POLITECNICO DI MILANO

DEPARTMENT OF ELECTRONICS, INFORMATION AND BIOENGINEERING

DOCTORAL PROGRAM IN INFORMATION TECHNOLOGY

DATA ANALYSIS AND MODELS FOR LONG-DISTANCE BIRD MIGRATION

from correlations on ring recoveries to machine learning on geolocator measurements

Doctoral Dissertation of:

Mattia Pancerasa

Advisor:
Prof. Renato Casagrandi

Co-Advisor:
Prof. Roberto Ambrosini

Tutor:
Prof. Andrea Castelletti

The Chair of the Doctoral Program:
Prof. Barbara Pernici

Abstract

Climate is one of the fundamental shapers of ecosystems, thus its ongoing changes deeply influence the behavior, distribution and dynamics of plant and animal populations. Migratory birds are among the species most affected by this phenomenon, as they need to fine-tune their phenology according to the climatic conditions of their breeding and wintering areas. To investigate how and to what extent alterations of climate regimes may determine key changes in the movement ecology of migratory birds, a detailed knowledge of their staging sites, a trustable reconstruction of their migration routes and of the time schedules of their journeys is very necessary. The classic methods for studying migration, such as bird ringing, can now be complemented by new technologies, such as GPS loggers or light level geolocators, that allow to record proxies of organisms' positions throughout their routes.

Focusing on a model species, the barn swallow (*Hirundo rustica*), in this work we first developed a method to investigate the occurrence of climatic connections between the African wintering and European breeding areas of this migratory passerine bird: surprisingly significant correlations between the average temperatures in the wintering and breeding locations of individuals emerged at the precise weeks of individuals' spring migration. Correlations have high significance only in the proximity of barn swallow wintering sites and if the temperature series refer to the precise weeks of migration. Second, we reconstructed migratory routes of 88 barn swallows using the measurements provided by light level geolocators, verifying the repeatability of the estimation method we used. The results obtained allowed us to identify four groups of individuals, as well as a possible effect of the year of migration on many indicators of the migration schedules obtained from the reconstructed routes. Third, using the routes data as reconstructed in the second research step, we have automated a long manual phase of data pre-processing by implementing filters based on Machine Learning algorithms. The migratory routes reconstructed using the automated pre-processing are completely comparable with those obtained from the manual selection of geolocator data. The work confirms that models based on data gathered with ICT devices may be helpful tools to let us gain insights on the influence of environmental and climate changes on species and ecosystems connectivity.

Contents

List of figures

List of tables

1 INTRODUCTION

1.1 Migratory birds and the climate change: a strong bond

Birds have always provided ideas and opportunities for humans to understand the mechanisms through which nature works. The extraordinary biodiversity of the Galapagos avifauna was for Charles Darwin one of the major sources of inspiration for a milestone of biology and modern science such as the theory of species evolution (Darwin, 1859). In the large family of birds, migratory species are followed with particular interest for their ability to adapt their behavior to the changes in the environment in which they live (Newton, 2007), with purpose of investigating how the species evolve or modify their strategies as a result of the changes they experience.

Moreover, like many other migratory animals, birds play an ecologically relevant role throughout the biosphere, transporting each year significant amounts of nutrients, energy and other organisms (including parasites and pathogens) and forming part of the trophic chains of different areas of the planet (Bauer and Hoye, 2014). These ecological links are today at risks: many long distance migratory species have for years been subject to a strong population decline (Sanderson *et al.*, 2006) mainly due to impacts caused by human activity such as habitat alteration, pollution and illegal killing (Berthold, 2001). Climate change worsens this situation, mainly acting on the mechanisms used by migratory species to decide the spatio-temporal dynamics of their long journeys (Cotton, 2003).

Migratory birds have for years been a valuable source of biological information for the study of the impacts of climate change on a large scale: they are highly mobile animals, relatively easy to find and recognize (Møller *et al.*, 2010). The numerous campaigns of observation and monitoring of their reproduction areas allowed to detect the variation of the arrival dates of many species (Gordo, 2007), providing one of the first signs of the sensitivity of biological mechanisms towards the complex abiotic and biotic changes induced by anthropogenic climatic changes. This peculiarity has made them a model for the study of the impacts of climate change on the phenology of plants and animals, elevating them to the role of 'winged sentinels' of climate change (Wormworth and Sekercioglu, 2011). It is therefore important to know which cues can influence the migration of these individuals, for example by acting on their departure and stopover decisions during their trips.

Until now, these studies have been carried out exploiting information of bird capture or recovery locations, as information on the places they visited during the migration was scant. Only in recent years, new technologies have been developed to track directly or indirectly the movement of these species (Bridge *et al.*, 2011). The science of geolocation of moving objects has reached remarkable goals, allowing people to know precisely and send to anyone their position on the planet through devices weighing a few tens of grams and with a reduced cost (i.e. any smartphone with a GPS sensor). Unfortunately, even today, we cannot adopt a similar approach for most species of migratory birds, because they are simply unable to successfully complete their journeys of hundreds or thousands of kilometers even carrying a simple GPS data logger weighing 2.5g (Bridge *et al.*, 2011).

Currently this problem is overcome by less precise but lighter devices: light-level geolocators. A light level geolocator records the light intensity experienced by the bird throughout the period in which it is applied (usually for a round trip migration). Once recovered, it is possible to estimate the route traveled by the bird through the combination of physical models based on astronomical equations (Meeus, 1991) and statistical analysis of uncertainty filtering.

Thanks to the use of geolocators, in recent years it has been possible to obtain important information on the phenology and behavior of individuals even of small-sized species (e.g. Winkler *et al.*, 2017). The integration of these data with the information obtained from the classical methods of ornithological studies is a very active field of research,

which may lead to the clarification of several scientific issues still open, including the relevance of the climate and its changes on the migration process.

1.2 Thesis structure

In this thesis we developed and applied data analysis and modeling procedures to study the whole migration of a focal species, which is a long-distance migrator: the barn swallow (*Hirundo rustica*). Some basic information on the biology and migration of this species are provided in Par. 1.3.

In Chapter 2, we look for the presence of climate signals between the breeding and wintering areas of the barn swallow during the focal period of spring migration. We focused our attention on one of the most relevant environmental variables, the temperature, calculating the correlation between the average monthly temperature of the wintering and breeding areas close to the dates of departure and arrival of the barn swallows. The significance of the obtained results was investigated by means of randomization tests and temporal sensitivity analyzes. This chapter is elaborated from the work published in Pancerasa *et al.* (2018).

With the aim to go beyond the mere information provided by the departure and arrival positions, in Chapter 3 we reconstructed the migratory routes of 88 Italian and Swiss barn swallows from the measurements of light level geolocators. This is one of the first studies able to reconstruct the whole migration paths for a relatively large number of individuals of a small-size species. After verifying the reliability of the software used to reconstruct the routes, we selected some summary indicators of the migration at the individual level and analyzed the variability of the individual routes by means of linear models.

Finally, since one of the critical phases of the preprocessing of light level geolocator measurements is a time-consuming manual classification procedure, we used the data obtained in Chapter 3 to develop machine learning algorithms able to automate this process. Chapter 4 describes this work, also illustrating a repeatability analysis of the different classification methods and verifying the reliability of the results by comparing the routes generated by the automated procedure with those obtained by manual selection.

Finally, Chapter 5 summarizes the main findings of this thesis and draws some conclusions on the research topics covered.

1.3 Focus species: the barn swallow (*Hirundo rustica*)

The barn swallow is a small (length: 17-19 cm; wing-span 32-34 cm) migratory bird, belonging to the order Passeriforms. The distribution of its breeding range covers the whole temperate zone of the Northern Hemisphere, with the only exception of one population of the American subspecies (*Hirundo rustica erythrogaster*), which, during the '80s, has started reproducing in the north of Argentina (Winkler *et al.*, 2017). The barn swallow feeds exclusively on insects, capturing them in flight (Turner, 2006). It was described as a species by Linnaeus in his 'Systema Naturae' in 1758, named *Hirundo rustica* (literally "swallow of the countryside"). In fact, it nests semi-colonially in artificial structures located in rural areas, preferably near hayfields and farms with diversified crops.

For this reason, from the second half of the last century, the barn swallow have been subjected to the impact of the changes in the agricultural sector, where the trend of large lots of intensive monocultures (with the consequent loss of biodiversity) and significant changes in the agricultural buildings has been imposed. (Donald *et al.*, 2001; Donald *et al.*, 2006). Concomitantly, the availability of insects and places to build the nest has declined for the barn swallow, a phenomenon that has led to the decline of many of European populations (Møller, 1994; Ambrosini *et al.*, 2002; Turner, 2006).

With the exception of some southern Spanish populations, the barn swallows that breed in Europe start in autumn a long migration to reach their wintering areas. The first arrivals in Western and Equatorial sub-Saharan Africa are registered from the end of September, but the peak is reached in the first days of December, due to the slowness of the younger individuals (those born in the previous months) at their first trip. The last individuals reach their wintering areas at the beginning of January. The swallows can travel for up to 300 km per day, covering the distance between Scandinavia and South Africa in a month (Møller, 1994). Most annual mortality of this species occurs during migration and winter; in particular, in the wintering areas, precipitation acts indirectly on the survival of the barn swallows influencing their foraging (Møller, 1994). Spring migration begins earlier for populations reproducing in northern Europe, but the peak of arrivals at the breeding

grounds is recorded between March and April, except in the northernmost regions. Males usually arrive before females at the breeding colonies, in order to find a suitable breeding site and start the construction of a nest. Young individuals (less than one year old) usually arrive after adults. When a young swallow returns to the breeding areas, it tends settle to a breeding colony different than its birthplace (the dispersal phenomenon), but dispersal differ between males and females. Usually, males disperse less than females and tend to return to their native colony in larger number, especially if it was a high-quality breeding site (with many hay fields and food-rich habitats) (Møller, 1994). Females, on the other hand, exhibit higher dispersion propensity (with a 98% probability of dispersion). This probably allows them to maximize their reproductive success and to avoid breeding with consanguineous individuals. The average dispersal distance of females from the native colony is 10 km, while that of males is only 5 km (Turner, 2006).

Figure 1.1: Map of the breeding (yellow), wintering (blue) and permanent presence (green) areas of the European barn swallows. Source: *birdlife.org*

2 ANALYSIS OF CLIMATIC CUES FOR LONG DISTANCE BIRD MIGRATION

2.1 Introduction

In natural populations, organisms are expected to do the right thing at roughly the right place and time, under the limits set by their physiological and behavioral constraints, because natural selection strongly penalizes the individuals that do not appropriately match their activities to current environmental conditions (see e.g. Visser and Both, 2005; Møller *et al.*, 2008). For example, plants budding and flowering at the wrong time, and animals breeding or migrating at the wrong place and time suffer severe reproduction and viability costs (Stenseth and Mysterud, 2002; Both *et al*., 2006; Parmesan, 2006; Saino *et al*., 2009).

Organisms have evolved to track cyclical changes in ecological conditions, that typically occur with circannual periodicity, by exploiting environmental cues, like change in photoperiod, that announce forthcoming ecological changes (Berthold, 1996; Gwinner, 1996; Coppack and Both, 2003). While seasonal ecological changes occur predictably, fluctuations of major ecological factors that heavily impact on most organisms, like temperature or precipitations, over shorter time frames may occur rather unpredictably. The need to accommodate such fluctuations is the apparent evolutionary reason why many organisms have retained some level of temporal flexibility in the time schedule of

their activities ('phenology'). For example, birds at temperate latitudes adaptively time their breeding in spring according to photoperiod (Gwinner, 1996), but they also show the ability to adjust the exact time of breeding according to the current weather conditions, that may vary unpredictably among sites and years (Both, 2010; Gunnarsson and Tómasson, 2011). Plants and non-migratory animals can directly sense the progress of seasonal variation in local ecological conditions and flexibly adjust their physiological state and behavior according to environmental cues to prepare to the next shift in life-stage (Williams *et al*., 2014; Ensminge *et al.*, 2015; Jones and Gilbert, 2016). Unless sudden, abrupt changes in ecological factors occur, this affords them an opportunity of fine-tuning their life-cycle according to the current extrinsic conditions and retain (fairly) appropriate phenology.

On the other hand, migratory animals that periodically move over large distances, alternating between breeding and non-breeding areas, have no direct clue as to the conditions that they will experience along their migration journey and at destination, weeks to months later. Migrants are therefore considered to be particularly susceptible to environmental uncertainty and thus, for example, to the negative effects of human-driven, rapid climate change, including advancement of spring phenology at temperate latitudes (Walther *et al*., 2002; Parmesan and Yohe, 2003; Parmesan, 2006; Rubolini *et al*., 2007; Robinson *et al*., 2009) and increased frequency of extreme meteorological events (Meehl *et al.*, 2000; Parmesan *et al.*, 2000; Walther *et al*., 2002; Bertacchi *et al.*, 2016). The fitness advantages of appropriate timing of life-history events, however, is expected to select for the ability to capitalize on any environmental cue that allows to buffer the negative effects of environmental unpredictability on individual performance. Migratory animals may thus be expected to exploit any association that may exist between the ecological conditions during one stage of their annual life-cycle (e.g. staging in the non-breeding area, or wintering) with the conditions that they will later experience *en route*, during subsequent migration, or at destination (Przybylo *et al.*, 2000; Møller *et al*., 2004).

At one extreme, it may even be expected that, in order to appropriately tune their decisions on timing of migration and arrival to the breeding sites, migrants choose as wintering areas those where the most accurate information on future conditions at destination can be gathered. This may partly contribute to the migratory connectivity that migratory birds exhibit, whereby individuals that breed in the same geographical region also tend to share

the same wintering area (Ambrosini *et al.*, 2009; Fraser *et al*., 2012; Cormier *et al*., 2013; Hahn *et al*., 2013; Knick *et al*., 2014; Finch *et al*., 2015; Ambrosini *et al*., 2016, but see Finch *et al*., 2017). In addition, this may explain why migrants display some ability of tuning their arrival time according to the contingent weather conditions at destination, despite they cannot directly sense them (Cotton, 2003; Gordo *et al*., 2005). However, the hypothesis that migrants have the opportunity of making decisions on their migration schedule based on expected conditions at destination and that the location of their wintering staging areas depends, at least partly, on the extent of information that they can gather on the ecological conditions they will experience at the other end of their migration journey, has been explored only very sparsely (Gordo, 2007).

Saino and Ambrosini (2008) investigated the presence of correlations between the monthly average temperatures of macro-areas in sub-Saharan Africa and Europe in the focal period of spring migration, finding that the climatic conditions of the former negatively predicted the latter ones within a temporal range of a couple of months. To the best of our knowledge, no study of this type has ever tested these climatic connections at a finer spatial scale, for example by using migratory birds ringing data. The next section provides a brief introduction to this data source, in order to better understand its potential.

2.1.1 Ringing data

Bird ringing consists in applying a small aluminum or plastic tag to the leg or to the wing of captured birds (Figure 2.1a). This tag is marked with an identification code, which allow identifying the marked individual at any re-encounters. Tags are designed and applied specifically for not affecting the behavior, survival and reproductive success of the marked individual. During ringing, some ecological data related to the marked bird as sex and an estimate of age are also usually recorded, whenever they can be assessed observing the bird in the field, as well as some indicators of its physiological status such as the feather conditions and the amount of subcutaneous fat. Usually the birds are caught directly in their nest (especially if newborns) or through the use of mist nets (Figure 2.1b), which facilitated the simultaneous capture of many individuals and species (Møller *et al.*, 2010).

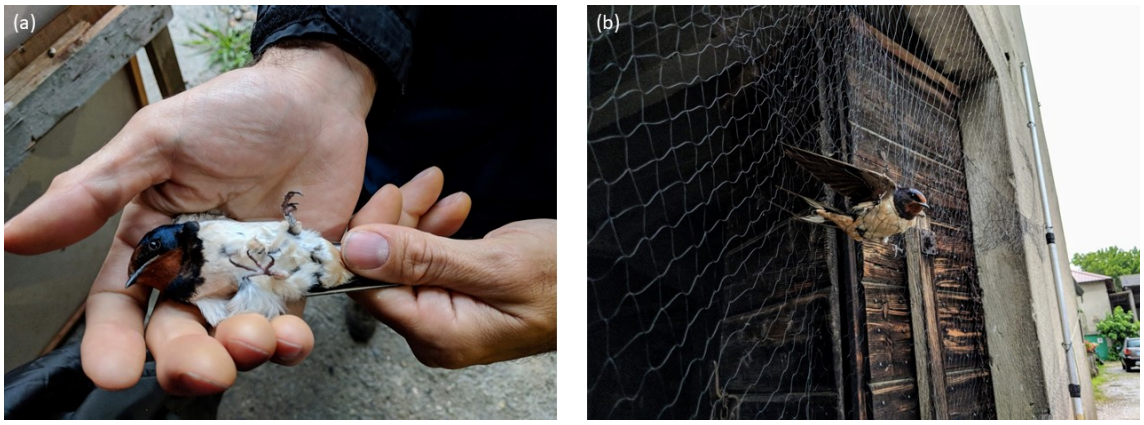

Figure 2.1: (a) A barn swallow with a metal ring on its left leg. (b) A barn swallow trapped in a mist net.

The ringing of migratory birds was the first study method historically used to try identifying where these species moved during the winter seasons. Since the beginning of the last century, several national European and North American associations of ornithologists have launched scientific ringing campaigns (Møller *et al.*, 2010), subsequently converging their data into transnational databases such as those managed by the European Union for Bird Ringing (EURING, euring.org), the North American Banding Council (NABC, nabanding.net) and the South African Bird Ringing Unit (SAFRING, safring.adu.org.za). This simple method has allowed studying the behavior, the phenology and the response to the anthropic pressures of entire populations and species (Fiedler *et al.*, 2004). However, ringing data are affected by a problem of large spatial and temporal heterogeneity of sampling effort that some analysis try to correct (Korner-Nievergelt *et al*., 2010; Nadal *et al.*, 2018).

Given their practicality, affordability and availability at large spatial and temporal scales, ringing data are still one of the main sources of information for scientific ornithological studies, particularly for those focused on the identification of the breeding and wintering areas (e.g. Frederiksen *et al*., 2018; Nadal *et al.*, 2018), migratory connectivity (Ambrosini *et al.*, 2009), departure and arrival from migration (Ambrosini *et al*., 2014) and exploitation of possible environmental cues to adjust migration phenology (this thesis).

2.1.2 Focus of the present analysis

In this work, we used information for a uniquely large set of data on ringed barn swallows to test if correlations exist between temperatures in the wintering sites south of the Sahara

Desert just before the start of northward spring migration and the temperatures at their individual breeding sites at the time of spring arrival from migration, several weeks later. We focus on temperature because this is the main driver of the progress of spring ecological events relevant to barn swallow ecology and breeding biology (Turner, 2006). Second, we test the prediction that temperatures at the sites where barn swallows spend their wintering period in Africa are correlated with those recorded at the breeding sites weeks later, when migration is completed, as expected under the hypothesis that individual barn swallows choose their wintering areas also depending on the level of temperature-connectivity with the breeding sites. Finally, we checked the persistence of these signals throughout the previous century, so as to check the possible impact of climate change on these ecological connections.

To perform our analyses, we relied on the information from ringing data for 270 barn swallows that were captured during breeding in Europe and were later recovered during wintering in Africa, or vice versa, during the period 1930–2009. For each individual, we estimated the putative departure time from Africa when spring migration started according to information from a recent geolocator study (which will be presented and more extensively used in Cap. 3) and from bird monitoring, and spring arrival time to the breeding site in Europe according to a model of the progress of spring arrival of barn swallows.

2.2 Materials and methods

2.2.1 Barn swallow ringing data

Ring recoveries were obtained from the EURING (du Feu *et al*., 2016) and SAFRING (Underhill and Oately, 1994) databanks. Out of the 73610 records in the original datasets, we selected the only 270 individuals ringed and re-encountered (i.e. recaptured alive or found dead, in any circumstance, 'ring re-encounters' hereafter) during stationary periods in the breeding (North Africa and Europe, simply 'Europe' hereafter, as 99.6% of the records of breeding individuals used in this study occurred in Europe) and the wintering grounds (Africa). In particular, those periods are December-February in Africa (south of the Sahara Desert) and June-July in Europe and North Africa (see the study of Ambrosini *et al.*, 2009 for a similar approach). Selected ring re-encounters spanned 1930–2009 and

were within 34.46°N–65.07 °N and 4.53°W–59.67°E in the breeding grounds and within 7.75°N–34.45 °S and 7.92°W–35.00°E in the wintering grounds.

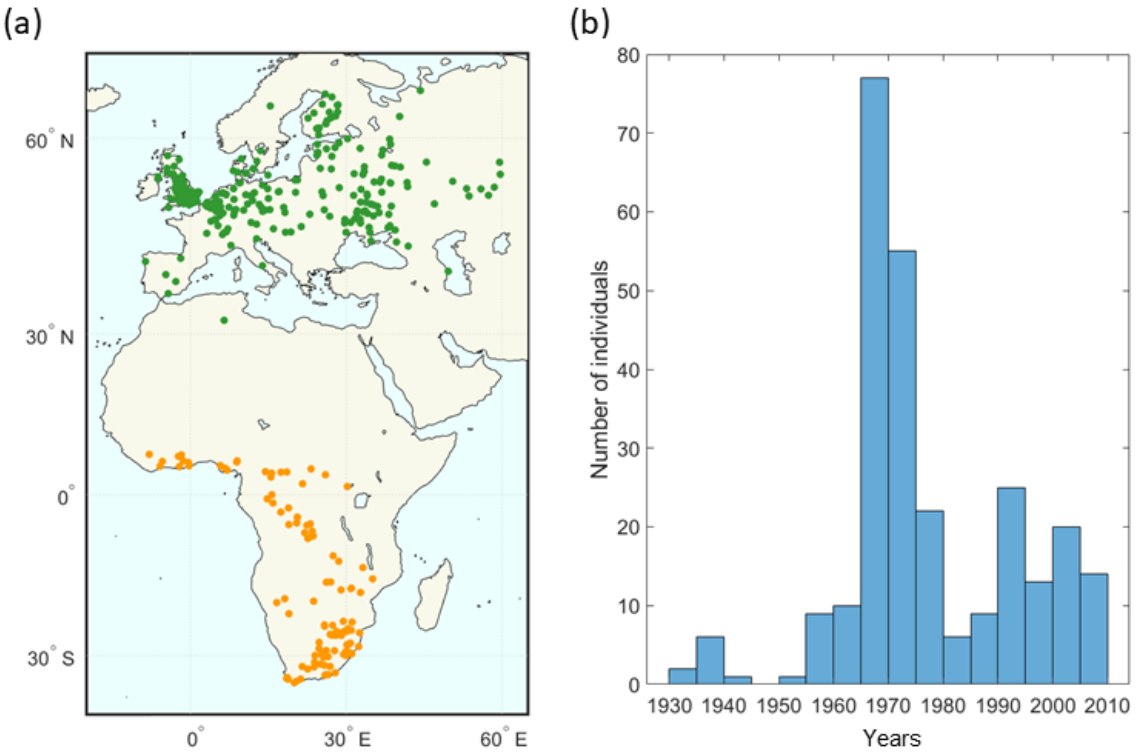

Figure 2.2: Spatial and temporal distribution of ringing data used in the correlation analysis. (a) Geographical displacement of wintering (orange) and breeding (green) positions. (b) Histogram of individuals year of recovery in Europe.

As it is well known in the ornithological literature, ringing data show high spatial and temporal heterogeneity (Thomson *et al.*, 2003) and, no exceptions, our dataset is also subject to this same problem, as shown in Figure 2.2. However, as there is no reliable data regarding ringing sampling effort nor proxies, we didn't try to correct the ringing dataset. Rather, as our goal was not to build a spatio-temporal model of the migration process, we retained all the samplings, because the relevant information for the present study is the geographical location of the breeding and the wintering sites of the single individuals, which is clearly well represented by its ringing and recovery locations.

2.2.2 Departure and arrival dates of spring migration

We first estimated the arrival dates from spring migration in each breeding location according to Ambrosini *et al.* (2014), which reports a map of estimated arrival dates of the first 15% of barn swallows in Europe and North Africa (10°W–26°E, 26°N–66°N, resolution 4°×4°, latitude × longitude) based on an analysis of ringing data spanning

1908–2008. We estimated the arrival date at each breeding location by ordinary kriging with a stable variogram model (sensu Wackernagel, 1995) of estimated arrival dates at each cell as identified in Ambrosini *et al*. (2014). The kriging algorithm was used also to extrapolate the arrival dates of barn swallows ringed or recovered in Europe outside the area covered by that study (i.e. to the east of 26°E, n = 88 individuals). However, to reduce uncertainty in the estimated arrival dates for these latter individuals, we used their median estimated arrival date (7 May = i.e. Julian date 125) as the arrival date of all the individuals breeding to the east of 26°E.

At present, we are aware of no model allowing an estimation of departure dates from each African location. Preliminary analysis of the correlations showed the presence of two clear groups in the wintering areas, a division similar to those obtained through a geographical clustering by Ambrosini, Møller and Saino (2009) in an analysis of the migratory connectivity on barn swallows ringing data (see Par. 2.3.1). We have therefore selected for each cluster a departure date based on information available from studies of barn swallows that wintered in the same geographical areas. For all barn swallows wintering south of 7°S (the parallel that geographically divided the two clusters) , we used the mean departure date from South Africa as reported in Altwegg *et al*. (2012) (10 February = 41st day of the year). For all barn swallows wintering north of 7°S, we selected the mean departure dates reported in Liechti *et al*. (2015) (2 March = 61st day of the year). Since in both the studies the variability around these dates was of the order of half a dozen of days, we checked the robustness of this choice with a temporal sensitivity analysis described in Par. 2.2.5.

2.2.3 Large-scale, long term temperature data

To test for correlations between temperatures in the wintering and breeding locations of each individual in the focal period of spring migration, we used temperature data obtained from the atmospheric reanalysis ERA20C of the European Centre for Medium-Range Weather Forecasts (Poli *et al*., 2016). The ERA20C dataset was chosen for two reasons. First, because instrumentally recorded temperature data are not available with adequate resolution (neither in space nor in time) for our whole study areas, particularly in Africa. Second, because among the different global reanalyzes currently available, ERA20C is

the one with the finest spatial horizontal resolution (approximately 125 km) for the period 1900–2010.

Operatively, we selected the 2-metre temperature data (which represent an estimate of air temperature measured by meteorological stations, usually located 2 meters above the ground) at 6 hours intervals over a 1° × 1° geographical grid and calculated mean daily temperatures at each node. Then, we computed mean daily temperatures at the two exact coordinates where each barn swallow was ringed or recovered by spatial bilinear interpolation. In this way, we could obtain a time series of mean daily temperatures from 1900 to 2010 for the exact geographical positions where each barn swallow was ringed and re-encountered. From each time series, as detailed below, we extracted a short-term time series $\tau_{E,t}$ [$\tau_{A,t}$] by selecting temperatures that are relevant to spring migration in Europe [Africa] in the 30-years interval ending with the year of recovery in Europe. We opted for a 30-years timespan in analyzing temperatures, in accordance with suggestions by the World Meteorological Organization[1], because we wanted to work over temporal windows that are relevant to climatic rather than meteorological conditions. In order to smooth daily fluctuations and obtain temperature conditions of year t which are relevant to influence departure of barn swallows from Africa ($\theta_{A,t}$) and their arrival to Europe ($\theta_{E,t}$), we averaged all temperatures within the 30 days centered, respectively, on the specific departure and arrival dates described above. Thus, two migratory-relevant temperature series, computed over a climatic suitable and consistent temporal horizon, were assigned to each individual: one for the African location, $\tau_{A,t} = [\theta_{A,t}, \theta_{A,t-1}, \dots, \theta_{A,t-29}]$ and one for the European location $\tau_{E,t} = [\theta_{E,t}, \theta_{E,t-1}, \dots, \theta_{E,t-29}]$.

[1] For more information: www.wmo.int/pages/prog/wcp/ccl/faq/faq_doc_en.html

2.2.4 Position randomization

Continental-scale randomization

To test for climatic correlations between breeding and wintering locations of individual barn swallows, we first calculated the partial correlation coefficient (r_{par}) between $\tau_{A,t}$ and $\tau_{E,t}$ at African and European actual locations, i.e. the locations retrieved from the ringing data, while controlling for the effect of year. Partial correlation enabled us to control for the effects of long term temporal trend in temperature data (e.g. climate change), and is computed as:

$$r_{XY \cdot Z} = \frac{r_{XY} - r_{XZ}\, r_{ZY}}{\sqrt{1 - r_{XZ}^2}\,\sqrt{1 - r_{ZY}^2}}$$

In our case $X = \tau_{A,t}$, $Y = \tau_{E,t}$ while as Z we used an integer vector from 1 to 30, representing the time index for each value of $\tau_{A,t}$ and $\tau_{E,t}$.

To verify the significance of the analysis it is not possible to rely on typical statistical tests (e.g. a binomial test of the number of significant correlations found on the total number of individuals) as the used samples (i.e. the series $\tau_{A,t}$ and $\tau_{E,t}$ for each individual) are not independent, due to the spatial and temporal correlation in temperature for swallows sampled in nearby periods and/or locations.

To assess whether partial correlation coefficients were significant at a broad (i.e. continental) spatial scale, we then computed the same partial correlation coefficients for all individuals by holding the European location and year fixed and using 361 additional positions in Africa. The African additional positions used for this broad spatial scale simulation were distributed according to a 2° × 2° regular grid (south of 15 °N) whose nodes did not occur neither on the sea nor in desert areas (see exemplificative cyan dots in Figure 2.3). Desert locations were identified as those where the average daily *Total Precipitation* (as retrieved from ERA20C reanalyzes) was lower than 0.65mm over the period 1900–2010 (Marshak, 2009). The absolute values of the 362 partial correlation coefficients (one between the actual wintering and breeding locations plus 361 for the simulations over the entire sub-Saharan Africa) calculated for each barn swallow were then listed in decreasing order of magnitude, thus obtaining the rank of the value for the correlation between the actual wintering and breeding positions.

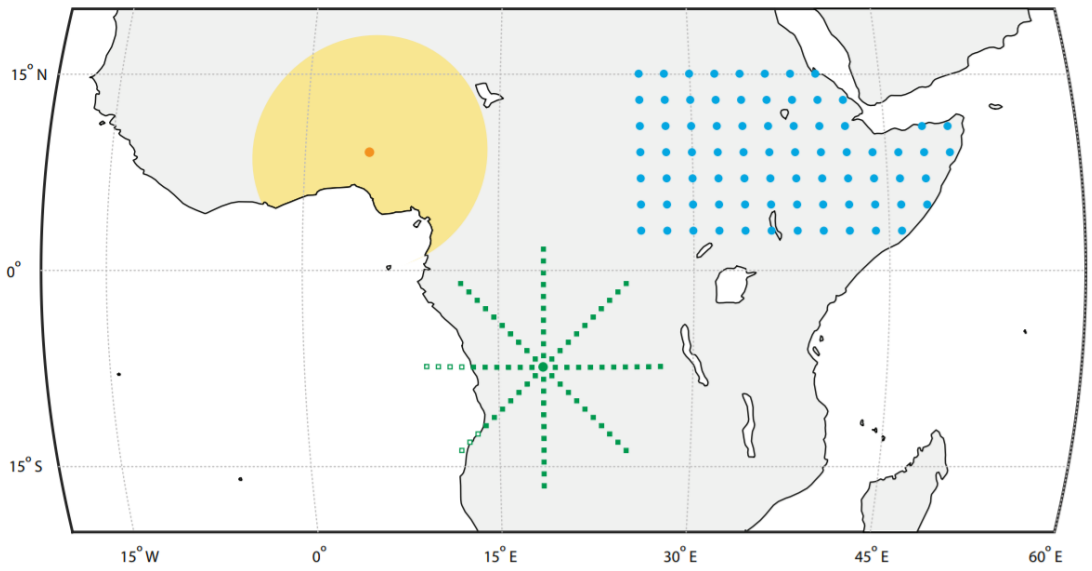

Figure 2.3: Exemplificative representation of randomization tests used to evaluate the strength of the correlations between the African and the European temperatures relevant to barn swallow migration and their correlation peaks. Cyan dots are some of the 361 nodes of the sub-Saharan Africa subcontinent grid (2°×2°) used to perform the broad scale simulation test. The circular yellow area (radius of 1000 km) is where we randomly extracted (with a uniform probability distribution) the locations alternative to the focal barn swallow wintering location (orange center) to perform the local scale randomization test (ocean and desert areas are excluded). The wind rose-like radial grid surrounding a hypothetical barn swallow wintering location (green) used in our simulation to search for correlation peaks: filled green squares are for locations where r_{par} between $\tau_{A,t}$ and $\tau_{E,t}$ was computed, white filled squares were discarded locations.

Local-scale randomization

A second type of spatial randomization test was then performed to check the robustness of our results at a finer (say 'local') geographical scale. To this end, we assessed whether the number of significant partial correlations was larger than those arising from a null model where the positions of barn swallows in Africa were randomly selected 999 times within a distance of 1000 km around the true wintering position, while avoiding points located on the sea or in desert areas (see for example the portion of the yellow circle in Figure 2.3). It is worth noticing that there is an important asymmetry in the relationships between recorded locations of barn swallows captured (or found) in Europe and in Africa. While the home range radius of individuals in the European breeding grounds is of about 1 kilometer (Ambrosini *et al.*, 2002), in the African wintering areas it can be as large as hundreds of kilometers (Turner, 2006).

It is therefore important to explore whether there are any structured spatial patterns of partial correlations surrounding the actual location where the barn swallow has been

found in Africa, e.g. the location is close to a correlation peak. To investigate this possibility, we computed the partial correlation coefficients between $\tau_{A,t}$ and $\tau_{E,t}$ also for a set of points that were homogeneously distributed in the region surrounding the wintering position. To this end, we built a radial grid of points (fled green squares in Figure 2.3) centered on each of the barn swallow locations. Nodes of every grid were placed at 45° to one another (starting from the north), at distances of 100–1000 km (at 100 km intervals) from the central position (green dot in Figure 2.3). Grid nodes located on the sea or in desert areas (see 'Continental scale randomization') were disregarded (open squares in Figure 2.3). For each barn swallow, at each grid node we calculated the partial correlation between the local temperatures and those at the European breeding location and recorded the distance from the grid center of the node where correlation was significant and strongest (the correlation peak).

2.2.5 Temporal sensitivity analysis

Since there is some uncertainty on the exact period of migration of each individual, we also analyzed the sensitivity of the number of significant correlations to changes in the dates of both departure from Africa and arrival to Europe. This was done by advancing or delaying of at most 15 days (with steps of 5 days) the dates of departure and/or arrival over which $\tau_{A,t}$ and $\tau_{E,t}$ were computed, recording the number of partial correlations that occurred each time.

Finally, we verified the presence of partial correlations throughout the period covered by ERA-20C (1900-2010), repeating the same steps described in Par. 2.2.3 for each year since 1929 (right extreme of the first 30-year time window on the atmospheric reanalysis time span) to 2010.

2.3 Results and discussion

2.3.1 Correlation analysis at the continental scale

Our broad-scale simulation test suggested that a large fraction of the individuals did strongly select wintering locations where the temperature correlations were stronger: indeed, for 59 (21.8%) individuals, the absolute value of the partial correlation coefficients with temperatures in their European breeding locations was higher (i.e.

within the top 10%) for the actual wintering locations than for the 361 alternative locations of this broad-scale simulation test (Figure 2.4a). This percentage is well above the 10% (dashed line in Figure 2.4a) that would be a priori expected if selection did not occur.

Also, for 61 (22.6%) individuals, pre-migration temperature in the African wintering location ($\tau_{A,t}$) was found to explain at least 10% of the variance in temperature at the breeding site in Europe ($\tau_{E,t}$). The locations of these 61 individuals were clearly separated in two geographical clusters in Africa (Figure 2.4b), whose latitudes were either North of 7°S (*cluster N*) or South of 18°S (*cluster S*). Interestingly, the partial correlation coefficients between $\tau_{A,t}$ and $\tau_{E,t}$ were opposite in sign for either geographic clusters for almost all barn swallows (>95%): 18 out of 19 barn swallows whose wintering location was in Western and Central equatorial Africa (cluster N, Figure 2.4c) exhibited positive temperature correlations (mean 0.373, standard deviation 0.056) with the relevant temperature time series at their breeding locations in Western Europe, and 40 out of 42 barn swallows wintering in Southern Africa (cluster S, Figure 2.4d) showed negative temperature correlations (mean −0.407, standard deviation 0.064) with their breeding sites in Eastern Europe.

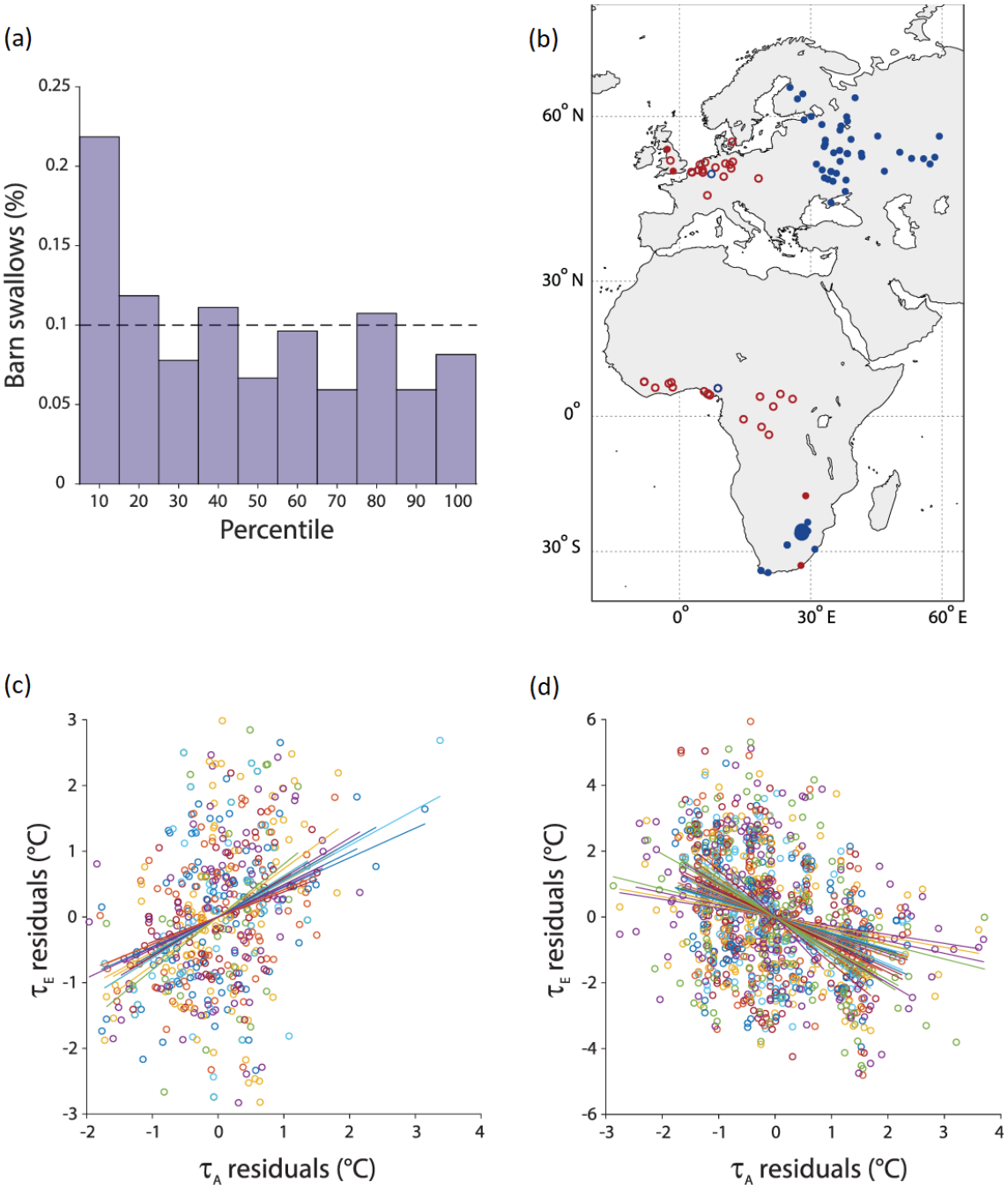

Figure 2.4: Continental scale analysis of correlations between temperatures at departure of barn swallows from Africa and at their arrival in Europe. (a) Ranking of partial correlations coefficients between temperatures at departure time from Africa ($\tau_{A,t}$) and at arrival time in Europe ($\tau_{E,t}$). Climatic series in the actual African locations are contrasted to alternative locations in the whole sub-Saharan African subcontinent (see broad scale simulation test in Methods). the dashed line is the expected distribution if no site selection occurred (complete random process). (b) Geographical locations of the 61 barn swallows for which $\tau_{A,t}$ explained at least 10% of the variance of $\tau_{E,t}$. Circles identify individuals that winter either north of 7°S (cluster N) while dots those that winter south of 18°S (cluster S). Colors code the sign of the partial

correlation coefficient between $\tau_{A,t}$ and $\tau_{E,t}$ (red for positive and blue for negative partial correlation). Dot size is proportional to the number of individuals found at any location. (c) Scatterplot of temperature anomalies in breeding vs wintering areas for individuals of cluster N whose migratory relevant temperature conditions in Africa explain more than 10% of variance of their European equivalent. Data referring to the same individual are denoted by a unique color: each circle represents the values of wintering and breeding temperatures anomalies for the focal individual in one of the 30-years of climatic reference for it. (d) As (c), but for cluster S.

It is noticeable that the correlations identified at departure sites were highly time-specific. Indeed, by repeating the same analysis shown in Figure 2.4c,d under the hypothesis of a six weeks delayed migration, we found no significant correlations and much lower signals (Figure 2.5).

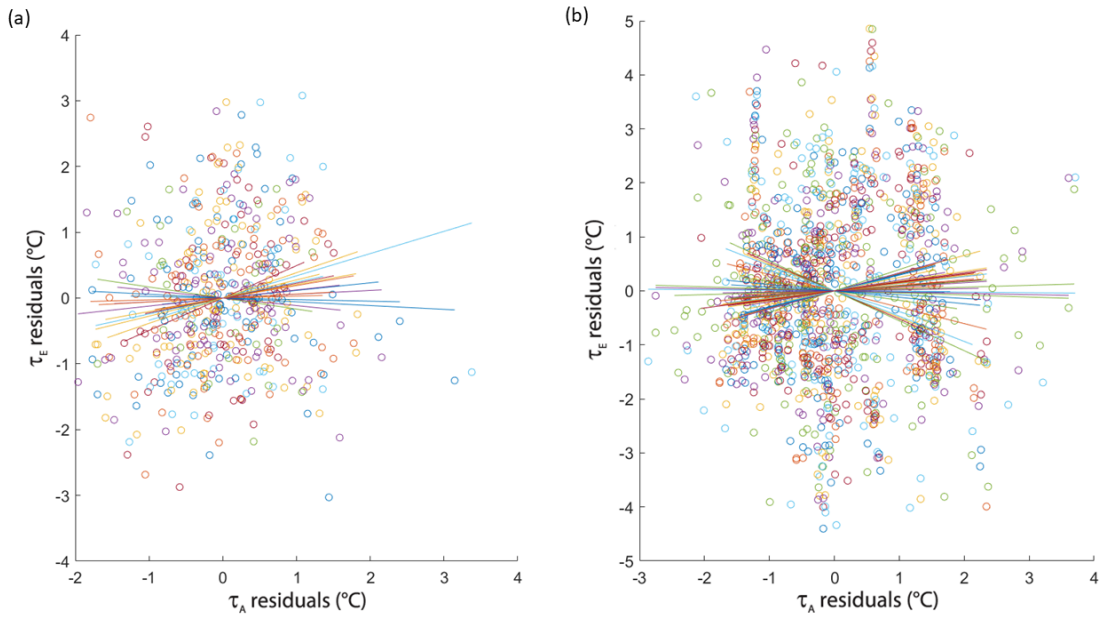

Figure 2.5: (a) same as Figure 2.4c, but after moving departure date 6 weeks later. (b) Same as Figure 2.4d, but after moving departure date 6 weeks later.

Our crude clustering based on latitude of barn swallows wintering locations alone is almost identical to the one proposed by Ambrosini et al.(2009), which was based on migratory connectivity using a *k*-medoids algorithm (Kaufman and Rousseeuw, 1987) on distance matrices computed on ringing data of barn swallows captured both in Europe and Africa. We thus found that the clustering based on geographical locations is almost indistinguishable from a specific climatic partitioning based on the signs of partial correlation coefficients between temperatures at departures and arrivals for our migratory species. These results are compatible with the idea that there might be climatic guidance

to site selection for the long-distance migrating barn swallows breeding in different European regions. For this reason, in subsequent analyzes, we focused only on positive correlations for cluster N and negative ones for cluster S. For the sake of clarity, we specify that we retained all the 270 individuals selected in Par. 2.2.1 in each of the spatial randomization and temporal sensitivity analysis of the subsequent paragraphs.

Temperature correlations between the wintering and the breeding sites may also contribute to the mechanism by which migratory birds are responding to climate change effects. Several trans-Saharan migratory species are advancing the time of spring arrival to the breeding sites in Europe and this has been attributed to the advantages of keeping track of rapid advances in spring phenological events that occur in Europe. If current climate change is preserving the existing patterns of spatio-temporal correlations between temperatures in sub-Saharan Africa and in Europe, we may expect that these correlations would boost the process of adjustment of migration phenology to current climate change. On the other hand, disruption of temperature correlations would hinder adjustment adaptive adjustment of migration phenology with negative effects on populations of long-distance migrants.

2.3.2 Correlation peak at the local scale

The interpretation that choice of the wintering location was guided by climatic signals is reinforced by the analysis of statistical significance of the correlation between temperatures in wintering and breeding locations at the local geographical scale. The number of individuals showing a one-tailed statistically significant correlation between $\tau_{A,t}$ and $\tau_{E,t}$ exceeded that expected by chance alone (binomial test for the deviation of the proportion of significant correlations from 0.05: $p < 0.00001$ in both clusters). Because spatial autocorrelation of temperature may violate the binomial test assumption of independence of the observations, we ran the local-scale randomization test. At each of 999 replications, we randomly extracted one position within 1000 km of the wintering site of each individual and calculated the partial correlation between temperatures at the random African position ($\tau_{A,t\,rand}$) and temperatures at the breeding site ($\tau_{E,t}$). The number of significant correlations between $\tau_{A,t}$ and $\tau_{E,t}$ computed at actual wintering positions (18, 26.9% for cluster N and 42, 20.7% for cluster S) was larger than the number

of correlations between $\tau_{A,t}$ rand and $\tau_{E,t}$ for all the 999 replications (Figure 2.6, number of significant correlations from randomization: cluster N: mean±SD: 7.28±2.08, range: 1–13; cluster S: 27.45±3.79, range 17–39).

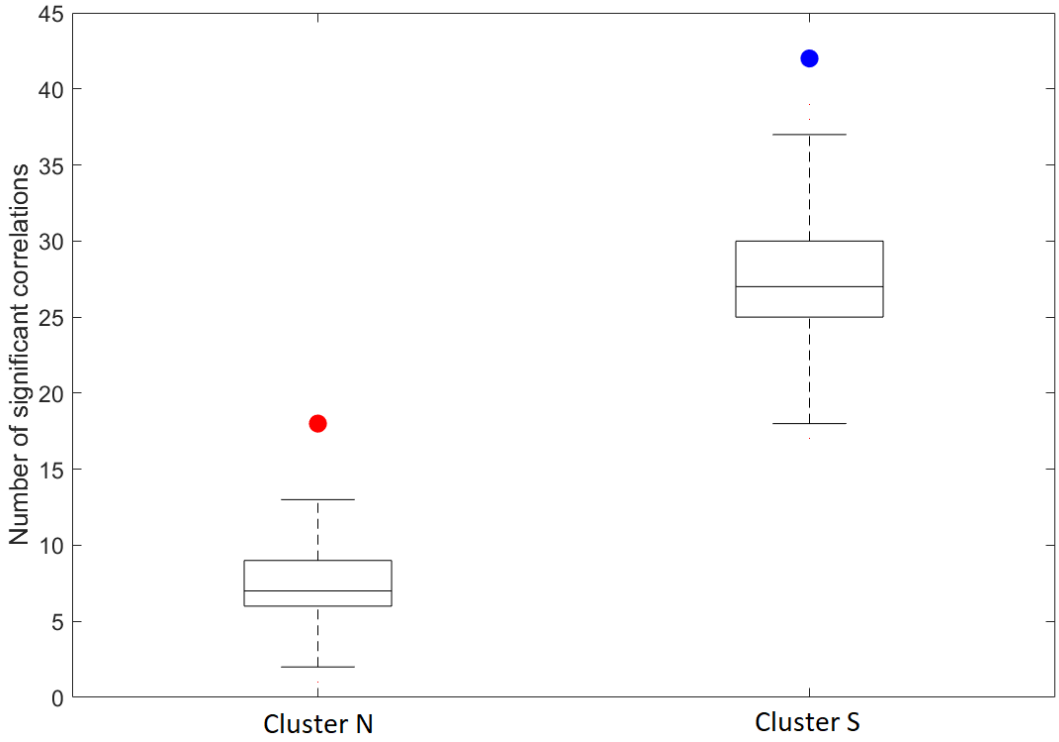

Figure 2.6: Boxplot of the number of significant correlations measured from local randomizations. Red and blue dots show the numbers obtained by using actual wintering positions. Cluster N has 67 individuals, while cluster S has 203.

Hence, the temperature correlations with the breeding location appeared to be consistently stronger for the actual wintering location than for other random locations within the same African region.

In the analysis of correlation peaks, the frequency distribution of the distances from the center of the grid (i.e. the wintering site) used to search for the peak showed that a remarkable proportion of them (27.27% for cluster N; 32.29% for cluster S) was located within 200 km of the wintering site (red bars in Figure 2.7), a distance that is of the same order of magnitude of the individual home range of barn swallows during wintering in Africa (Turner, 2006). To test if the frequency distribution of correlation peaks resulted from spatial autocorrelation of temperatures (i.e. from a pure climatic process), rather than from site selection, we re-ran the same analysis 999 times by centering the grids at each run on a random position in Africa within 1000 km from actual location as in the

local scale randomization described in Methods. In both clusters N and S, the observed frequency distributions markedly differed from those obtained by randomizations (grey bars in Figure 2.7). Indeed, the frequency distribution for the actual wintering locations (red or blue bars in Figure 2.7) have a mode rather close to the actual wintering position (ca. 200 km), whereas the frequency distribution from the randomized locations (grey bars) increased with distance, with local maxima around 800 km in cluster N (Figure 2.7a) or 600 km in cluster S (Figure 2.7b).

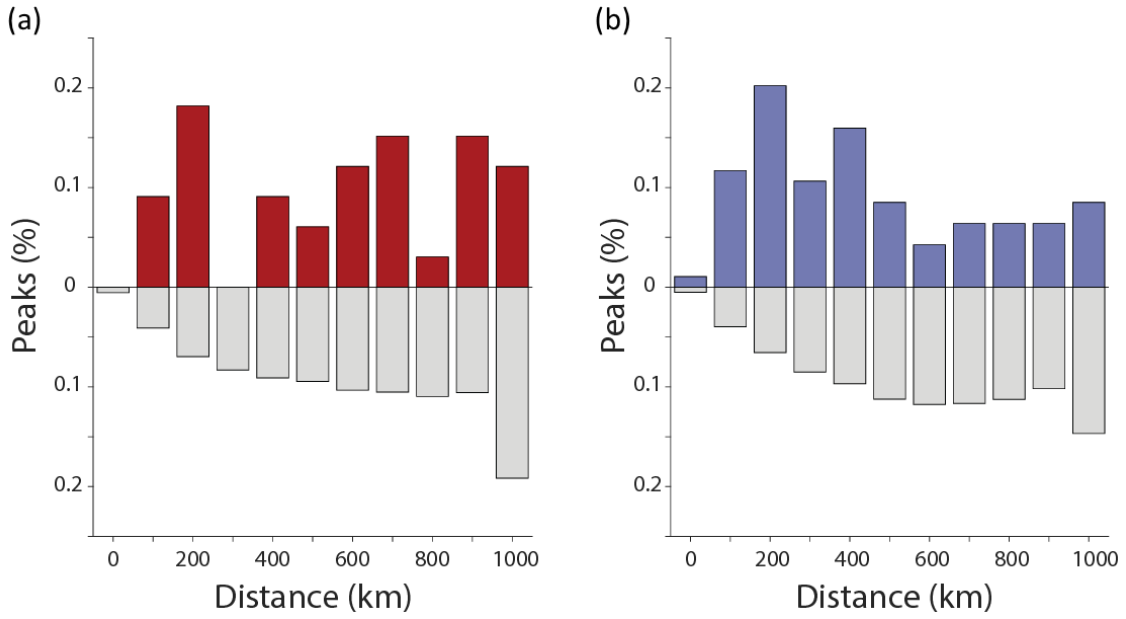

Figure 2.7: Frequency distributions of the distances of the correlation peak between temperatures relevant to migration from Africa to Europe and (red or blue bars) the actual wintering locations of barn swallows, or (grey bars) the randomly generated positions in Africa (local scale randomization) in either cluster N (a, red) or cluster S (b, blue).

To compare these patterns with a null random case, we analyzed the results of the 999 local-scale randomizations of Figure 2.7 and counted the number of times when the fraction of correlation peaks occurring within 200 km was higher at the actual locations of barn swallows (red or blue bars) than at random ones (grey bars). The result was unequivocal: this occurred 992 times in cluster N (99.2%, Figure 2.7a) and always (999 times) in cluster S (100%, Figure 2.7b).

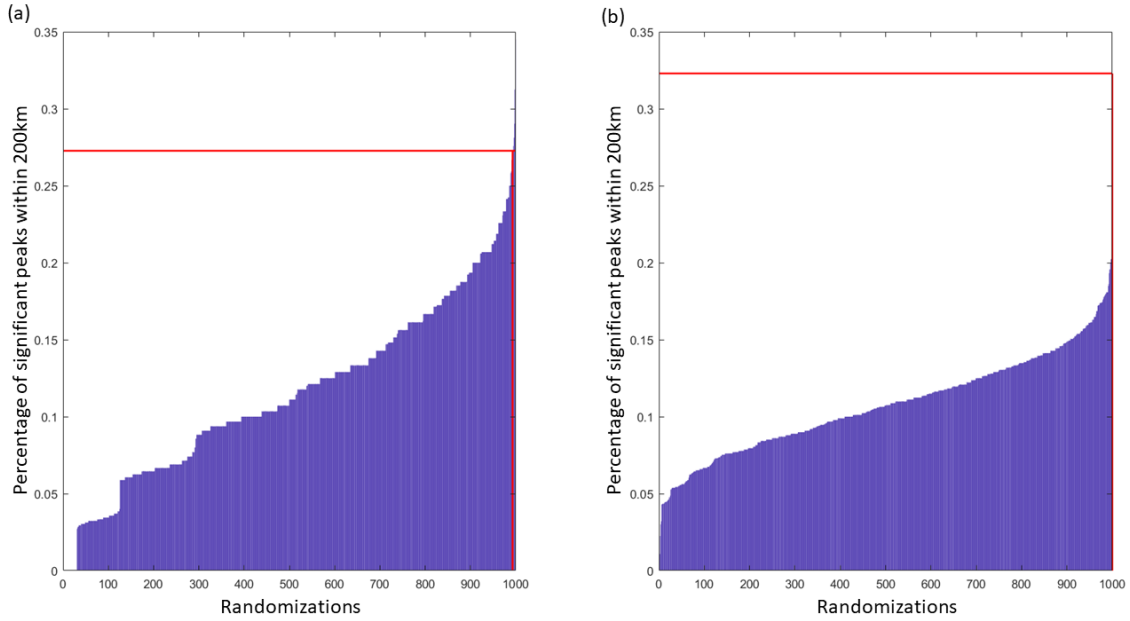

Figure 2.8: Barplots of the 999 percentages of peaks within 200 km from the randomized wintering positions for (a) cluster N or (b) cluster S. The red lines indicate the result obtained using the actual wintering positions.

If the correlation peaks had been randomly distributed around the center of our grid, the probability of finding correlation peaks within a distance of 200 km would have been around 4% (i.e. the ratio between the areas of two circles with radius 200 and 1000 km, respectively). The fact that the frequency distributions of correlation peaks obtained for the actual wintering sites markedly differed from those obtained for the locally randomized positions in both clusters strongly supports the idea that the two processes have different nature and that, also at a local geographical scale, barn swallows may choose as wintering locations those where temperatures have stronger correlation with temperatures in the breeding locations.

This result should be interpreted as an indirect test of the actual effect of temperature correlations between the wintering and the breeding sites on migration and wintering strategies. If such correlations are influential on life-history decisions is still an open research question. It could be expected that the sites where individual birds choose to spend their non-breeding season are non-randomly located with respect to their temperature correlations with the breeding sites. Wintering sites of individual barn swallows in sub-Saharan Africa have larger temperature correlations with the breeding site than with other locations in Africa. This pattern held both at the subcontinental scale

of sub-Saharan Africa and at a local geographical scale (i.e. within 1000 km from the actual wintering location). This might indeed suggest that the choice of the wintering location partly functions to maximize the information on annual conditions at the breeding site that is available before the start of migration.

2.3.3 Temporal robustness

To assess the robustness of these patterns of correlation with respect to the choice of the reference time periods assumed for departure from Africa and arrival to Europe we shifted these periods by a maximum of 15 days in both directions (back and forth), in steps of five days. A maximum of significant correlations clearly emerged for the time periods that we used in the analyses above, especially for cluster N (Figure 2.9a). We remark that such periods considered to be relevant for migration were chosen purely on the basis of information currently available on the actual phenology of barn swallow migration (see Par. 2.2.2).

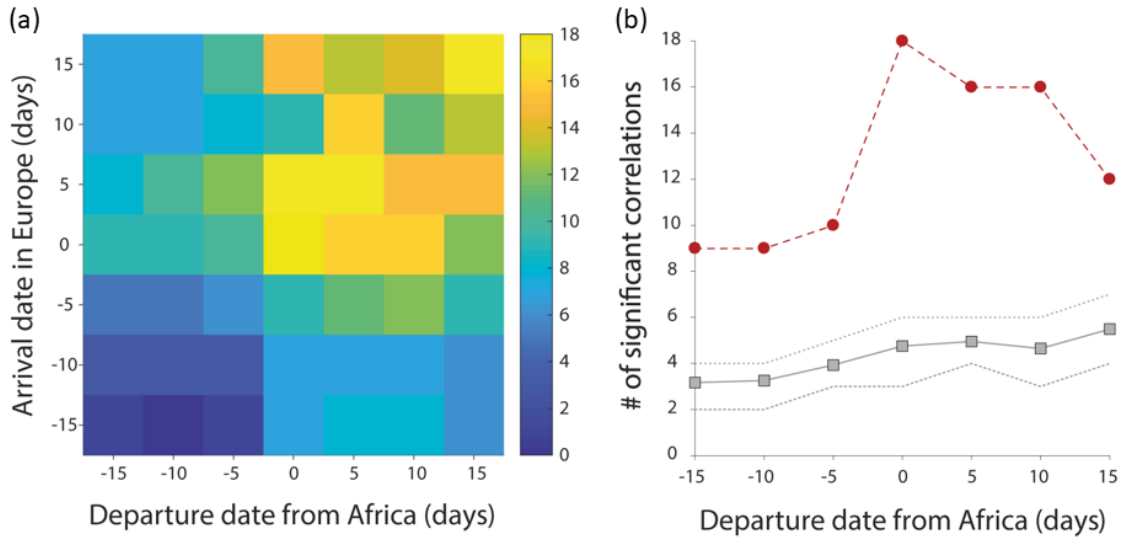

Figure 2.9: Temporal sensitivity analysis. (a) The number of significant positive partial correlations for barn swallows in cluster N at different temporal shifts (positive meaning delay) of the departure date from Africa (x-axis) and the arrival date in Europe (y-axis). (b) Sensitivity of significant correlations between $\tau_{A,t}$ and $\tau_{E,t}$ to temporal shifts of the departure date using actual positions in Africa (red circles) or 999 local randomized positions (gray squares). Dotted gray lines indicate the 25–75 percentiles.

The most important axis of variation in our temporal sensitivity analysis is the shifting of departure date from Africa, because it is known with less accuracy than time of arrival to

Europe. While holding the time of arrival to Europe constant (time shift on the y−axis=0 in Figure 2.9a), but shifting the departure time from Africa, the number of significant correlations between $\tau_{A,t}$ and $\tau_{E,t}$ in the actual wintering sites markedly outnumbered that obtained from 999 local scale randomizations of positions (Figure 2.9b). Interestingly, the maximum number of significant correlations was achieved exactly for the chosen departure period (i.e. for temporal shift in Africa equal to 0). The result obtained in cluster S was weaker and showed that there might be a slight increase of partial correlations with increasing shifts of the period of departure from Africa (Figure 2.10). However, we stress that arrival dates to Europe are known with lower precision for cluster N than or cluster S, as we used the median arrival date for all those individuals breeding outside the area covered by the study of Ambrosini *et al*. (2014).

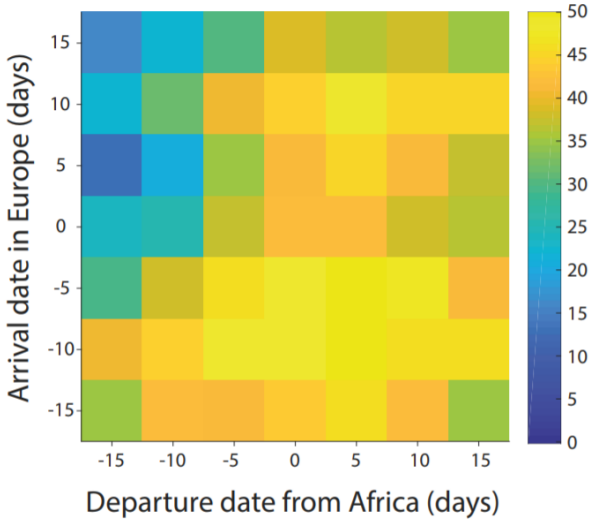

Figure 2.10: Number of significant negative partial correlations for barn swallows in cluster S for different temporal shifts (positive meaning delay) of the departure date from Africa (*x*-axis) and the arrival date in Europe (*y*-axis).

A temporal sensitivity analysis of the obtained results can be performed on a different temporal scale, not related to the uncertainty of the exact timing of spring migration, rather to the persistence of climatic correlations over decades (Figure 2.11). As for the robustness of the reference year (i.e. the last of the 30-year time window used to calculate the partial correlation between $\tau_{A,t}$ and $\tau_{E,t}$), the value of the partial correlation coefficient of the cluster N individuals with a significant partial correlation in their actual reference year remains substantially positive throughout the whole analysis period (Figure 2.11a), in some cases with significant values for many years. Cluster S presents a similar

situation, even though many positive, yet not significant, partial correlations occurred in recent years (Figure 2.11b).

The individual trends of the partial correlation of cluster S are visually highly temporary correlated between them. This is mainly caused by the greater proximity of the wintering areas of these individuals (Figure 2.4b) and the synchronicity of their temperature conditions in Europe, also due to the choice of a unique arrival date for ringing data located east of 26°E (as explained in Par. 2.2.2 at page 12). It is noteworthy that the period of maximum correlation intensity between those areas falls in the years in which the barn swallows have actually been found.

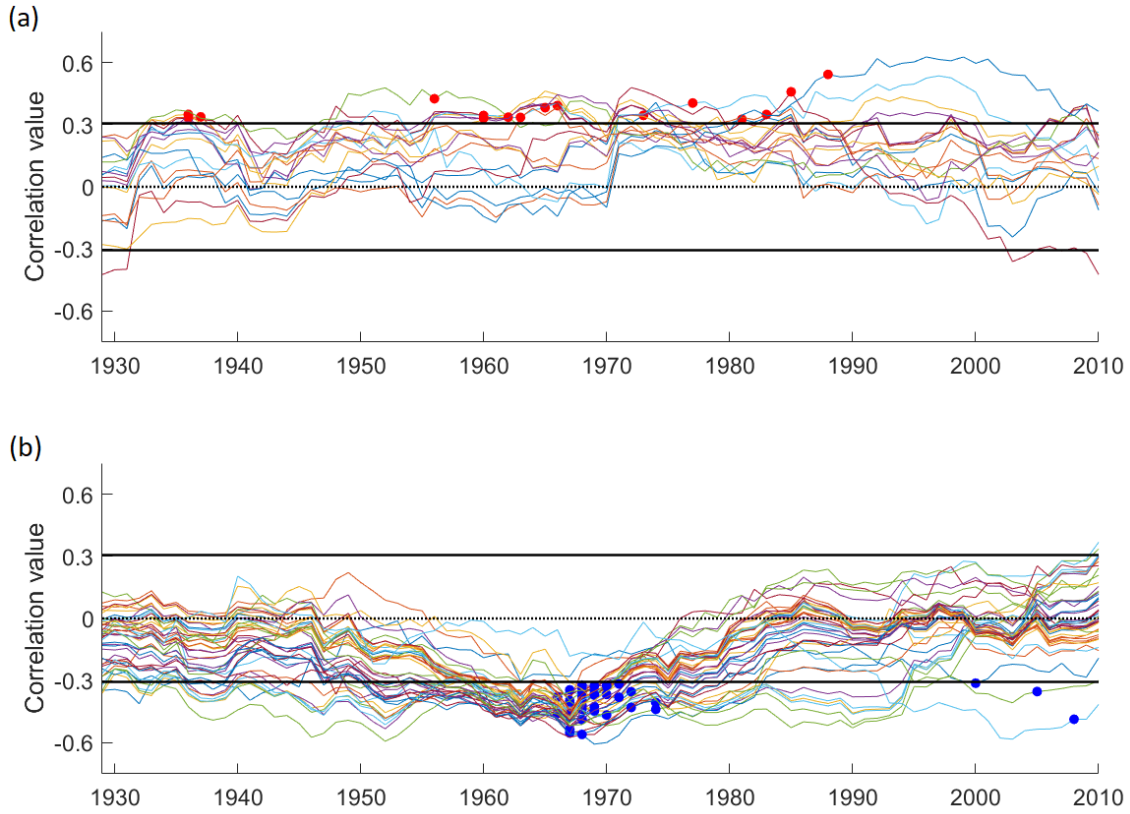

Figure 2.11: (a) Temporal trends of partial correlation coefficient of the significant individuals of cluster N. *x*-axis represent the last year of the 30-years window used to calculate the partial correlations (i.e. reference year). Each line represents the trend for a single individual. Dots show the partial correlation values calculated in their actual reference years. Continuous black lines mark one-tailed significance levels. (b) same as (a) but for cluster S.

Also the individuals characterized in our first analysis by not significant correlations present here a result in line with the barn swallows with a significant one. In particular,

we found a series of moderately positive partial correlations between 1965 and 1990 for the cluster N and a good number of significant negative partial correlations between 1955 and 1980 for the cluster S (Figure 2.12). In recent years there has been a clear shift towards negative partial correlations for cluster N and a balanced situation of low partial correlations for cluster S. From this result, , which might have important implications in terms of ecological success of our migratory species, it is still however difficult to hypothesize a possible influence of climate change on climate connectivity between the wintering and breeding areas of the barn swallows, because of the small number of recent individuals found both in Africa and in Europe compared to those that had been identified fifty years ago (see Figure 2.2b).

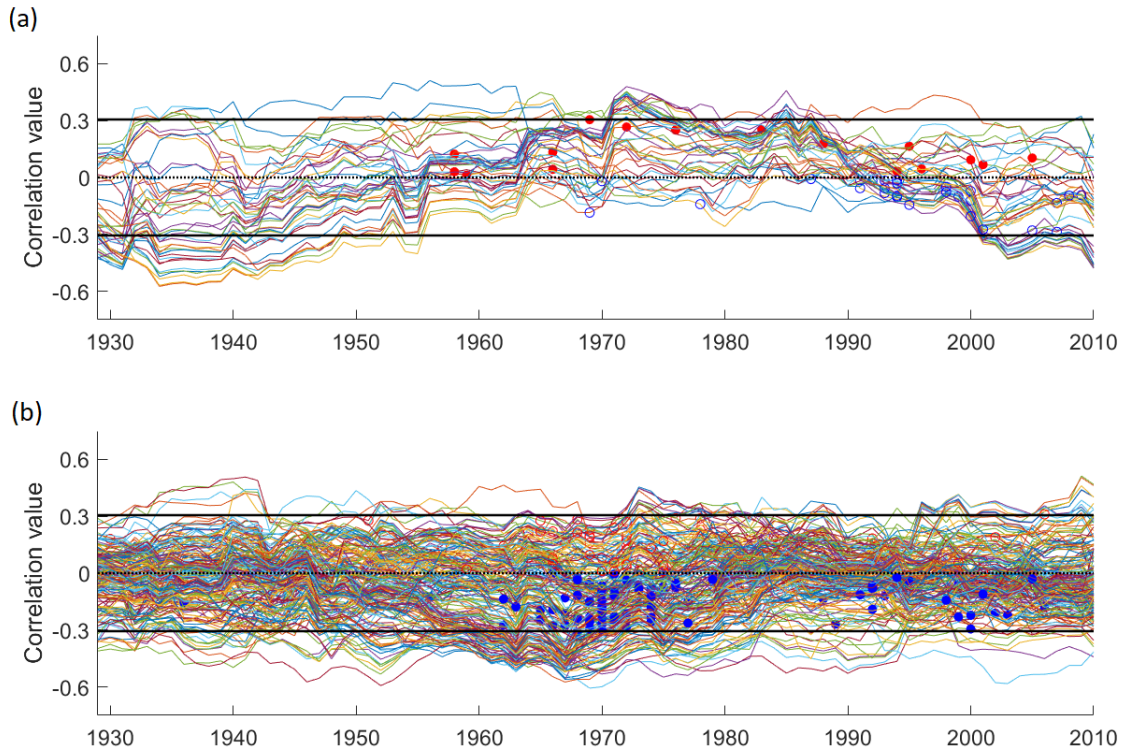

Figure 2.12: Temporal trends of partial correlation coefficient of not significant individuals of (a) cluster N or (b) cluster S. *x*-axis represent the last year of the 30-years window used to calculate the partial correlations (i.e. reference year). Each line represents the trend of correlation value for a single individual. Dots show the partial correlation values calculated in their actual reference years. Continuous black lines mark one-tailed significance levels. (b) same as (a) but for cluster S.

Figure 2.12a shows also a high number of negative partial correlations in the cluster N before 1950. This has to be balanced with the great uncertainty of the ERA-20C outputs in the first half of the 1900s, in particular considering the limited availability of measurements available in Sub-Saharan and Equatorial Africa in that time (Poli *et al.*,

2016). Furthermore, the only data of barn swallow positions that are available in those years show a significant positive partial correlation (Figure 2.11a).

Figure 2.13 summarizes the results shown in the previous parts, showing the number of significant partial correlations combined with the number of individuals sampled at the change of the reference year. In line with previous results, the N cluster is characterized by a strong predominance of positive correlations throughout the second half of the last century (Figure 2.13a). Starting from the year 2000, there is a sign reversal in significant partial correlations. This result is in line with the analysis shown in (Saino and Ambrosini, 2008) that found significant negative partial correlations by investigating at large scale the monthly average temperature ranges related to spring migration between sub-Saharan Africa and Europe.

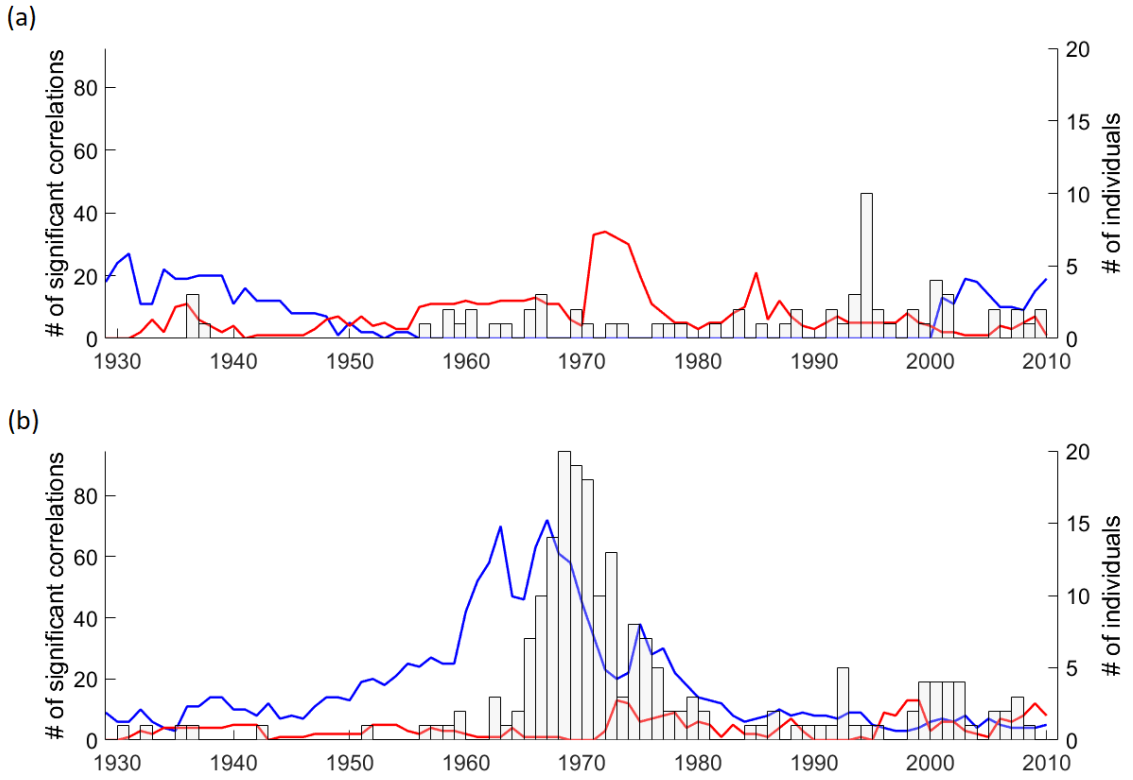

Figure 2.13: Trend of the number of significant positive partial correlations (red line) and negative (blue line) of the cluster N (panel a, 67 individuals) and cluster S (panel b, 203 individuals). x-axis represent the last year of the 30-year-old window used to calculate the partial correlations (i.e. reference year).

However, the number of barn swallows belonging to the N cluster is not sufficient to identify any link between the presence of correlations along the last century and the actual presence of individuals in the analyzed locations. The S cluster instead provides this

possibility: Figure 2.13b shows a co-occurrence, albeit with a shift of a decade, between the high number of significant negative partial correlations in the 60s and 70s and the actual presence of individuals in the sampled areas.

2.4 Conclusions

Understanding the influence of past and current on bird migration is a crucial first step towards the ambitious goal for predicting possible impacts of climate change on these species. The timing of spring migration is a critical point of their phenology: a too early arrival would catapult them into an environment with still unfavorable ecological conditions for breeding, while excessive delays would not allow birds to take advantage of the resource peaks that emerge in this season. Migratory birds regulate first the timing of their journey in their wintering areas, delaying or anticipating the departure. However, the environmental mechanisms that determine this variability are not yet clear.

Using a long-distance migratory species for which considerable information on wintering areas exist, here we speculated that cues may exist that allow individuals to adjust their timing of departure from the wintering site. This requires that correlations exist between the ecological conditions at departure and conditions at destination around the expected time of arrival, several weeks later and thousands of kilometers ahead. The first implication of the present analyses is that for our reference species *Hirundo rustica* correlations do indeed exist, suggesting that migratory barn swallows may actually have some information on the temperatures at destination while they are still on their wintering grounds. The sign of the correlations found geographically divides the individuals analyzed in a similar way to a clustering produced from breeding and wintering positions.

We have also found that the barn swallows wintering locations occur more frequently in areas where the climatic connection with their reproduction areas is greater. The randomization tests of the wintering positions have shown that this result is true both on a local and continental scale. Temperature connections are also robust temporally: the greatest number of significant correlations in the N cluster occurs exactly in the starting and arrival dates reported by other ornithological studies, while the S cluster has a high number of significant correlations even in a wider dates interval. By varying the reference year of the single individuals, we have shown that the highest number of captures and recoveries in the S cluster occurred in the decades characterized by maximum climate

connectivity. The present results on the barn swallow are therefore particularly relevant to the interpretation of the effects of large-scale climatic correlations on the expression and evolution of migration behavior and migratory connectivity of widely distributed species, for which differential climatic connections between parts of the wintering and breeding ranges can occur.

3 ESTIMATE OF BARN SWALLOW MIGRATORY ROUTES FROM LIGHT LEVEL GEOLOCATORS

3.1 Introduction

In a regime where notable environmental changes occur at the global scale, as the one characterizing our recent decades, it becomes particularly important to understand if and how the movement pattern of long-distance dispersing species may be affected. Not surprisingly, then, the tracking of migratory animals is a very active field of biological studies (Wikelski *et al*., 2007; Robinson *et al*., 2010; Tomkiewicz *et al*., 2010; Guilford *et al*., 2011; Cooke *et al*., 2013; Teague O'Mara *et al.*, 2014). Knowing the positions visited and the routes traveled by migratory organisms is in fact a crucial information to design management policies oriented for example toward species conservation (Cooke, 2008; Hays *et al*., 2014) or the protection against disease spread (Gilbert *et al*., 2010). This research field is particularly challenging and very interdisciplinary, because it requires the integration of knowledge coming from biology and environmental science with that coming from the information technology sector of engineering. The continuous development of new hardware devices –which permit to monitor, record and sometimes transmit the position of individuals, over long time and large space extensions – opens

novel research perspectives that must be accompanied by analogously advanced ways of interpreting the newly available data through proper modelling tools and software techniques.

Migratory birds are ideal model taxa for enhancing the current research in the field, since an incredible variety of movement patterns is offered to investigation: every year, billions of individuals belonging to several species make unbelievable journeys, timely occurring in the right seasons, and head for weeks for hundreds or thousands of kilometers, sometimes at inter-continental scales, toward wintering or breeding areas. Some of these movements can be tracked with high-precision systems, such as GPS or other satellite receivers. The necessary equipment can however be too heavy to be carried by individuals of small species (like the barn swallow), for which every single gram of added weight can make a huge difference in terms of success or failure of their migration event and their survival (Barron *et al.*, 2010). However, these species can be tracked through the use of another type of device: light level geolocators.

3.1.1 Light level geolocators

Light-level geolocators (from now geolocators), called also *geologgers*, are currently the smallest devices from which it is possible to obtain data that can be used to estimate the routes made by long distance migratory birds (Bridge *et al*., 2011). Thanks to their small size, they could be carried by the majority of birds, including most of passerines, although with some impact on the survival and reproduction of tagged individuals (Scandolara *et al*., 2014).

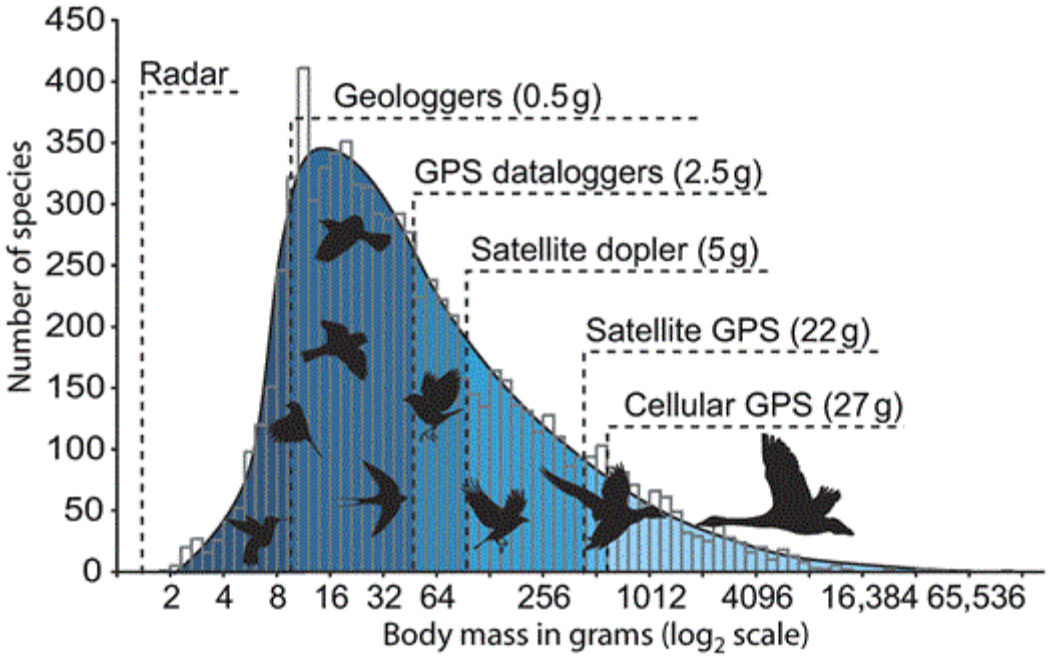

Figure 3.1: Frequency distribution of bird body masses (histogram and blue fitted continuous distribution, in grams) in relation to possible devices that can be carried by them and that use various tracking technologies. Minimum bird sizes for each technology are represented according to the 5%-body-weight rule: a threshold recommended by Barron *et al.* (2010) . Source: Bridge *et al*. (2011).

The simplest models of geolocators consist of a small battery, a detector of solar irradiance and an accurate real-time clock and allow to record the two information at regular time intervals, usually for a period ranging from 6 months to 5 years[2]. Most geolocator models do not transmit data, so they must then be recovered to download the recorded data, which implies that the individual that has been equipped with the instrument must be recaptured. Data must then be analyzed after recapture using appropriate software that can pre-filter them for treatment and estimate the positions of the bird carrying the geolocator based on day length and sunrise/sunset times (as detailed

[2] For more information on the variety of models and characteristics of geolocators, see: www.migratoryconnectivityproject.org/manufacturers

below at Par. 3.2.2). The price of such devices usually does not exceed 100 USD, making economically feasible the study of individual migration at the population level.

Compared to heavier and more expensive tags like GPS, the main disadvantage of geolocators is that it is needed to recapture the individuals on which they are applied, making this technology unsuitable for species characterized by large dispersal. Also, and technically more limiting, their accuracy estimating the position of the individual is several orders of magnitude lower than that provided by satellite tags: on average 50 kilometers in longitude and 200 kilometers in latitude (Phillips *et al*., 2004) versus a few meters or submeters.

A technical complication while studying species that migrate near equinoxes, like in our case, is that it is particularly difficult to estimate the latitude based on the duration of the day, because it is almost the same at each latitude on the planet. Latitude estimation is more difficult also near the equator, where the duration of the day varies very few even with latitudinal shifts of several hundred kilometers (Hill, 1994), and at the polar latitudes during the solstices, due to the lack of twilight events (polar night and midnight sun). A further complication in the estimation process is due to the noise of the light measurement close to twilight events, whose definition must be as accurate as possible (see Par. 3.2.2).

On the other hand, however, many applications for which it is interesting the study of migratory birds do not need high spatial and fine temporal resolution of the surveys. Even today, migratory routes and wintering areas of entire populations or even of some species are still ignored or known only with great approximation (Robinson *et al*., 2010; Bridge *et al*., 2011). The estimated positions that can be reconstructed thanks to geolocators do provide useful information such as the identification of stationary areas and periods of migratory individual (Liechti *et al*., 2015) and the analysis of the general features of migration routes (Briedis *et al*., 2018).

Despite the above mentioned possibly strong limitations, geolocators are currently the only technology able to track the migration of species whose weight is in a range between 10 and 50 grams (e.g. the barn swallow): only major innovations in battery technology, which are the heaviest component of satellite tags (Bridge *et al*., 2011), could lead to geolocator obsolescence.

3.1.2 Geolocator data analysis

The increasing popularity of the use of geolocator for the study of animal migration has led in recent years to the development of different software for the analysis of their measurements, such as `Ukfsst` (Lam *et al.*, 2008), Trip Estimation (Sumner *et al.*, 2009), `Trackit` (Lam *et al.*, 2010), `GeoLight` (Lisovski and Hahn, 2012), `probGLS` (Merkel *et al*., 2016) and `FLightR` (Rakhimberdiev *et al*., 2017). The process of reconstructing animals' paths is usually divided into two phases:

1) the estimation of the bird visited locations (from the light data obtained via the geolocator);
2) the filtering process of such estimates, that could be implemented as post hoc smoother or as a filter in a Bayesian analytical framework.

Phase 1 can be performed using the threshold method (Hill and Braun, 2001) or the template-fit approach (Ekstrom, 2004). The threshold method requires an exact definition of sunrise and sunset times, determined using a constant and predefined light intensity threshold. The estimate of the latitude is then made starting from the duration of the day (or night), while the longitude can be estimated thanks to the timing of solar noon (or midnight). The threshold method is still widely used, but its estimates may be very biased due to two main factors. One is the presence of noise in light levels measurements (because of weather conditions or the specific environmental settings where the bird is temporarily located). The other is that migratory animals can have also large movements between a twilight event and the subsequent one (Lisovski *et al*., 2012). In contrast, the template-fit method is based on an empirically derived relationship between the solar angle above the horizon at a certain latitude and the measurement of light intensity (Ekstrom, 2007), using many light measurements close to twilight events. Repeated measurements are used to decrease the influence of noisy light data as we will show in the next Par. 3.1.3. In contrast, the template-fit method is based on an empirical relationship between the solar angle above the horizon at a certain latitude and the measurement of light intensity, using different light measurements close to twilight events to decrease the influence of shading effects (Ekstrom, 2007). More details about the template-fit method are provided in Par. 3.1.3.

Phase 2 is based on the reconstruction of the path of the individual through a *Hidden Markov Model*, specifically designed according to the ecological migratory behavior of the taxon under study. The migration performed by birds is usually characterized by prolonged sedentary periods (i.e. breeding and wintering), interspersed with long movements with few changes of direction, but with sporadic stationary periods of refueling (Newton, 2007). Between the above mentioned software used to elaborate geolocator derived data, `FLightR` *R* package is currently the only one that implements a specific model for migratory birds, The model uses behavioral functions to describe a bird as belonging to either sedentary or migrating species, and offers the possibility to edit behavioral parameters for the species under study such as, for example, the minimum and maximum distances from the sea within which an individual can fly or have a stationary period.

3.1.3 A glance at `FLightR`

Despite its recent publication, `FlightR` has been already used in a dozen studies dealing with migratory birds route estimates (e.g. Kardynal and Hobson, 2017; Winkler *et al*., 2017; Brlík *et al*., 2018; Kramer *et al*., 2018; Mu *et al*., 2018; Witynski and Bonter, 2018)and we decided to use it also in the present study to analyze quite a large geolocator dataset (described below at Par. 3.2.1). We provide here a moderately detailed description of its functioning (Figure 3.2), as we will discuss some of its functionalities in Par. 3.2.3. For a complete description the interested reader can refer to (Rakhimberdiev *et al*., 2015).

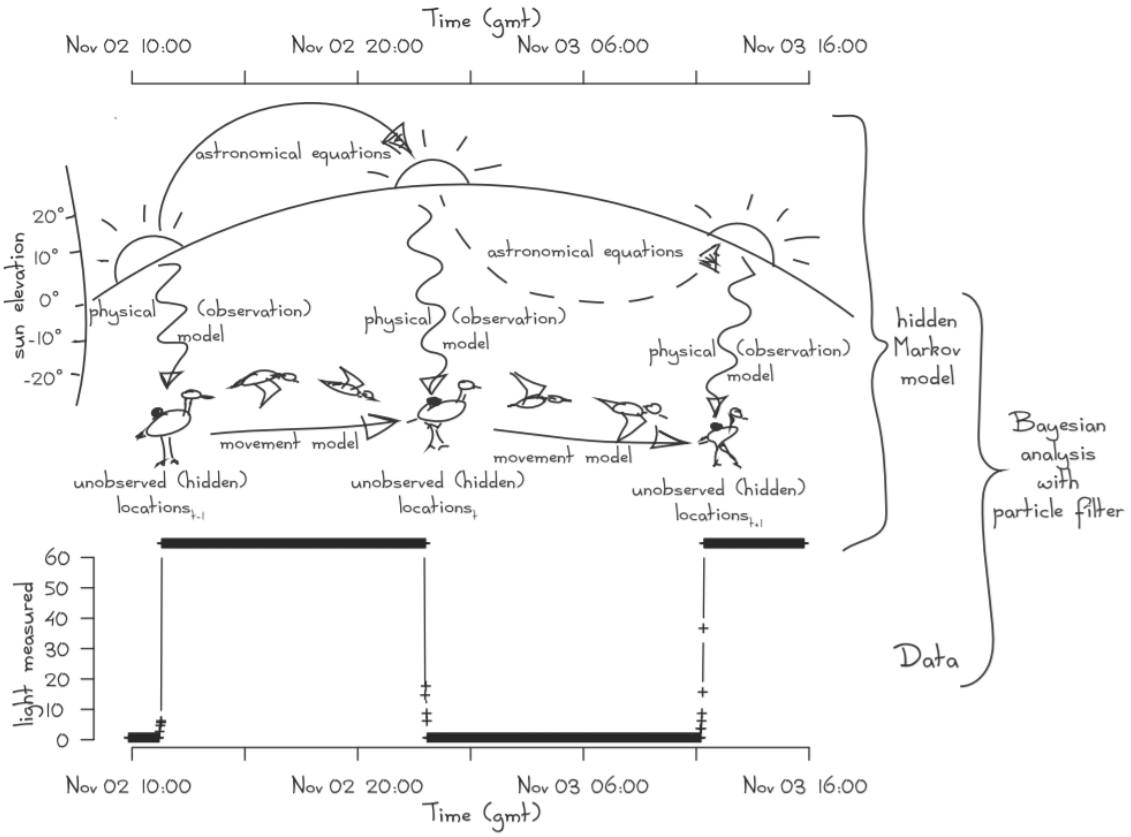

Figure 3.2: Sketch of solar geolocation principles and `FLightR` method of analysis. A solar geolocator (shown in black on bird's back) records light levels and times (example raw data in the lower panel). When the animal moves, its position is unobserved (hidden), but it can be estimated by the pattern of light changes measured at twilight. `FLightR` combine a physical (observation) model about how light levels change with position and time with some basic knowledge of the patterns of movement between twilights (movement model) along with all previous and subsequent positions in a hidden Markov model framework. Then, using the particle filter, `FLightR` arrive at the most likely position and movement for each twilight. Source: Rakhimberdiev *et al*. (2015)

Physical observation model

Starting from an input file (later explained in Par. 3.2.2), `FLightR` recovers for each twilight event i a set of light measurements j. Then the algorithm uses standard astronomical equations (Meeus, 1991) to link the coordinates $\boldsymbol{\alpha}$ of a potential twilight location k at time τ_{ij} to solar angle relative to horizon (θ_{ij}):

$$\theta_{ij} = l(\boldsymbol{\alpha_k}, \tau_{ij}) \quad \textbf{(1)}$$

The physical observation model used by `FLightR` is elaborated from the template-fit method of Ekstrom (2007) and express the relationship between the aforementioned solar angle and the light reaching Earth surface (Surface Light: SL_{ij}):

$$log(SL_{ij}) = f(\theta_{ij}) + K_i + \varepsilon_{ij}; \quad \varepsilon_{ij} \in Norm(0, \sigma_i) \qquad \textbf{(2)}$$

with:

$$f(\theta_{ij}) = -u(\theta)^2 - log\left(erfc(u(\theta))\right); \quad u(\theta) = 21.5 \times sin(\theta) \qquad \textbf{(3)}$$

where $erfc$ is the complementary error function and K_i is the attenuation (or cloudiness) variable of twilight i, that has to be estimated. `FLightR` assumes that the solar light reaching the Earth surface has an exponential relationship with the *expected* light measured by the geolocator (ELM_{ij}):

$$log(ELM_{ij}) = I + S \times log(SL_{ij}) \qquad \textbf{(4)}$$

where tag intercept I and tag slope S are specific for each individual device. In addition, `FLightR` assumes that observed light measured by the geolocator is related to the expected light measured by another exponential relationship:

$$log(OLM_{ij}) = \beta_i + Z_i \times log(ELM_{ij}) + E_{ij}; \;\; E_{ij} \in Norm(\mu_i, \sigma_i) \qquad \textbf{(5)}$$

Parameter β_i is related to the behavior of the bird and the local weather/orography conditions at the twilight i.

The slope Z_i varies both with twilight and with geographical position of the measurements. `FLightR` requires a calibration dataset of the light sensor at a known location in order to separate the Z_i variability in time and space. The calibration algorithm assumes that, at a known location, Z_i has a log-normal distribution with parameters Z_{calib} and σ_{calib}, which are estimated using measurements of a couple of days from the known location. Then, to evaluate likelihood of the tag presence at an unknown location k, using equation 5, `FLightR` estimates local slope $\hat{z}_{ik}$ and its uncertainty $\sigma_{\hat{z}_{ik}}$. Then, the software builds a joint probability of $\hat{z}_{ik}$, $\sigma_{\hat{z}_{ik}}$ and the calibration parameters Z_{calib} and

σ_{calib} and uses this result as the likelihood of occurrence of the bird at location k during the twilight i (see Rakhimberdiev *et al*. 2015 for details).

Movement model

`FLightR` movement model was designed specifically for migratory birds. For the specific behavior of the species at hand, the model is requested to describe movement patterns where the individual is primarily sedentary for long periods (up to 6 months) the bird rapidly migrates between breeding and wintering locations within quite a short time period (usually 1-2 weeks). It should also possibly identify the short stationary periods that may occur during migration, where the birds refuel for a few days before continuing their journey.

The implemented movement model is a simplified 'double' model (Morales *et al*., 2004; McClintock *et al*., 2012) with just two behavioral state: 'Sedentary' and 'Migrating'. In the context of these two states, the simulated bird position is initialized at a defined location $\boldsymbol{\alpha_0}$ and then updated through the following procedure:

$$\boldsymbol{\alpha_{i+1}} = \begin{cases} \boldsymbol{\alpha_i} + \boldsymbol{d_i}, & with\ probability\ p_i \\ \boldsymbol{\alpha_i}, & with\ probability\ 1 - p_i \end{cases} \quad \textbf{(6)}$$

The movement $\boldsymbol{d_i}$ follows an uncorrelated random walk with a distribution based on bird behavior described as:

$$\boldsymbol{d_i} = \begin{bmatrix} S_i \times cos(\Phi_i) \\ S_i \times sin(\Phi_i) \end{bmatrix} \quad \textbf{(7)}$$

Where S_i is the length of the movement step and Φ_i is movement direction. Both these two values are sampled from the following distributions:

$$\Phi_i \sim vonMises(\varphi, \kappa) \quad \textbf{(8)}$$

$$S_i \sim truncNorm(\mu, \sigma, a, b) \quad \textbf{(9)}$$

`FLightR` sets default values for parameters a at 45 km and for parameter b to 1500 km, which respectively represent in this case the minimum and the maximum travelled distances by the simulated bird when its state is 'Migrating' and are kept fixed for the whole simulation process. Parameters φ and k in the von Mises distribution reflect the direction of migration and its concentration, while the parameters of the truncated normal

distribution shape the distribution of inter-twilight flight distances. Figure 3.3 show the Probability Density Function of von Mises and truncated normal. `FLightR` allows to set the values of parameters a, b and k.

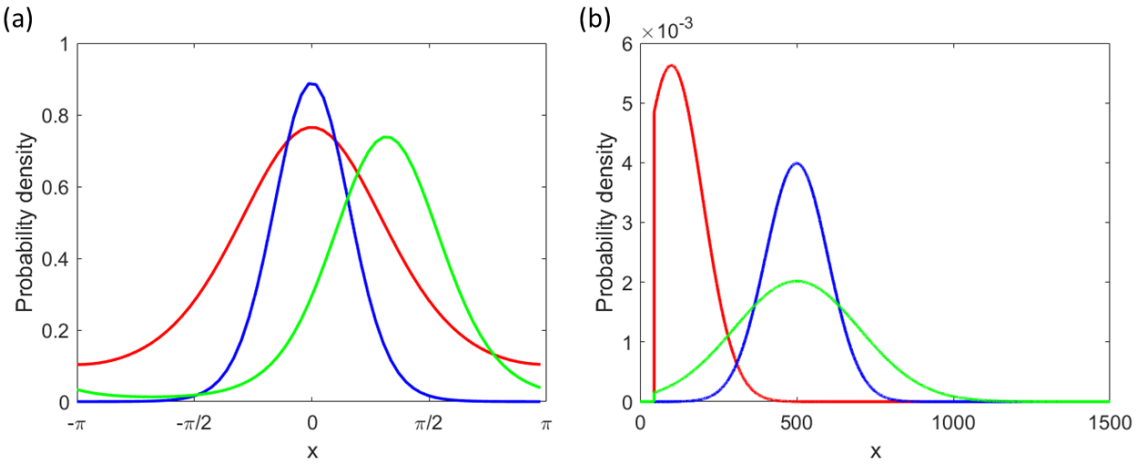

Figure 3.3: (a) Probability Density Function of von Mises distribution with $\varphi = 0$ and $k = 1$ (red), $\varphi = 0$ and $k = 4$ (blue), $\varphi = 2$ and $k = 1$ (green). (b) Probability Density Function of truncated normal distribution with a $= 45$ and $b = 1500$, varying $\mu = 100$ and $\sigma = 100$ (red), $\mu = 500$ and $\sigma = 100$ (blue), $\mu = 500$ and $\sigma = 200$ (green).

This movement model could be run with or without a behavioral mask which defines the maximum and the minimum distances at which the bird could stay or flight on seas and oceans. Hence, birds may fly over water, but cannot switch to sedentary state in this habitat.

Bayesian estimation with particle filter

The uncorrelated random walk designed in the movement model has five unobserved variables at each time step. Due to the presence of non-Gaussian noise, `FLightR` uses a particle filter (Reini, 1996) to compute their posterior distribution, simulating movement model on discretized positions on a 50 km node distance grid within the defined geographical range. The algorithm adopted by `FLightR` is based on the one proposed by Doucet *et al.* (2000) as expanded by Andersen *et al*. (2007).

At the initialization phase, the algorithm creates a high number (`FLightR` default setting: 1 million) of particles (i.e. georeferenced points) at the actual release location. Then the position of each particle is updated through the movement model, computing the particle-specific likelihood value associated to the twilight event retrieved from the physical observation model (i.e. properly filtered data). At each temporal step, all

particles are assigned with a weight that is computed as the product between all previous likelihoods and the current likelihood. Then they are resampled proportionally to the weights, to remove particles that are in unlikely positions according to the light measurements by replacing them with more copies of the most likely ones. This procedure is repeated over the subsequent steps. Behavioral mask (if defined) is applied in the weight computation phase, setting to zero the likelihood of a particle that violates one of its assumptions.

To avoid degeneracy problem, which often occurs in long particle filter runs (Van Der Merwe *et al.*, 2001), `FLightR` applies a method called *block sampling* (Doucet *et al.*, 2006), which uses as weight for particles resampling the product of the particle likelihood at the actual position and at the n (default: 90) previous steps. Following the approach used by Andersen *et al*. (2007), `FLightR` allows to include in the simulation the information on the recapture location (i.e. the last available twilight position): the last n states of the particles are resampled with weights proportional to a normally distributed probability density function with mean position placed at the recapture point coordinates and standard deviation (SD) to be given as a measure of precision (`FLightR` default is 25 km).

At the end of its run, the particle filter provides a way to get a numerical estimate of the central tendency and of the associated uncertainty of the route travelled by the bird without making any assumption on the data distribution ('non-parametric' estimate). This could be done through the calculation of appropriate statistics (e.g. mean, mode, standard deviation and percentiles) on the state of the particles at each time step.

One of the major drawbacks about trajectories reconstructed by `FLightR` is in that the particle filter cannot properly deal with outliers (Arulampalam *et al*., 2007). This effect results to be particularly evident in all cases where `FLightR` estimates are based on noisy and 'shadowed' twilight events occur, i.e. data characterized by big differences in sunrise/sunset hours with respect to those of the nearby days and/or data whose light curve following/preceding the twilight event has a shape that is qualitatively different from those commonly measured during undisturbed events (Figure 3.4).

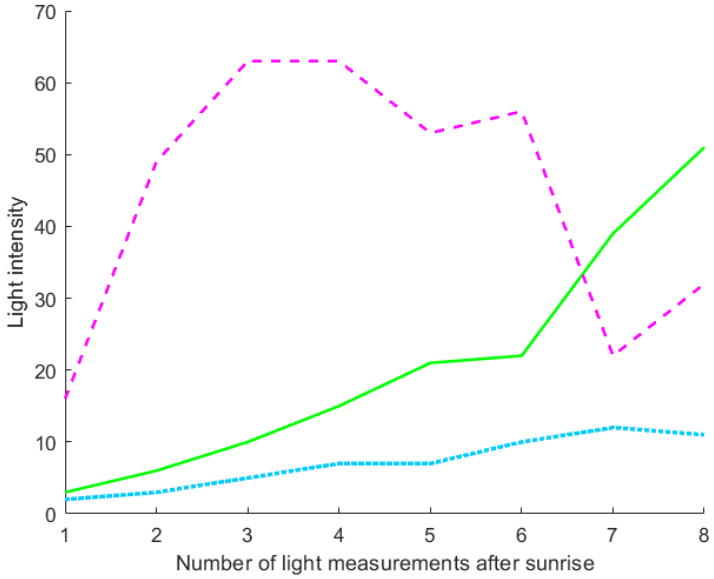

Figure 3.4: An example of a light curve at a natural clear sunrise (solid, green), at a shadowed sunrise (dotted, light blue) and at a fast sunrise (dashed, pink). This last pattern is typically registered when the bird exits a cavity after the actual sunrise.

Although `FLightR` has a feature to analyze and remove possible outliers in the estimated positions, the authors of the software recommend operating a careful selection of twilight events before proceeding with the whole procedure. This pre-filtering phase of the analysis is carried out manually, relying on specific *R* packages, such as `TwGeos` (Wotherspoon *et al.*, 2016), for an help in data display and visualization; details are shown in Par. 3.2.2.

3.1.4 Focus of the present analysis

Using the procedure outlined above, in this work we reconstructed the migratory routes of 88 individual barn swallows, belonging to three different breeding areas in Southern Switzerland and Northern Italy, equipped with miniaturized light-level geolocators during two consecutive annual cycles (2010-2011 and 2011-2012). These data have already been partly analyzed and results of such analyses were published in Scandolara *et al*. (2014) and Liechti *et al*. (2015). However, those papers dealt only with estimates of the timing of migration and of wintering staging grounds, because no attempt were made to reconstruct the routes followed by each individual.

The identification of routes followed by individuals, other than very interesting *per se*, is also preliminary to study whether migration paths vary according to some biological

features of animals (such as for instance their sex or age) and/or are subject to inter-annual variation, as it may be the case if the routes are strongly affected by contingent condition (such as for instance, weather).

As already shown in Par. 3.1.3, `FLightR` provides an estimate of the migratory routes performed by individuals through a particle filter. Also, as mentioned earlier, barn swallow migration occurs close to the equinoxes, when latitude can be estimated only with very wide approximation based on light variation curves. In such dates, then, the estimated latitude tends to be strongly dependent on movement priors, with the risk of making the particle path in those days quite similar to a random walk. In this case, the mean position of particles could no longer provide a reliable estimate of the bird location, being strongly dependent on the particular random extraction performed by the algorithm for the specific twilight event.

Given these premises on the possible strong role played by uncertain priors, before using migration routes reconstructed with `FLightR` for any ecological inference, we need as a first step of our analysis to verify the reliability of `FLightR` estimates. We therefore performed a repeatability analysis on a sample of 20 individuals, running the algorithm ten times on the pre-filtered geolocator data of each individual and comparing the results of the different runs in terms of *i*) variation between each position estimate, and *ii*) differences between the overall traveled routes. For this analysis, we used the mean position of particles at each time step of `FLightR` as an indicator of the estimated position of an individual at a given time.

After having verified the reliability of the procedure for reconstructing migration routes, we then proceed with routes reconstruction. Thanks to the large number of data available, it was then possible for us to perform some regression analyzes by comparing seasonal differences in migration routes of individuals (i.e. spring vs autumn paths) from different breeding areas and according sex and year of migration.

3.2 Materials and methods

3.2.1 Geolocators deployment

Geolocators were applied to and recovered from three different barn swallows populations: one in southern Switzerland (Magadino, hereafter N area; coordinates of the approximate center and approximate elevation: 46°09′N, 8°55′E, 211 m a.s.l.) and two in northern Italy (Piedmont, hereafter SW area, 45°33′N, 8°44′E, 160 m a.s.l.; Lombardy, hereafter SE area, 45°19′N, 9°40′E, 60 m a.s.l.; Figure 3.5), during a time span of three years (2010-2012). Full details on breeding areas, field procedure, and the number and type of geolocators deployed are reported in Scandolara *et al*. (2014) and Liechti *et al*. (2015).

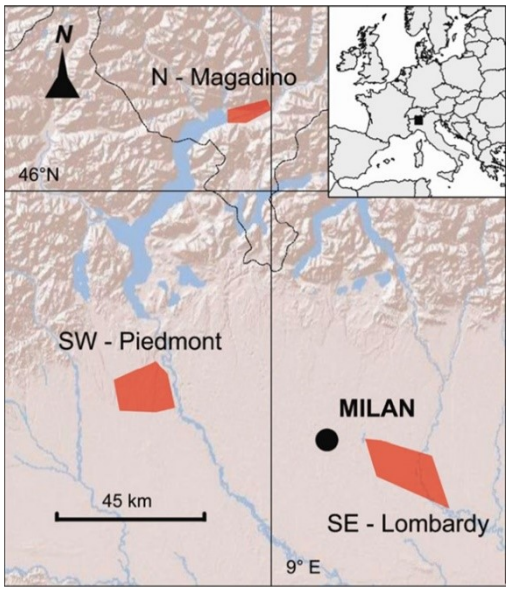

Figure 3.5: Geographical position of the three study areas (shaded polygons) (N – Magadino, Switzerland; SW – Piedmont, Italy; SE – Lombardy, Italy). Inset: position of the three barn swallows populations (in black) within Europe. Source: Liechti *et al.* (2015).

In addition to what was reported in those studies, 33 further geolocators in the SE study area were deployed in 2012. However, only four of them reported full migration routes, which were reconstructed here using `FLightR`, but excluded from subsequent analyses because of the very low sample size for that study year. The present analyses are therefore based on information on a sample of individuals that slightly differ from that used in Liechti *et al.* (2015).

The geolocator models applied were SOI-GDL2.10[3] (for 2010 individuals) and SOI-GDL2.11 (for 2011 individuals), which measure the light intensity every minute, recording its average value every five minutes. Light values may take integer values from 0 (full dark) to 64 (maximum detectable light intensity).

The total number of geolocators analyzed is 88, 22 of which (equal to 25% of the total) did not record light data for the entire non-breeding season. The data recorded, however, were sufficient to reconstruct all the fall migration tracks and to individualize the wintering positions. Table 3.1 shows sample size for each year and by population of origin.

Population of origin	**2010 migration**	**2011 migration**	**Total**
SW	22 (15)	9 (9)	31 (24)
SE	3 (3)	13 (11)	16 (14)
N	31 (19)	10 (9)	41 (28)
Total	56 (37)	32 (29)	88 (66)

Table 3.1: Number of geolocators recovered by year of migration and by population of origin. In brackets is the number of geolocators with a complete set of light measurements for the full (spring + autumn) migration.

3.2.2 Geolocator pre-processing

As seen in Par. 3.1.3, `FLightR` uses light curves at twilight events to provide an estimate of the geographical location of the individual at that time. It is therefore necessary to

[3] Geolocators were provided by the Swiss Ornithological Institute: www.vogelwarte.ch/indirect-trackinggeolocator.html

identify sunrise and sunset times from the raw light data recorded by the geolocator in each day. As anticipated above, some of the light measurements provided by geolocators may be affected by shading due to meteorological or environmental conditions (e.g. due topography, vegetation or buildings) that the bird has experienced (Lisovski *et al*., 2012). This phenomenon can affect both the information used by `FLightR` to compute the likelihood of the particles position at each twilight event.

The light curve of a shadowed geolocator shows a shorter daylight than that of a geolocator under optimal light conditions, which strongly affects the identification of sunrise and sunset times. In addition, brightness values measured nearby shadowed twilights show a different pattern compared to non-obscured twilights (Figure 3.4). If `FLightR` is run on light curves that include shadow events during twilights, it would provide highly biased positions estimates, and therefore completely distorted routes (see the example shown in Figure 3.6).

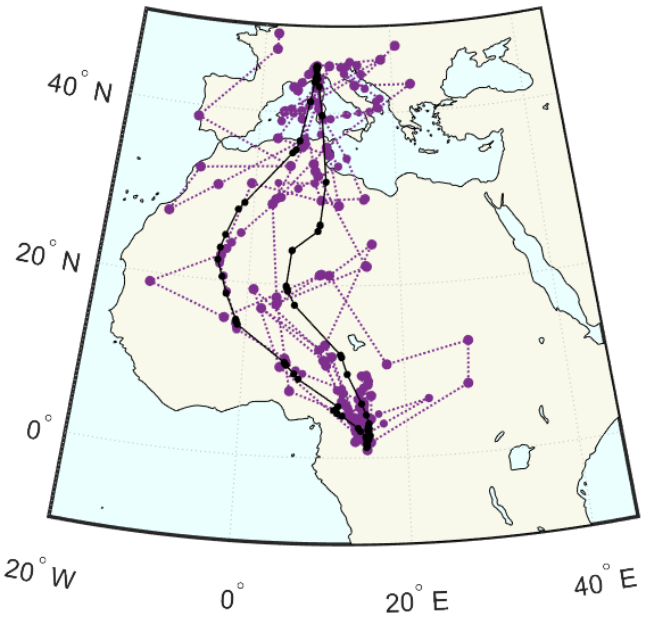

Figure 3.6: `FLightR` route estimate from uninterpreted geolocator measurement (purple, raw data for the barn swallow ID: 5PD, belonging to the SE population) compared with the same route estimated after the twilight selection process (black). Dots indicate particles mean positions at each twilight.

We made the identification of non-obscured twilight events and the consequent selection assisted by `TwGeos` (Wotherspoon *et al.*, 2016) *R* package. `TwGeos` operates in four steps.

For each individual, we selected the period of the year in which the geolocator was actually carried by the bird (see Figure 3.7), eliminating the eventual light values registered before and after that interval (geolocators cannot be turned on or off, but are active from when the battery is installed to when it is removed).

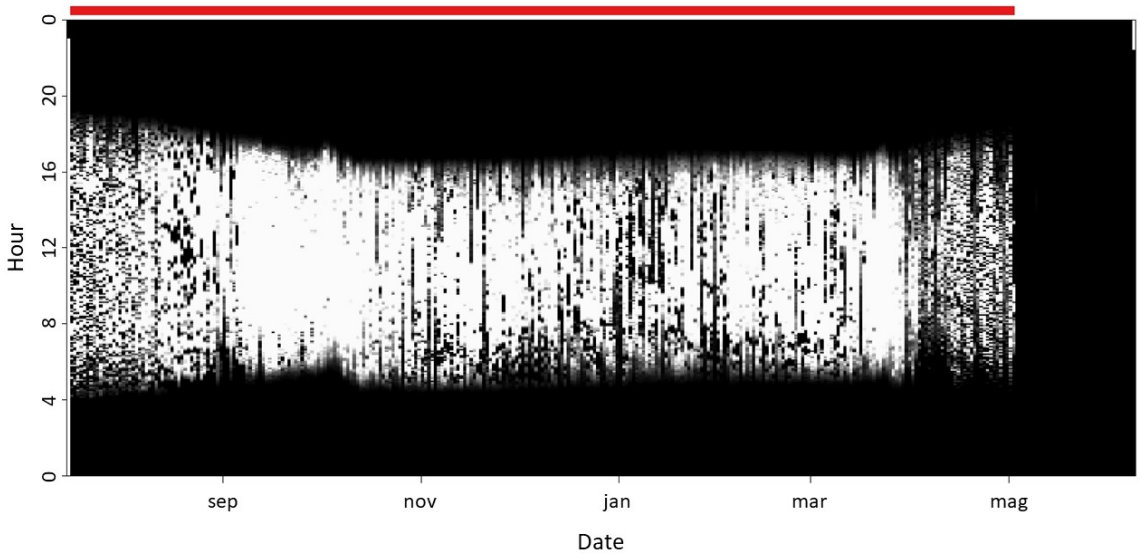

Figure 3.7: `TwGeos` step 1: selection of the correct time span of geolocator measurements. Light measurements are shown on a gray scale (white: maximum measurable luminosity, black: no light detected). Red bar shows the selected interval for the subsequent steps. The red bar indicates the interval selected on the geolocator data. Full dark values after the beginning of May correspond to a period when the geolocator was still activated, but put in a box after its recollection from the bird.

By clicking on any night point of the graph, `TwGeos` automatically identifies the sunrise and sunset events corresponding to that day (Figure 3.8), associating to each of them the (linearly interpolated) time in which the light curve crosses a set threshold before or after a night (automatically identified by `TwGeos`).

We set this threshold to the minimum value of light detection (1 on 64).

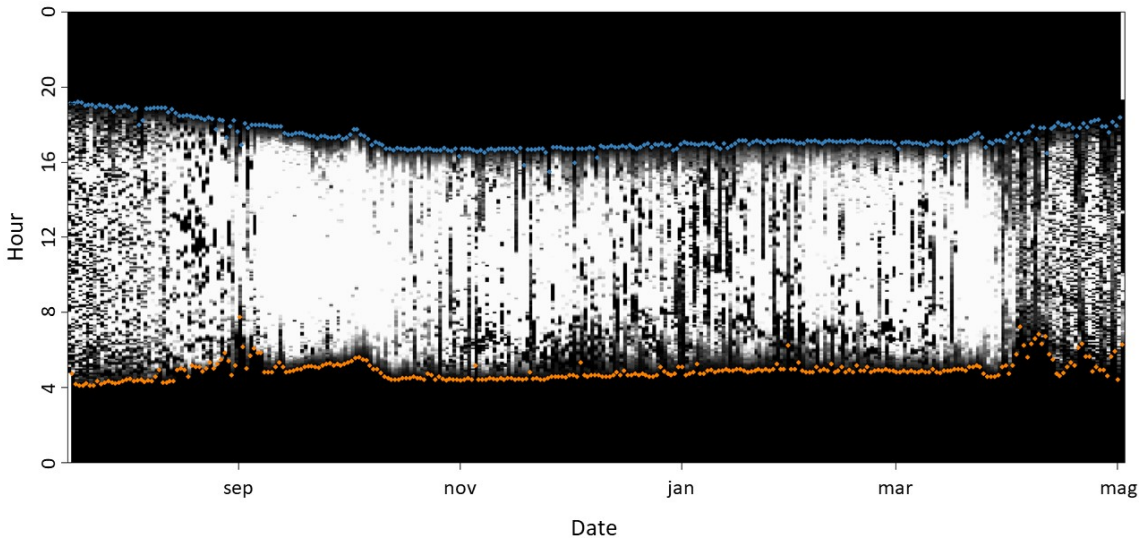

Figure 3.8: `TwGeos` step 2: identification of twilight events. Orange and blue dots represent suggested sunrises and sunsets respectively.

In the phase 3, it is possible to manually enter sunrise and sunset events not automatically identified in the previous phase 2. This operation is necessary when there are long series of missing data in the luminosity measurements (e.g. the geolocator no longer records any light value for at least a whole day), because `TwGeos` fails to detected the twilight events before or after prolonged periods of failure of the geolocator light sensor.

Finally, in the phase 4 `TwGeos` provides the possibility to review one by one all the identified twilight events, in order to manually eliminate the shadowed ones. As previously written in this paragraph, this step is crucial for the successful recostruction of migration routes with `FLightR`. Luckly, `TwGeos` is programmed to facilitate and speed up this task as much as possible, showing to the user, in addition to the variation of the inter-twilights light measurements (i.e. the light patterns in between different days, see Figure 3.9a), the trend of the intra-twilight light curve (i.e. the light patterns within a specific day in between sunrise and sunset, see Figure 3.9b), and the possibility of contrasting the latter to those of the previous and the following days. In phase 4, many of the twilight events that occurred before migration departure (or after migration return) are usually deleted, as light patterns close to these events are very disturbed by bird movements inside and outside areas surrounding nesting places. Indeed, barn swallows are strictly synanthropic during the breeding season, and nest almost exclusively in buildings, particularly barns and cattle sheds, which can clearly “shadow” light curves (Turner, 2006).

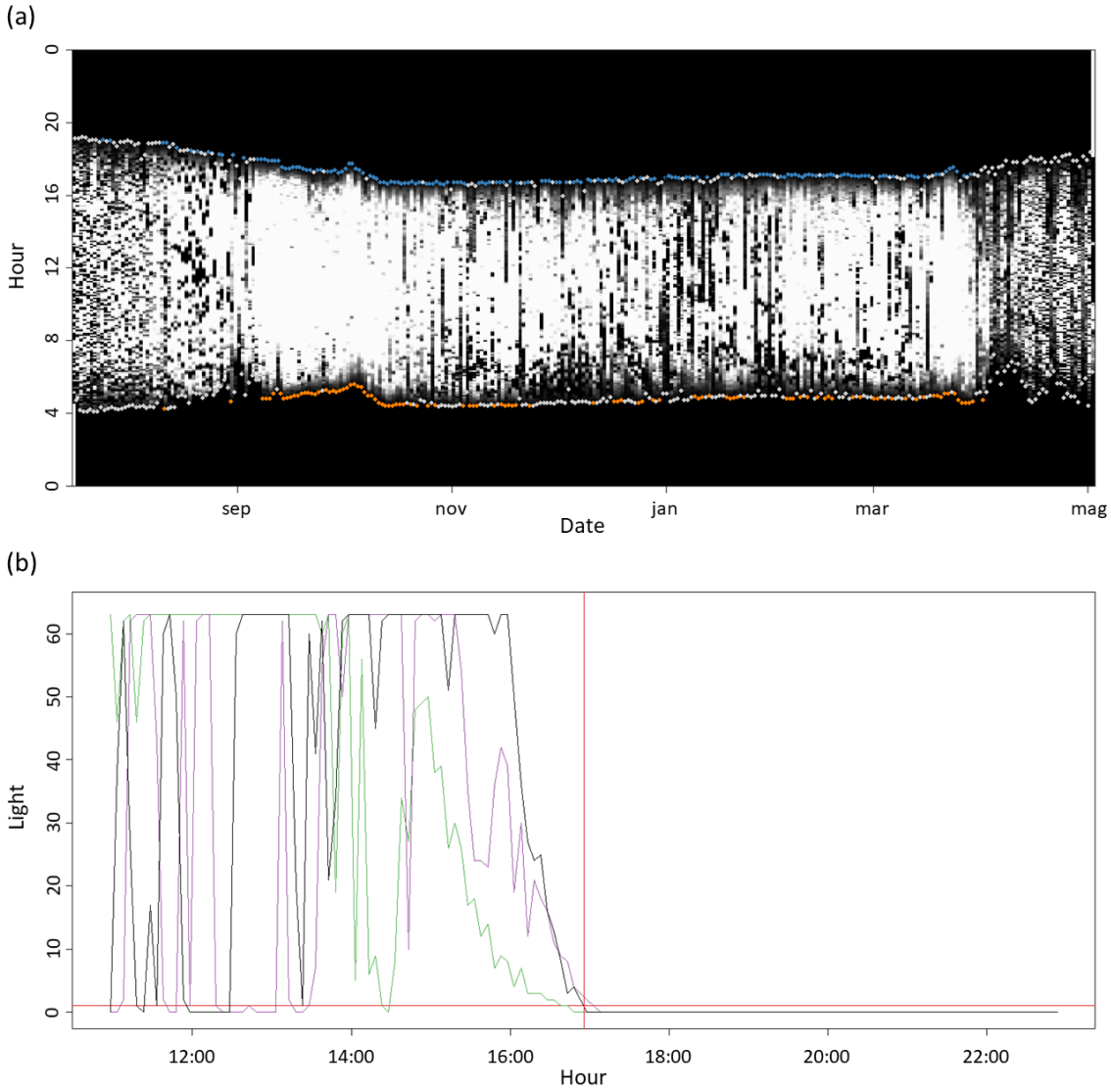

Figure 3.9: `TwGeos` step 4. (a) inter-twilight light and hour variation of one individual of the SE population (geolocator ID: 5PC). Gray dots represent twilight events that have been discarded after manual processing by an expert; (b) intra-twilight light variation for 31 December 2012 sunset (black line), the day before (green line) and the day after (purple line). Twilight selection was made by the expert by evaluating the light curve near to (~ 40 min) the twilight event (vertical red line). This sunset was kept by the expert since it has a pretty smooth decrease in light intensity through time within the day, while the previous one (green line) is obscured (with a sudden decrease followed by a revamping) and was removed. The purple sunset is a borderline case (we kept it in our selection).

For each geolocator, we therefore created a TAGS file (the standard input format for `FlightR`, containing the light measurements and the classified twilights events) applying the *twGeos2TAGS* function to the file of classified sunsets and the corresponding light measurements of the device.

3.2.3 `FLightR` data analysis

Each TAGS file was loaded by `FLightR` using the *get.tags.data* function and for each individual the installation and removal dates of the geolocator were assigned as starting and ending simulation days. Tag-specific information about the sensitivity of the light-sensor, requested by `FLightR` were set using the *log.light.borders* function to values of [1.2; 4] and *log.irradiance.borders* to [-2; 2]. Each input was then processed through the following procedure.

Calibration

Since `FLightR` estimates positions on the bases of luminosity values, it is important to provide it with calibration data, i.e. reference ground-truth values for mapping measured light intensity into geolocator registered scores (from 1 to 64). Each geolocator applied in 2011 was provided with its own calibration data. These measurements were obtained by leaving each device to the side of a building near the Swiss Ornithological Institute in Sempach (CH), at the coordinates (47.128203° N; 8.19224° E) for at least three days between June 2011 and July 2011. Such data were used to calibrate the geolocators with the *make.calibration* `FLightR` function. In particular, the variance of the Observed Light Measurements log-slope σ_{calib} (see Par. 3.1.3 at page 40) was set to 0.3, a value larger than that observed during calibration, but more representative of the conditions experienced by the instrument during the migratory routes. In fact, the measurements taken during the calibration period were very clean as the instrument was in a position with almost no shadowing.

Calibration data were instead not available for geolocators used in 2010, but it has been demonstrated that the data measured by SOI 2.10 and SOI 2.11 geolocator models (used for this research) are consistent between instruments (Meier *et al.*, 2018). Therefore, for all 2010 devices we therefore used the calibration data of another geolocator applied in 2011 to one individual of the N population (ID: 3MY).

Likelihood estimation and particle filter run

Using the *make.grid* function, we set the boundaries of the spatial extent of the `FLightR` simulation to [-20° E; 40° E] in longitude and to [-35° N; 55° N] in latitude. This spatial range includes all historical records of barn swallows breeding in Italy and Switzerland

(Ambrosini *et al.*, 2009). Since barn swallow stationary periods cannot occur in open water, we imposed a behavioral mask with a maximum allowed distance of 50 km from the coast during stationary periods and of 300 km for migration periods. This latter setting allowed including almost all the Mediterranean basin in the analysis, which is reasonable as the barn swallows, like several passerines, migrate on a wide front across this sea (Ambrosini *et al.*, 2014).

We then estimated the likelihood of grid positions at each twilight event by providing the function *make.prerun.object* with the light data processed by `TwGeos`, the results of the calibration procedure, the specifications of the spatial extent and the location of application and removal of the geolocator from the individual.

Finally, we launched simulations of the particle filter, using one million particles per geolocator (per simulation run) and allowing the use of the information on recapture location (*know.last* = TRUE, *precision.sd* = 25).

Estimated routes check

We then obtained an estimate of the migratory routes performed by the 88 analyzed individuals, expressed as a set of statistics (e.g. mean, median, mode, 1st and 3rd quartiles) of the positions of the particles at each not discarded twilight event. To visually inspected each single route, we plot its mean positions at each twilight event on a geographical map, identifying possible outliers (e.g. positions that deviate significantly from the direction followed by the individual during migration up to that moment and in the following). We then double-checked light curves of twilights events associated to possible outliers, and, if we found that they could be shadowed twilights that were undetected during the preliminary checks, we further inspected and deleted them.

3.2.4 Repeatability analysis

To assess repeatability of different sessions of `FLightR` on the same classified twilight data, we ran 10 times the particle filter procedure of 20 different TAGS files and their correspondent posterior probability distributions, obtaining 10 repetitions of 20 individual migratory routes. To get an estimate of variation of mean positions among `FLightR` runs, we computed the standard deviation (both for latitude and longitude) between the

particles mean position at every single twilight event of the 20 repeated analyses of the same geolocator. The mean value of such standard deviations calculated among all individuals can be considered as a measure of *inter-repetition variability* in position and therefore as a measure of repeatability of positions estimates by `FLightR` (Figure 3.10a). It is interesting to compare such inter-individual variation with another quantity that we refer to as *inter-particles variability* and defined as follows. First, we computed for each run the time series of standard deviations of particles positions at each twilight. Second, we averaged such quantities between runs of the same geolocator and, third, between geolocators (see Figure 3.10b). Note that all the runs from the same geolocator have identical twilight series (because they were runs on the same light data with the same set of discarded or non-discarded twilights), while runs on different geolocators do not, because *i)* departures from wintering areas and arrivals to breeding colonies are not synchronous between individuals and *ii*) the twilights removal due to shadowing occurs erratically for each geolocator.

We also checked the consistency of the whole routes estimated by different `FLightR` runs by calculating an appropriate overall distance among them (see below). We computed the distance both between the ten repeated runs of `FLightR` from the same geolocator (intra-geolocator) and routes from different individuals (inter-geolocator). We then used a Mantel test (Sokal and Rohlf, 1995) to assess whether the distances between paths repeatedly reconstructed by `FlightR` for the same individual were significantly shorter than those between routes reconstructed for different individuals. The Mantel test is a statistical test of correlation between two matrices, commonly used in ecological research to test the relationship between a distance matrix (in our case reporting the geographical distances between estimated paths) and another distance matrix or an explanatory variable (in our case a binary variable indicating whether the two paths were estimated from the same geolocator or not). The significance of the correlation between the two matrices is then assessed with a randomization procedure whereby some rows and column of the two matrices are randomly shuffled and the Pearson correlation coefficient is calculated after each permutation. The significance of the test is the proportion of such permutations that have a lower correlation coefficient than the one computed for the actual (observed) matrices.

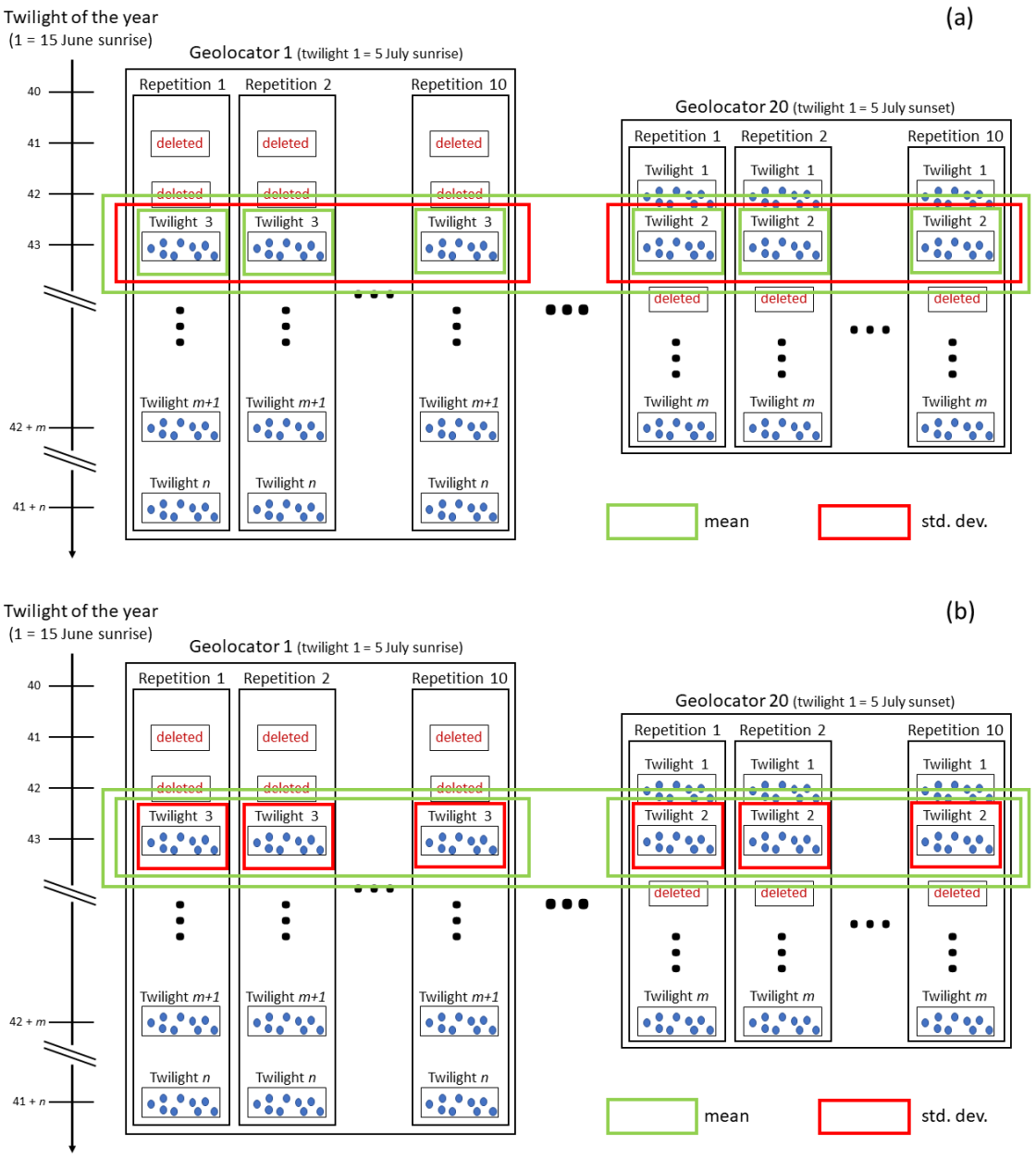

Figure 3.10: Schematic representation of the procedure used to create the time series from the 10 runs of `FLightR` on 20 different geolocators. The results of each run are represented as vectors along the time (vertical) dimension defined by twilight day-of-the-year. Each non-deleted twilight event is represented by its abstract set of particle positions. a) Intra-geolocator variation: for each twilight of each run, we calculated the mean position of the particles, then we computed the standard deviation within the 10 runs of each geolocator and then averaged the results within different geolocators (all those for which data were available for that twilight). b) Intra-run variation: for each twilight of each run we computed standard deviation between particle positions, then we averaged the results between runs and geolocators. Deleted twilights are treated as missing values while averaging between different geolocators. Twilights included in less than four geolocators were discarded.

Select a proper distance metric for comparing two spatiotemporal paths, such as migratory routes, is far from being easy. For the sake of simplicity, we decided to compare only the spatial dimension of the migration routes (i.e. the 'paths', as indicated in Ranacher and Tzavella, 2014) or the 'trajectories'if we use the jargon of automation theory), ignoring the temporal dynamics of the migration process. This means that if two hypothetical individuals followed the same two routes, but traveled in different periods or at different speeds, we considered the two routes as identical. This is tenable since the focus of our current analysis is the reliability of the path reconstruction by `FLightR`, without making inference on barn swallow migration ecology, which can be investigated only after having assessed the reliability of the procedure followed to reconstruct migration routes.

Selecting a metric to evaluate path distance measure was not a trivial task either. After, having explored many possibilities (see e.g. the recent review by Ranacher and Tzavella, 2014) we adapted to geographical distances the One-Way-Distance (OWD) metric by Lin and Su (2005). In details, we computed OWD between route π_A and route π_B as follows:

- we divided both routes in downward ($\pi_{A,down}$, $\pi_{B,down}$) and upward ($\pi_{A,up}$, $\pi_{B,up}$) parts, using as separation point for each of the two its minimum mean latitude reached by particles as rconstructed by `FlightR`. This corresponded to the wintering grounds in the large majority of the cases;
- we then calculated the distance between the two routes in the downard direction ($d_{AB,down}$) as the sum of great circle distances between all mean positions of $\pi_{A,down}$ and their "corresponding" positions in $\pi_{B,down}$, dividing the result by the total length of $\pi_{A,down}$. Corresponding positions are those locations in both paths that are closest in a geographical sense (i.e. have minimum great circle distance);
- we the calculated $d_{BA,down}$ using the same procedure as in the previous point, but swapping $\pi_{A,down}$ and $\pi_{B,down}$;
- we computed OWD_{down} as $d_{AB,down} + d_{BA,down}$;
- we computed $\mathrm{OWD_{up}}$ with the same procedure, but using $\pi_{A,up}$ and $\pi_{B,up}$;
- we finally obtained the One-Way-Distance as $OWD_{down} + OWD_{up}$.

3.2.5 Routes analysis

Using `FLightR` estimated mean positions for each geolocator, we analyzed the migratory routes at a large scale, comparing seasonal differences in migration routes within individuals as well their variation between breeding areas, years and sex classes.

We selected a set of variables for describing the entire migratory process of the barn swallows (Table 3.2).

Variable name	**Description**	**Source**
Sex	Sex of the barn swallow (male or female)	Liechti *et al.* 2015
Year	Year of the fall migration (2010 or 2011)	Liechti *et al.* 2015
Pop	Breeding population of the barn swallow (N, SW or SE)	Liechti *et al.* 2015
DepBC	Departure date (day-of-the-year) from breeding colony, visually determined by inspecting individual light curves	Liechti *et al.* 2015
DevLon*	Position index of the route, expressed as the longitude of the location which had the maximum deviation from 9°E, a meridian that is approximately the average longitude of the three breeding origin areas	Present study
Det*	Computed as $\frac{M-G}{G}$, where M is the actual length of the migration path of the individual and G is the great circle distance between the breeding colony and wintering site	Present study
Stat*	Total duration of stationary periods during the migration path	Liechti *et al.* 2015
Speed*	Migration speed, derived as total length of migration path divided by total duration of migration. The latter is computed as the time difference between departure and arrival to which it is further subtracted the total duration of stationary periods that occurred during the route	Liechti *et al.* 2015 + present study

LatWG	Latitude of the wintering ground	Present study
LonWG	Longitude of the wintering ground	Present study
ArrWG	Arrival to the wintering ground, selected as the first date when `FLightR` mean position was within a distance (chosen to be 50 km, see main text) from the mode of the wintering position estimated by `FLightR`	Present study
ArrBC	Arrival date to the breeding colony, visually identified by inspecting individual light curves	Liechti *et al.* 2015

Table 3.2: Variables used in the analysis of the migration of the barn swallows described in Par. 3.2.1. The asterisk next to the name of a variable indicates that the variable has been calculated both for fall (F) and spring (S) migration.

Although it is possible to derive from `FLightR` an estimation of the time intervals of stationary periods (through which it is also possible to identify arrival and departure dates from the wintering ground), we preferred here to retrieve this information using the method applied in Liechti *et al.* (2015), in which they were obtained by direct observation of intra-day light variations and the rate of change in sunrise and sunset times. We retrieved wintering locations from their median positions estimated by `FLightR` with the function *stationary.migration.summary*: these results were very similar to those estimated by the method of Liechti *et al.* (2015) (based on `GeoLight` *R* package) (Pearson correlation coefficient: r_{lat}=0.975, r_{lon}=0.989; average ± standard deviation of differences: lat=1.77±1.75, lon=0.30±0.71). However, it was not possible to get precise dates of arrival and departure for wintering periods, as the *stationary.migration.summary* function is significantly influenced by the choice made during twilight events selection. Liechti *et al.* (2015) estimated the date of the first stationary period south of the Sahara, but not the date of arrival at the wintering location. We obtained such information here using the date of the first twilight event whose average position was within a threshold of 50 km from the position of the wintering ground. Unfortunately, the (average particles) positions of four individuals were never within 50 km of their respective estimated wintering location. For these individuals we increased the aforementioned distance threshold by steps of 50km, reaching a maximum distance of 300 km with one of them.

The identified variables were then sequentially analyzed by linear regression models, eventually centering (i.e. subtracting the mean of the group) explanatory variables by sex, age or population to reduce collinearity among predictors entered simultaneously in the same regression model. For instance, as later shown in Par. 3.3.2 as latitude of wintering ground differs between years, we computed the difference between the wintering latitudes in a year and the average of the wintering latitudes of the same year and we used this difference in the analyzes that included both wintering latitude and year.

3.3 Results and discussion

As indicated in Par. 3.2.1, of the 88 analyzed barn swallows geolocators, 22 (25%) presented an incomplete series of light measurements, nevertheless including enough data to estimate at least the autumn migration route and the position of the wintering location. The sample of 20 barn swallows for `FLightR` repeatability analysis was chosen among the 66 geolocators with complete routes.

The estimated migratory routes (analysed as `FLightR` particles mean positions) are shown in Figure 3.11. Each line corresponds to an individual, while colours identify the population of origin of the barn swallows (Blue: SW, Orange: SE, Yellow: N). Four individuals reached during their migration the southern part of Africa, an unusual destination for Italian and Swiss barn swallows. These southern wintering locations are more typical of individuals breeding in Britain or Scandinavia, but were identified also in the analysis made by Liechti *et al.* (2015).

At the best of our knowledge it is the first time that it is possible to obtain the estimate of the migratory routes for such a high number of European passerine birds. It would be difficult to analyze the migration patterns at the population level in statistical terms, taking into account the uncertainty associated to each position of each individual. Therefore, before going deeper with further considerations about the routes, it is necessary to investigate the reliability of this result, analyzing the repeatability and the uncertainty of the `FLightR` estimates.

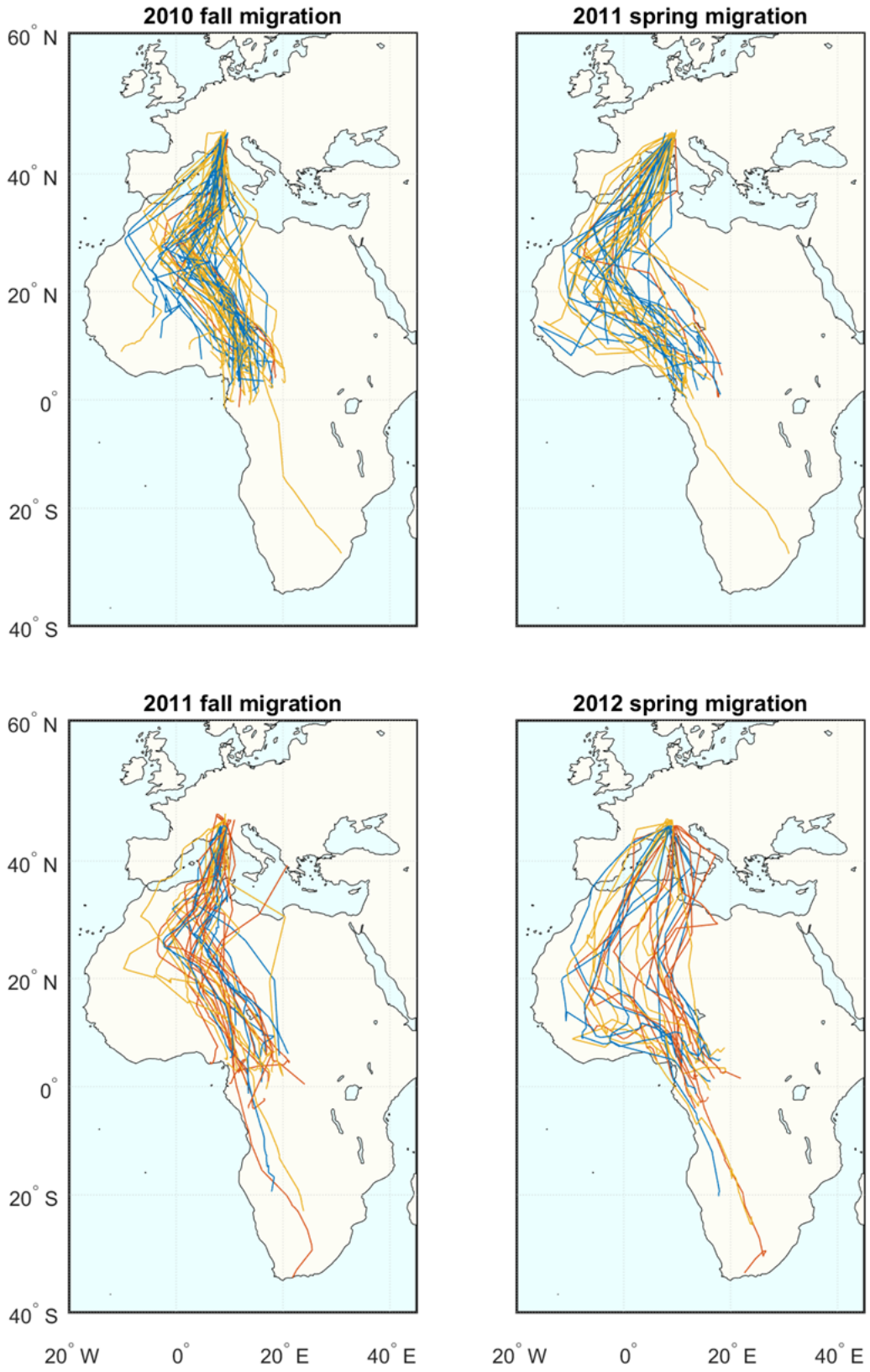

Figure 3.11: Reconstruction of the 88 fall (66 spring) barn swallow routes estimated using `FLightR`. Each line connects mean positions of a single individual at each twilight. Color refers to population of origin (Blue: SW, Orange: SE, Yellow: N).

3.3.1 Inter-repetition variability vs inter-particle variability

Figure 3.12 shows the global averages (both inter-repetitions and inter-geolocators; continuous lines) of (mean particles) positions in latitude (a) and longitude (b), contoured by the geolocators averages of inter-repetition variability (i.e. the inter-repetition standard deviation between particles mean positions; colored area) and inter-particle variability (i.e. inter-particle standard deviation averaged on each repetition and on each geolocator; dotted lines). An its careful observation reveals some incongruences: the average position is never perfectly stationary, even during the wintering period; mean latitude can decrease during spring migration; final average position does not correspond exactly to starting position (i.e. the breeding colony). These facts are mainly caused by the different number of geolocators (i.e. the sample size) used to estimate the average position at each twilight. Indeed, some twilights recorded by some geolocators may have been excluded because shadowed. To generate the two plots in Figure 3.12, we discarded twilight events contained in three or less geolocators, replacing them with the linear interpolation of neighboring values. We applied a moving average of 10 twilight events to the global average position (continuous line) to smooth out high frequency oscillations due to the different number of the sample for each twilight event.

In line with the known problems of geolocators inaccuracy (see Par. 3.1.1), `FLightR` results show greater uncertainty in latitude estimation, where the inter-particle variability (dotted lines) reach 4.5° near the autumn equinox (black vertical line on the left). This uncertainty is smaller (less than 1°) during barn swallows staging periods (July-August: birds are still in their breeding colonies; end of October – middle January: birds are in their wintering grounds), growing significantly during migration movements, where the proximity to the dates of the equinoxes becomes also relevant. The figure, however, shows that this uncertainty is relatively small with respect to the large latitudinal range covered by barn swallows through their migratory journeys.

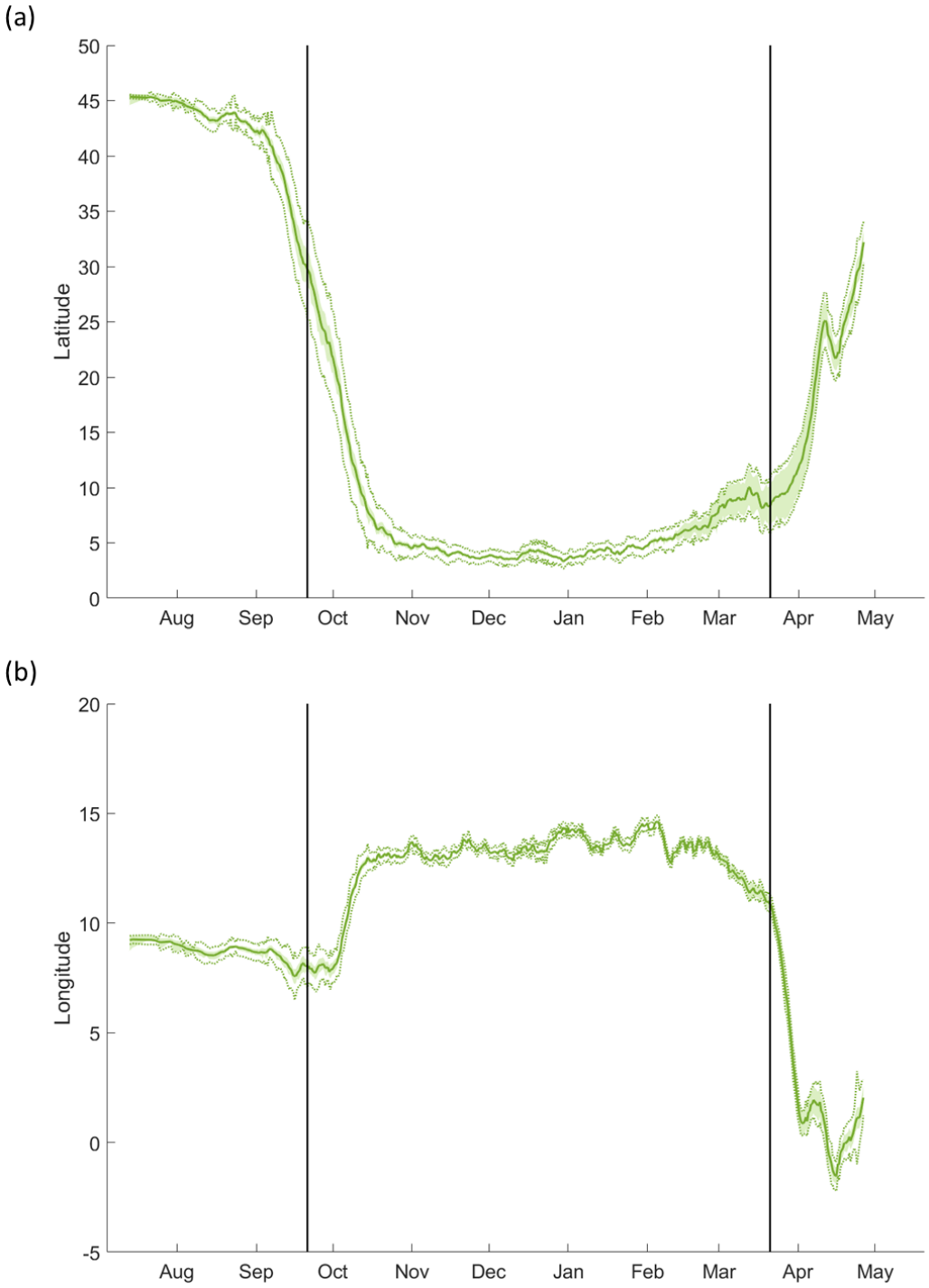

Figure 3.12: (a) Plot of `FLightR` average variability on estimated average latitude over time. Continuous line represents particles mean latitude computed at each twilight event averaged on all the repetitions of all the geolocators, smoothed with a 10 twilights mobile window. Dotted lines show `FLightR` inter-particles variability (standard deviation of particles latitude → mean between the different repetitions of the same geolocator → mean between the different geolocators). Colored area represents `FLightR` inter-repetition variability (mean of particles latitude → standard deviation between the different repetitions of the same geolocator → mean between the different geolocators). Data are temporally aligned to twilight date and time as shown in Figure 3.10. (b) Same as (a), but for `FLightR` longitude estimate.

The inter-particle variability in longitudes (Figure 3.12b, dotted lines) have a smaller range, remaining lower than 0.5° during the residential periods and reaching a peak of almost 1.5° at the end of spring migration. As with latitude, the inter-particle variability is of an order of magnitude lower than the average variation of the positions during the annual migration cycle (continuous line).

The inter-repetition variability (colored areas) is always less than or equal to the inter-particle variability (dotted lines), both in latitude and longitude. The only exception is represented by the first twilights of July, where a single run of the analyses of one geolocator estimated a departure date for fall migration five days earlier than that estimated in the other repetitions, resulting in five positions very far from those of all the other runs of the same geolocator. The migration route estimated in this particular repetition, however, was substantially consistent with the general migration pattern of all the others during the rest of migration.

The analysis at the level of the whole migratory paths indicated that different estimates from the migration routes of the same individuals were significantly more similar (i.e are at a shorted OWD to one another) than those from different individuals (mean ± SD inter-geolocator OWD: 24.46±11.96, intra-geolocator: 3.44±2.34; Mantel test: r_M = -0.350, p < 0.001, number of permutations: 999), as also clearly shown in Figure 3.13.

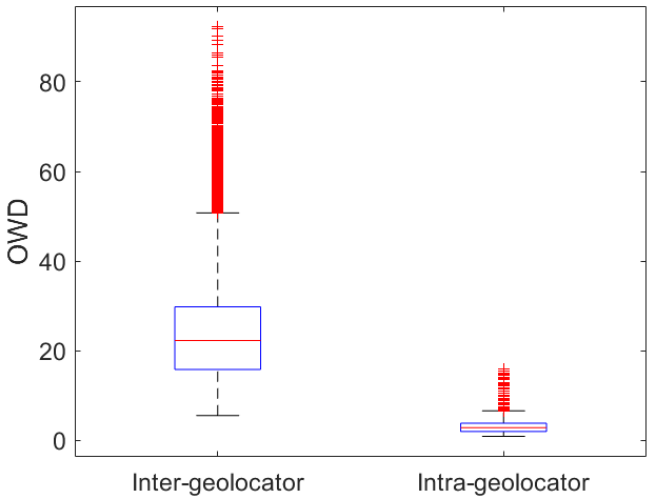

Figure 3.13: Boxplot of One-Way-Distances measured between routes estimated by `FLightR` from different individuals (Inter-geolocator) and between repeated estimates of routes of the same individual (Intra-geolocator).

From these analyzes it emerges that `FLightR` variability (both inter-particles and inter-repetitions) remains in a rather small range with respect to the scale of the movements performed by the barns swallow during their migration. In addition, the mean particle position obtained from a single run of analysis is a consistent estimator of the mean position that could be obtained with different runs on the same data. This suggests that any improvement in the precision of estimated positions could be obtained by running `FLightR` with a higher number of particles (e.g.: 10^7 instead of 10^6) during the filtering process rather than replicating the whole analysis with a lower number of run and then averaging the positions obtained at each run.

3.3.2 Analysis of migration routes

Migration routes and within individual variation

The migratory routes showed that barn swallows of our populations generally tend to migrate along a clockwise loop pattern, with many individuals that shifted from the central Afro-Palearctic flyway (roughly corresponding to Tunisia, east Algeria, Niger) during fall migration to the western Afro-Palearctic flyway (roughly corresponding to Mali, Mauritania, Morocco, west Algeria) during spring migration. Indeed, in terms of maximum longitude deviations from our focal meridian at 9°E positions visited by individuals during fall migration were significantly shifted westwards than those of spring migration (DevLonF vs DevLonS paired samples t-test: $t_{65} = -4.388$, $p < 0.001$). Also, a characteristic of fall migration is that individuals followed a more direct north-south direction with respect to spring migration, as clearly indicated by a significantly lower detour index (DetF vs DetS, paired samples t-test: $t_{65} = -3.882$, $p < 0.001$).

The seasonal longitude shift clearly emerges even visually from of Figure 3.14 which details the temporal variation of the inter-geolocator average both for latitude and longitude, divided by population of origin (colors) and by year of migration (line style). The phenomenon of westwards shifts is much more intense in the migration cycle started in 2010 (continuous lines), and it seems to be consistent between the North, South East and South West groups, since there are no statistically significant variations between the different populations of origin.

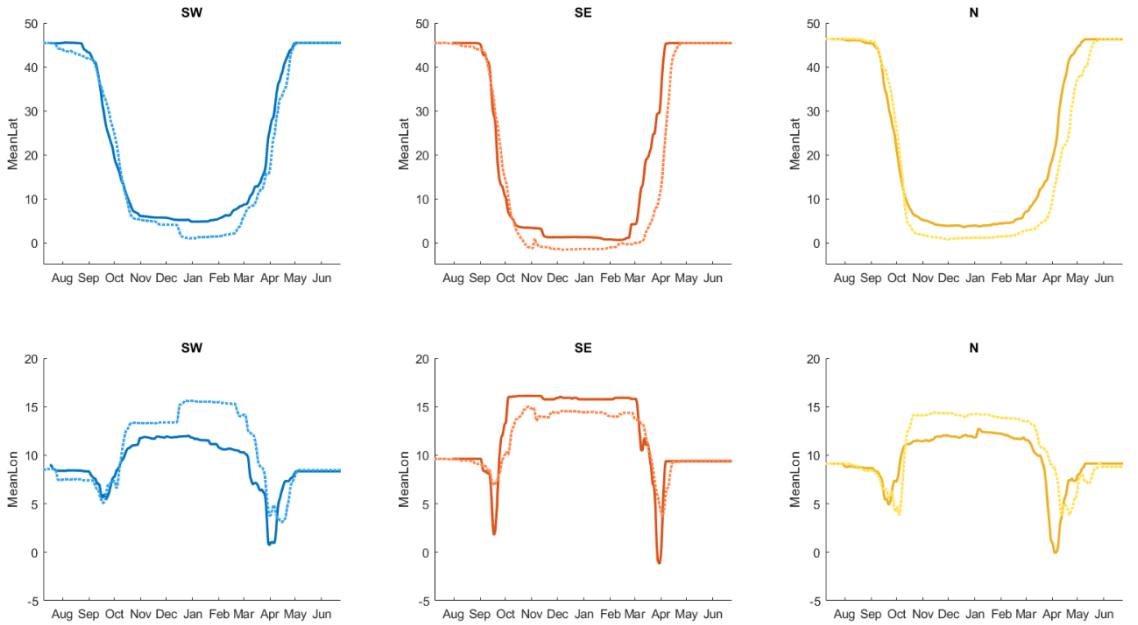

Figure 3.14: Time variations of the inter-individual mean latitudes and longitudes, derived from `FLightR` mean particle positions. Solid and dotted lines represent geolocators deployed in 2010 and 2011, respectively. Twilight events of all the geolocators are temporally aligned according to their date and time, in the same way we did to align data in the repeatability analysis in Par. 3.2.4. To perform the calculations using the same number of individuals at each twilight event, we used the position of the last available twilight as a proxy of position of an individual at any possibly deleted twilight. The number of individuals for each combination of year and population is summarized in Table 3.1, at page 47.

Interestingly, the index of the position of migration routes (DevLon) showed a clearly bimodal distribution both during fall and spring migration (Figure 3.15a). Individuals seem not to follow consistently routes to the east or the west of 9°E during fall and spring migration (χ_{21} = 2.082, p = 0.149, N = 66 individuals), and position indices were positively correlated (r = 0.316, p = 0.010). This occurred because many individuals approximately followed the same routes during fall and spring migration (41 dots, i.e. 62%, in the down-left and up-right quadrant in Figure 3.15b) while others shifted from a central to an eastern route (7 dots, 11% in the up-left quadrant) or from an eastern to a central one (down-right quadrant).

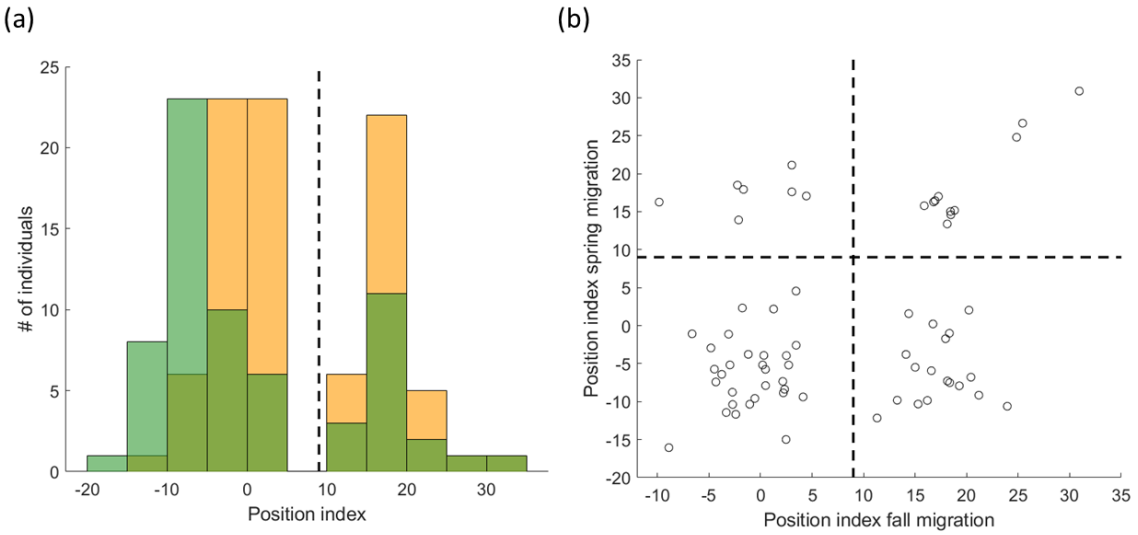

Figure 3.15: (a) Index of longitude of migration routes calculated as the longitude of the position that deviated most from the focal longitude 9 °E Orange bars represent fall migration, green bars spring migration. The vertical dashed line indicates 9 °E. (b) Position indices of fall and spring migration routes of the same individuals, indicated as the longitude of each route that differed most from 9 °E.

Figure 3.16 provides a schematic representation of the migration routes followed by individuals of each of the four groups of Figure 3.15. A multinomial test showed that the frequency distribution of individuals classified into the different routes differed among breeding population (LR-test: $\chi_{26} = 13.714$, $p = 0.033$), with more individuals that consistently followed central routes in both fall and spring migrations in the SE and N populations, but not between years or sexes ($\chi_{23} \leq 0.001$, $p \geq 0.999$).

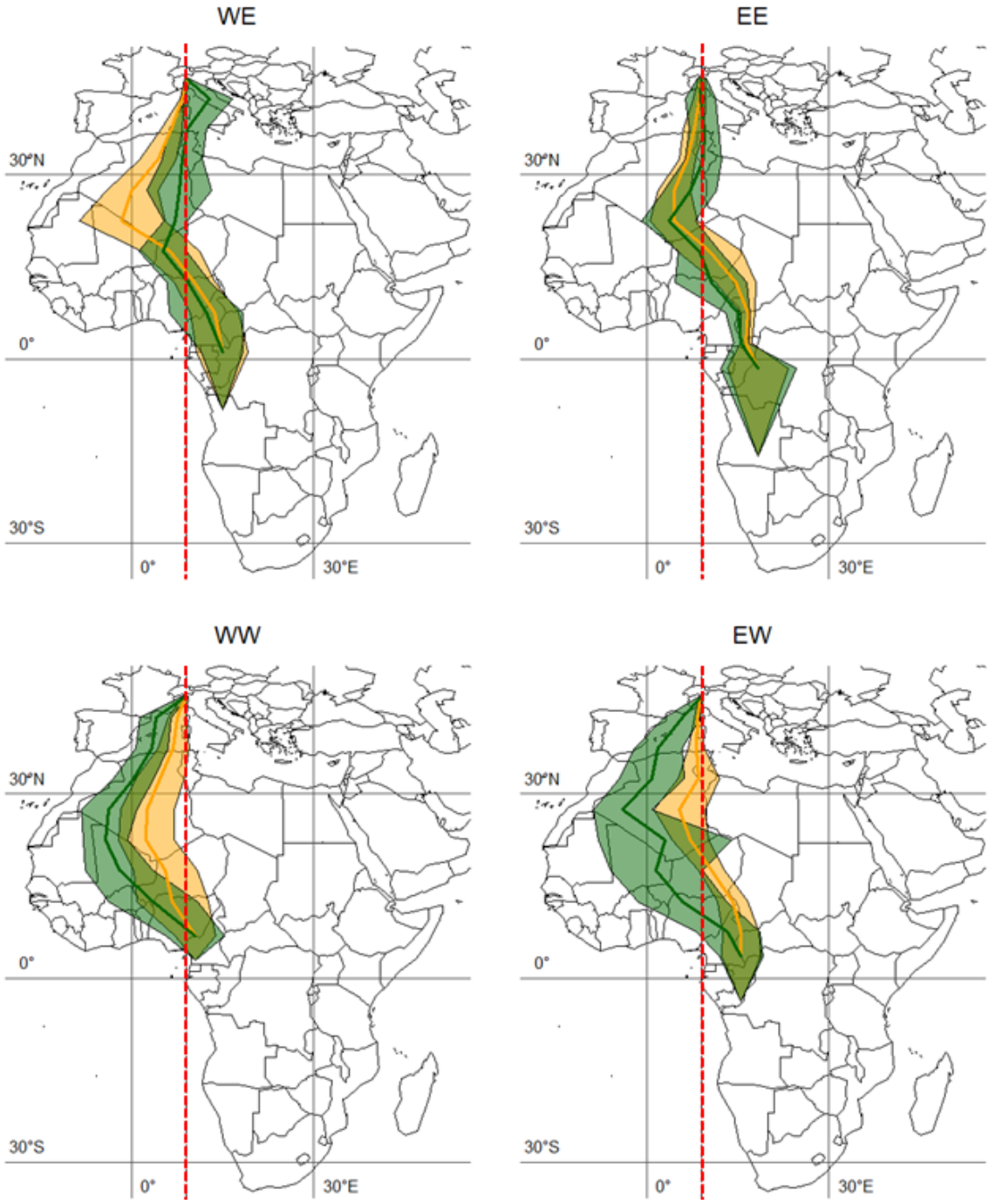

Figure 3.16: Schematic representation of the four groups of migration routes. Orange lines represent mean longitudes calculated for each belt of 5° latitude during fall migration and the orange polygon one standard deviation in longitude around that mean. Green lines and polygons represent the mean longitude and one standard deviation around it during spring migration. Dashed red line represents the focal 9°E meridian.

Fall migration

Departure time from the breeding colony differed between sexes and years but not between populations (Table 3.3). In particular, males departed on average 3 days later than females, while individuals tracked in 2011 departed on average 4 days earlier respect to 2010 individuals .We therefore centered departure time from the breeding colony to the mean value of each year by sex group, so that values of this variable reflect the deviation of departure date of an individual from its group and added this variable to regression model of maximum deviation in longitude from 9°E. This latter variable, however, did not significantly vary according to any predictor. Similarly, detour index did not vary according to the same set of predictors.

In contrast, the total duration of stationary periods before the arrival to the final wintering location decreased with departure date from the breeding colony, indicating that individuals that departed later (with respect to their year by sex group) spent less time in stationary sites. This result held also when we repeated the analyses excluding the four individuals with a wintering residence area in southern Africa (other details not shown). In addition, total duration of the stationary periods did not differ between individuals that reached southern Africa and those that spent the wintering season in central Africa (t-test: $t_{3.372} = -0.520$, $p = 0.635$).

Speed of fall migration (excluding stationary periods) did not change according to any predictor, and this was true also for excluded individuals that reached southern Africa (details not shown). Indeed, migration speed did not either differ between individuals that reached southern Africa and those that spent the wintering season in central Africa (t-test: $t_{4.367} = -0.861$, $p = 0.434$).

In contrast, and interestingly, latitude and longitude of the wintering grounds did significantly differ between years only (Table 3.3), both including and excluding the four individuals that reached the southern of Africa (details not shown). We therefore centered latitude and longitude of the wintering residence areas by year and entered this variable in the analysis of the date of arrival to the wintering residence areas. This latter analysis indicated that the arrival date strongly depended on departure date from the breeding colony and on the length of stationary periods during fall migration. All these results did not change excluding from the analysis the four individuals that reached southern Africa.

Indeed, their arrival date to the wintering ground did not differ significantly from that of the individuals that ended their migration at more northern latitudes (t-test: $t_{3.628} = -0.527$, $p = 0.629$).

	F	DF	P	Least-square means (SE)		
Departure from the breeding colony (DepBC)						
Sex	**5.001**	**1,81**	**0.028**	**M: 251.11 (0.85)**	**F: 247.97 (1.21)**	
Year	**9.742**	**1,81**	**0.002**	**A: 251.95 (1.00)**	**B: 247.13 (1.17)**	
Population	0.047	2,81	0.954	SE: 234.31 (1.67)	SW: 249.85 (1.21)	N: 249.50 (1.05)
Maximum deviation in longitude from 9° E during fall migration (devLonF)						
Sex	0.421	1,80	0.518	M: -0.987 (1.417)	F: -2.513 (2.019)	
Year	0.827	1,80	0.366	A: -2.922 (1.675)	B: -0.579 (1.958)	
Population	0.716	2,80	0.420	SE: 0.824 (2.789)	SW: -3.070 (2.027)	N: -3.004 (1.753)
cDepBC	0.190	1,80	0.664	Coef: -0.081 (0.186)		
Detour index during fall migration (DetF)						
Sex	1.358	1,80	0.247	M: 0.221 (0.017)	F: 0.254 (0.025)	
Year	0.562	1,80	0.456	A: 0.226 (0.020)	B: 0.249 (0.024)	
Population	0.380	2,80	0.685	SE: 0.225 (0.034)	SW: 0.233 (0.025)	N: 0.254 (0.021)
cDepBC	2.652	1,80	0.107	Coef: -0.003 (0.002)		
Total duration of stationary periods before arrival to the wintering grounds (StatF)						
Sex	0.091	1,79	0.764	M: 39.524 (4.482)	F: 41.524 (6.397)	
Year	0.332	1,79	0.566	A: 42.746 (5.285)	B: 38.048 (6.192)	
Population	1.719	2,79	0.186	SE: 31.597 (8.795)	SW: 39.489 (6.392)	N: 49.745 (5.563)
c-DepBC	**7.041**	**1,79**	**0.010**	**Coef: -1.578 (0.595)**		
DetF	3.771	1,79	0.056	Coef: 56.140 (28.908)		
Fall migration speed (SpeedF)						
Sex	0.271	1,78	0.604	M: 258.937 (15.253)	F: 245.753 (21.662)	
Year	0.061	1,78	0.805	A: 255.766 (17.888)	B: 248.924 (21.056)	
Population	0.148	2,78	0.862	SE: 255.559 (30.106)	SW: 257.718 (21.675)	N: 243.758 (18.978)
c-DepBC	0.059	1,78	0.808	Coef: -0.511 (2.100)		
DetF	1.225	1,78	0.268	Coef: -111.723 (100.137)		
StatF	1.946	1,78	0.167	Coef: 0.531 (0.381)		

Latitude of the wintering ground						
Sex	1.094	1,77	0.299	M: 2.903 (1.058)	F: 4.742 (1.503)	
Year	**7.107**	**1,77**	**0.009**	**A: 6.378 (1.240)**	**B: 1.267 (1.460)**	
Population	0.980	2,77	0.387	SE: 2.514 (2.087)	SW: 5.532 (1.503)	N: 3.421 (1.318)
c-DepBC	0.334	1,77	0.565	Coef: -0.084 (0.146)		
DetourF	0.864	1,77	0.355	Coef: 6.507 (6.998)		
c-StatF	0.011	1,77	0.916	Coef: -0.003 (0.027)		
SpeedF	0.193	1,77	0.662	Coef: -0.003 (0.008)		
Longitude of the wintering ground						
Sex	0.667	1,77	0.417	M: 13.900 (0.765)	F: 12.862 (1.086)	
Year	**5.745**	**1,77**	**0.019**	**A: 11.721 (0.897)**	**B: 15.042 (1.055)**	
Population	0.527	2,77	0.592	SE: 14.465 (1.509)	SW: 12.537 (1.086)	N: 13.142 (0.953)
c-DepBC	0.024	1,77	0.876	Coef: 0.016 (0.105)		
DetourF	3.049	1,77	0.085	Coef: -8.831 (5.058)		
c- StatF	3.089	1,77	0.083	Coef: 0.034 (0.019)		
SpeedF	0.015	1,77	0.903	Coef: 0.001 (0.006)		
Arrival date to the wintering ground (ArrWG)						
Sex	3.926	1,75	0.051	M: 321.466 (0.595)	F: 319.501 (0.844)	
Year	1.721	1,75	0.194	A: 321.187 (0.694)	B: 319.780 (0.817)	
Population	0.369	2,75	0.693	SE: 320.949 (1.172)	SW: 320.602 (0.849)	N: 319.900 (0.738)
c-DepBC	**154.547**	**1,75**	**< 0.001**	**Coef: 1.016 (0.082)**		
DetourF	**13.044**	**1,75**	**< 0.001**	**Coef: 14.418 (3.992)**		
c-StatF	**4148.266**	**1,75**	**< 0.001**	**Coef: 0.988 (0.015)**		
c-LatWG	**40.770**	**1,75**	**< 0.001**	**Coef: -0.478 (0.075)**		
c-LonWG	0.020	1,75	0.888	Coef: 0.015 (0.104)		
SpeedPost	**261.500**	**1,75**	**< 0.001**	**Coef: -0.071 (0.004)**		

Table 3.3: Post-breeding migration. Different letters indicate significant ($P < 0.05$) pairwise differences at post-hoc tests.

Spring migration

Interestingly, departure time from the wintering location at spring is related to the arrival date in Africa in the previous fall (Table 3.4). More precisely, individuals that arrived later to the wintering ground from fall migration, also tended to depart later. In fact, the regression coefficient for this variable also differed significantly from one ($t_{80} = -5.391$, $p < 0.001$), indicating that individuals that arrive late from fall migration tend to spend

less time in the wintering ground. These results did not change when the analyzed data did not include the four individuals that reached southern Africa (details not shown), also because their departure date from the wintering ground did not differ from those of the other individuals (t-test: $t_{3.628} = -0.527$, $p = 0.629$).

Maximum deviation in longitude from 9° E during spring migration significantly differed between years, with individuals following more western routes in 2011 than in 2012. In addition, individuals that have eastern wintering grounds tended to follow more eastern routes during spring migration, independently of the between-years difference in the average position of the wintering grounds. These results held also excluding the four individuals that spent the boreal winter in southern Africa, which had more easterly wintering grounds than those that spent the boreal winter at more northerly latitudes (mean longitudes ± SE were respectively 22.863 ± 2.530°E and 13.095 ± 0.605°E; $t_{3.353} = -3.755$, $p = 0.027$), but followed routes than did not deviate from 9 °E more than those of the other individuals ($t_{3.129} = -1.766$, $p = 0.172$). However, the analyses that excluded these individuals, revealed also significant differences in route position between populations ($F_{1,54} = 4.233$, $p = 0.020$), with individuals breeding in the SE area migrating along more eastern routes than those from the other areas ($t \leq -2.652$, $p \leq 0.027$ at post hoc tests). It is worth noticing that the longitudinal difference between the SE and the SW or N areas is lower than 2 degrees, thus is very negligible compared to the longitudinal distance between the eastern routes emerged during migration. In addition, this analysis also revealed a significant increase in maximum deviation from 9° E with latitude of the wintering ground (Coef: 0.959 ± 0.368 SE, $F_{1,54} = 6.665$, $p = 0.013$). In contrast, the detour index did not change according to any variable, and this was true also excluding the four individuals that reached southern Africa (details not shown).

The total duration of the stationary periods during the spring migration changed with departure date from the wintering ground and also with its longitude. This result did not change also excluding the four individuals that reached southern Africa (details not shown). In particular, individuals that departed later from Africa tended to stopover less. The regression coefficient also did not differ much from -1 ($t_{57} = -1.122$, $p = 0.267$), implying that each delay of one day in the departure from the wintering ground determines on average a reduction of approximately one day in the time spent at stopover

sites during spring migration. In addition, individuals that spent the boreal winter in more eastern wintering locations (that chose a more eastern spring migration routes as we said) also tended to stopover less.

Spring migration speed changed according to *i*) departure date from the wintering ground, *ii)* length of the detour of the spring migration route, and *iii*) time spent at stopover sites. In particular, individuals that departed later and spent more time at stopover sites, migrated faster, while those that made longer detours tended to migrate slower. These results held also when we excluded the four individuals that reached southern Africa. However, this analysis revealed also a significant relationship between migration speed and latitude of the wintering location, with individuals breeding to more northern latitudes that also tended to migrate faster (Coef: 16.028 ± 6.637 SE, $F_{1,51} = 5.831$, $p = 0.019$).

Arrival date to the European breeding colony from African wintering sites did not differ between sexes nor with the breeding areas, but it was earlier in 2011 than in 2012. In addition, individuals that departed later from wintering sites, made longer detours and spent more time at stopover sites also arrived later, while those that migrated faster and had wintering grounds located more at north arrived earlier to the breeding grounds, independently of the difference between years in the average position of the wintering grounds. The regression coefficients associated to departure date and time at stopover sites, however, also not differed from one ($t_{54} \leq -3.000$, $p \leq 0.004$), implying that, any delay of one day in departure from the breeding colony and any day spent in stopover areas determines a delay of less than one day in the arrival to the breeding colony. In other words, our results suggest that individuals compensate for later departure or longer stopover by accelerating migration progression. These results also held when we excluded in the analyses the four individuals with wintering grounds in southern Africa (details not shown).

	F	DF	P	Least-square means (SE)		
Departure from the wintering ground (DepWG)						
Sex	0.338	1,80	0.653	M: 388.877 (4.633)	F: 393.459 (6.739)	
Year	1.924	1,80	0.169	A: 385.308 (5.547)	B: 397.029 (6.383)	
Population	0.450	2,80	0.639	SE: 386.817 (9.158)	SW: 290.351 (6.689)	N: 396.297 (5.583)
ArrSRA	**10.969**	**1,80**	**0.001**	**Coef: 0.380 (0.115)**		
c-LatSRA	0.000	1,80	0.993	Coef: 0.005 (0.588)		
c-LonSRA	2.651	1,80	0.107	Coef: 1.293 (0.794)		
Maximum deviation in longitude from 9° E during spring migration (devLonS)						
Sex	0.001	1,58	0.981	M: -7.009 (1.514)	F: -7.075 (2.2356)	
Year	**9.940**	**1,58**	**0.003**	**A: -11.130 (1.833)**	**B: -2.953 (1.899)**	
Population	2.821	2,58	0.068	SE: -2.044 (2.749)	SW: -9.334 (2.137)	N: -9.747 (1.928)
DepWG	0.040	1,58	0.850	Coef: 0.010 (0.052)		
c-LatWG	0.121	1,58	0.730	Coef:- 0.062 (0.178)		
c-LonWG	**10.140**	**1,58**	**0.002**	**Coef: 0.899 (0.282)**		
Detour index during autumn migration (DetF)						
Sex	0.379	1,58	0.540	M: 0.359 (0.032)	F: 0.324 (0.047)	
Year	1.131	1,58	0.292	A: 0.370 (0.039)	B: 0.313 (0.040)	
Population	1.060	2,58	0.353	SE: 0.278 (0.058)	SW: 0.381 (0.045)	N: 0.365 (0.041)
DepWG	0.250	1,58	0.620	Coef: 0.001 (0.001)		
c-LatWG	0.604	1,58	0.440	Coef: 0.003 (0.004)		
c-LonWG	0.702	1,58	0.406	Coef: -0.005 (0.006)		
Total duration of stationary periods during spring migration (StatS)						
Sex	0.338	1,57	0.563	M: 38.892 (2.401)	F: 41.404 (3.565)	
Year	3.604	1,57	0.063	A: 36.205 (2.909)	B: 44.091 (3.053)	
Population	0.885	2,57	0.418	SE: 38.863 (4.440)	SW: 38.037 (3.396)	N: 43.544 (3.059)
DepWG	**124.136**	**1,57**	**< 0.001**	**Coef: -0.908 (0.082)**		
c-LatWG	0.470	1,57	0.496	Coef: -0.195 (0.284)		
c-LonWG	**4.932**	**1,57**	**0.030**	**Coef: -1.001 (0.451)**		
DetF	0.051	1,57	0.822	Coef: -2.238 (9.910)		

Spring migration speed (SpeedF)						
Sex	2.093	1,55	0.154	M: 327.909 (23.497)	F: 264.293 (35.799)	
Year	0.014	1,55	0.906	A: 298.550 (28.483)	B: 293.652 (30.042)	
Population	1.359	2,55	0.266	SE: 325.483 (42.652)	SW: 312.310 (32.693)	N: 250.511 (31.767)
DepWG	**11.560**	**1,55**	**0.001**	**Coef: 6.323 (1.860)**		
c-LatSRA	3.355	1,55	0.072	Coef: 5.016 (2.738)		
c-LonSRA	0.218	1,55	0.642	Coef: 2.166 (4.634)		
DetS	**9.393**	**1,55**	**0.003**	**Coef: -293.200 (95.669)**		
StatS	**15.166**	**1,55**	**< 0.001**	**Coef: 6.523 (1.675)**		
Arrival date to the breeding colony						
Sex	0.518	1,54	0.475	M: 470.108 (0.752)	F: 469.088 (1.145)	
Year	**17.123**	1,54	**< 0.001**	**A: 466.900 (0.902)**	**B: 472.296 (0.952)**	
Population	0.152	2,54	0.859	SE: 469.095 (1.354)	SW: 470.030 (1.036)	N: 469.670 (1.030)
DepWG	**147.841**	**1,54**	**< 0.001**	**Coef: 0.788 (0.065)**		
c-LatWG	**29.384**	**1,54**	**< 0.001**	**Coef: -0.484 (0.089)**		
c-LonWG	1.041	1,54	0.312	Coef: 0.150 (0.147)		
DetS	**61.417**	**1,54**	**< 0.001**	**Coef: 25.687 (3.278)**		
StatS	**187.331**	**1,54**	**< 0.001**	**Coef: 0.820 (0.060)**		
SpeedS	**43.378**	**1,54**	**< 0.001**	**Coef: -0.028 (0.004)**		

Table 3.4: Pre-breeding migration. Different letters indicate significant ($P < 0.05$) pairwise differences at post-hoc tests.

3.4 Conclusions

The present work allowed for the first time to reconstruct the migration routes of a large set (88 individuals) of barn swallows. Knowing the routes traveled by migratory birds is important information for ornithological and ecological studies. For centuries scholars have been able to observe these species in their areas of reproduction or wintering, without having any chance of inspecting in detail their migratory movements. The technological innovations of the last two decades have instead made it possible to install new IT devices directly on individuals, even in cases of light passerine birds like *Hirundo rustica*, obtaining the first reconstructions of the routes. The only tags that can be carried by most migratory species are geolocators, which only provide a proxy of birds' positions. As clarified step by step in this thesis chapter, reconstructing the routes traveled by the

birds from light measurements is a complex procedure, which requires the expert-guided use of dedicated modeling and statistical frameworks.

In this chapter we have reconstructed the migratory routes of 88 swallows, studied over two years and by three different populations. We used `FLightR` software, testing the consistency of the estimated positions on multiple repetitions of the analysis on the same inputs by the means of a repeatability analysis. The results are consistent with each other and with a previous study that identified the stationary periods of the studied individuals.

The reconstruction of the routes made it possible to analyze the migration patterns of the barn swallows under examination, identifying four different groups of migrants according to the route taken during their autumn and spring trips. Regression analysis on route indices revealed that the year of migration has a significant effect on wintering grounds location and spring route westward deviation, while there is less influence from the population or sex of the individual. This result could suggest a possible influence of the meteorological conditions encountered by the birds on their routes.

4 AUTOMATIC TWILIGHT SELECTION BY MACHINE LEARNING TECHNIQUES

4.1 Introduction

As seen in Chapter 3, `FLightR` bases routes estimation procedure on light values measured by the geolocators around twilight events. Each recorded twilight event that shows unnatural temporal variation of light levels around twilight (e.g. too abrupt changes of luminosity in short periods of time or non-monotonical changes of luminosity nearby darkness situations at twilights) need to be manually removed by an expert operating a visual selection. If this operation was not performed correctly, the reconstruction of the routes would be strongly influenced by shadowed twilight events, which are responsible of producing a highly distorted estimate of the geographical positions (see again Figure 3.6 at page 48).

To track the geographic locations visited by a single bird along its annual migration path, the manual selection described in Par. 3.2.2 at page 47 required for the study cases of the present thesis the unassisted visual inspection of at least 600 twilight events per individual, that is around fifty thousand data: quite a cumbersome and time consuming task. That is why some *R* packages have been developed to partially assist the user during this procedure. We described in Par. 3.2.2 software `TwGeos`, that automatically identifies

twilight events using a threshold method and easily displays light variations occurring during all sunrises or sunsets. Despite the help provided by `TWGeos`, the manual selection further needed to pre-process raw data remains quite a slow and delicate operation. On average, an entire day of work of an expert user is required to visually classify the twilight events of few geolocators. The expert discriminates between noisy (shadowed) and natural twilight events by inspecting two different patterns: the variation of light intensity values after sunrise/before sunset as measured by the geolocators at the focal day *i*, and the smoothness of the day by day variation of dawns and sunsets hours around day *i*. Reformulating the problem from a statistical learning point of view, the identification of valid twilight events can be interpreted as a binary classification task (keep datum vs discard datum) from a set of numerical variables ('features').

In order to obtain a substantial training dataset, we used here the above described more than one hundred geolocators tracks of barn swallows during fall and spring migration, resulting in the identification and manually classifying about 40'000 twilight events. Thanks to such an abundance of data, we could therefore apply, in addition to standard linear classifiers as Logistic Regression (LR), machine learning classification algorithms such as Random Forest (RF) and Deep Neural Network (DNN). From geolocator light measurements and the hours of the previously identified twilight events we build the features used as inputs by the classifiers. Finally, we tested the reliability of algorithms predictions by estimating from their classification output the migration route traveled by four target individuals, comparing them to the one originated from the expert selected twilights.

4.2 Materials and Methods

4.2.1 Processing of geolocators data

We relied on 65 SOI-GDL2.10 and 43 SOI-GDL2.11 geolocators data (Swiss Ornithological Inst., www.vogelwarte.ch/indirect-trackinggeolocator.html), the large majority of which were used in the ornithological study of Liechti *et al.* (2015) and in the work presented in Chapter 3. In the previous chapter we did not analyze all this dataset because some geolocators presented insufficient light data to estimate at least the fall migration route (5 individuals) or because the equipped barn swallows will be subjects of other ornithological studies not treated in this thesis (15 individuals).

SOI-GDL geolocators detect the light intensity every minute and store its average measure every five minutes by assigning an integer value on a scale between 0 (full dark) and 64 (maximum detectable luminosity). Each geolocator in the dataset registered an average of 381±144 twilight events, providing a total amount of 39572 twilight events. Using the same procedure explained in Par. 3.2.2, we used `TwGeos` *R* package to pre-process raw data, manually inspecting every suggested twilight event by labeling with 1 (= discard) those that showed light curves that were too different from the 'natural' ones (i.e. those that would be measured if the geolocator was placed in an open air location at the same geographical position, see again Figure 3.4) and/or whose timing differed in an inconsistent way from that of the corresponding events occurred the days before or after the focal date. As we noticed that the classification of certain twilights could be somewhat uncertain even for an expert (i.e. the light curve shows an intermediate pattern between the natural variation of accepted twilights and the luminosity increases of shadowed events) we re-classified the twilight events registered by the geolocators of four individuals of 2012 migration (the only ones of this year, see Par. 3.2.1), using them as target cases. The twilight events of these geolocators were not used in any phase of the ML algorithms construction (training, validation and test). We used the target set of twilight data only to test the repeatability of the expert classification and the ones performed by the ML algorithms by assessing the values of Interclass Correlation Coefficient (Shrout and Fleiss, 1979), usually defined, in the framework of random effects models, as the proportion of the total variance accounted for by differences among groups (aka classes, in statistical terminology):

$$ICC = \frac{\sigma_G^2}{\sigma_G^2 + \sigma_R^2}$$

where σ_G^2 is the between-group variance and σ_R^2 is the residual variance of the model. Repeatability can be interpreted as the expected within-group correlation among measurements (Sokal and Rohlf, 1995). In our case, the response variable is the binary twilight selection (‘keep’ = 0, ‘discard’ = 1, as labeled in TAGS file format, see Par. 3.2.2), while the geolocator ID and the twilight event ID are inserted as nested random effects (twilightID nested within geolocatorID). We computed ICC values from a

generalized linear mixed model assuming a binomial data distribution with logit link function, built with `lme4` *R* package (Bates *et al.*, 2015).

4.2.2 Features selection

The above described manual classification of thousands of twilight events evidenced that the predominant part of expert's choice was based on shapes of light curves in the close proximity to every single twilight event. Therefore, we selected as first relevant features for our machine learning algorithm the eight light measurements of each geolocator (intra-twilights luminosity measurements) either following sunrise or preceding sunset. For the large majority of twilight events, it was often sufficient for the expert to inspect the plot of such eight values in order to discriminate between reliable (natural) and unreliable (shadowed) data. A regular variation of intra-twilights light intensity is a necessary, yet not sufficient condition for accepting the recorded datum: some dusks and dawns had in fact to be more closely evaluated by the expert, who contrasted their timings to those recorded in nearby days (Figure 4.1).

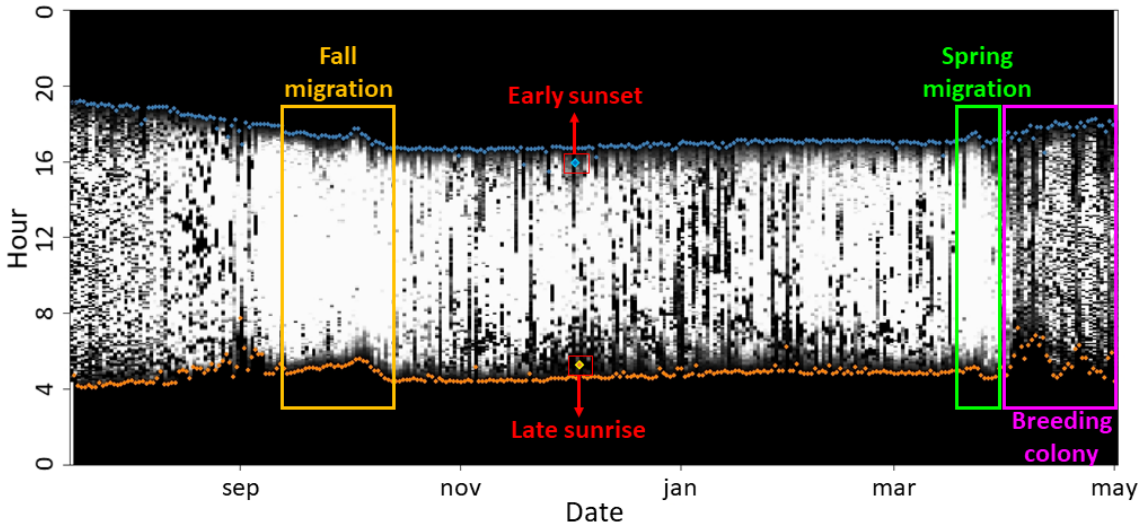

Figure 4.1: Light measurements of a light level geolocator visualized using `TwGeos` *R* package. *x*-axis represents date of the year, *y*-axis the hour of the day. Values on the gray scale represent light intensity measured by the geolocator. Orange and blue dots show the timing of twilights (sunrises and sunsets hours) as identified by `TwGeos`. We highlighted a late sunrise (yellow point) and an early sunset (cerulean point), and three probable phases of barn swallow annual phenological cycle: fall migration (yellow rectangle), spring migration (green rectangle) and the spring stay at the breeding colony (purple rectangle).

As additional input variables for our classifier, we therefore added the exact timing of all twilight events occurring in a nine-day window surrounding the focal event (i.e. day $i \pm$

4 days). Finally, to help the algorithm capturing the procedure used by the expert in the classification process, we added the following other four input variables that qualify different properties of the twilight hours:

1) the time difference between the twilight timing of the focal day i and the average twilight timings of top 50% of earliest sunrises/latest sunsets in a mobile window of nine days centered at day i (i.e., focal day ± 4 days). The aim of this variable is to identify the twilight events that occur at very different times from neighbors (generally late sunrises and early sunsets, see Figure 4.1);
2) same as 1), but with the average twilight timing computed over a mobile window of 19 days (i.e., focal day ± 9 days) to identify outliers on a wider time span;
3) the standard deviation of night duration on a mobile window of 9 days (i.e., focal day ± 4 days). This variable was selected to easily identify the twilight events of the periods in which a bird was at its breeding colony, because pattern of sunrise and sunset times is very variable in that period (see again Figure 4.1) due to the shadowing caused by the buildings where the barn swallows rest during the night. During manual classification procedure we discarded many of these twilight events;
4) the residual of a linear regression on twilight timings (either sunrises or sunsets) on a mobile window of 9 days (i.e., focal day ± 4 days). In this way, it is possible to identify outliers during the migration periods, where the sunrise and sunset times change considerably, but regularly, from one day to another (see again Figure 4.1).

4.2.3 Machine learning classifiers

Following the traditional machine learning terminology, the task we are dealing with is a supervised learning problem, more precisely a binary classification. It consists basically in splitting the elements of a given set (twilights, in this case) into two groups based on characteristics of the features of each element. The algorithms used to train classifiers require a dataset where each sample is qualified by its features and is already categorized.

Starting from these data, supervised learning techniques may allow to train a model predicting which group each twilight belongs to.

First, we implemented a Logistic Regression (hereafter LR), a simple classifier which takes a decision on the basis of a value resulting from a linear combination of the features (Cox, 1958). From a visual point of view, a linear classifier simply splits the high-dimensional feature space with a hyperplane and the classification of each sample is based on the positioning of its features relative to a linear decision boundary. Because of their simplicity and roughness, linear classifiers are nowadays mainly used as benchmark for a fair comparison with other, more articulated models.

Next, we introduced two more advanced non-linear machine learning models which allow to efficiently deal with problems where classes are not linearly separable: a Random Forest (hereafter RF; Ho, 1995) and a Deep Neural Network (hereafter DNN; Bengio, 2009).

The RF is an ensemble of classification trees: each tree is an algorithm that performs a recursive partition of the feature space, here performed by a Boolean test on a single variable at each node. As a direct consequence, the feature space in each tree is separated by orthogonal hyperplanes, which results in box-like decision (Biau and Scornet, 2015). Each classification tree is made on a random subset (both on instances and features) of the training dataset. The algorithm that build the tree operates with a top-down procedure, choosing at each step the variable that performs the best split of the data by the means of an evaluation function. In particular, we implemented the RF using the Gini impurity as evaluation function[1]. Finally, the RF performs the classification on each single item selecting the most recurrent class in trees decisions (Figure 4.2).

[1] The algorithm of a classification tree computes Gini impurity for each partitions split ('leaf'). Given a set of objects of different classes, Gini impurity is defined as the probability of obtaining two objects of different classes by a random sample on the set (i.e. the probability of sampling a discarded and a kept twilight event from the same leaf). The Gini impurity value for the whole tree is obtained by averaging leaves impurities, weighted by the number of objects of each leaf.

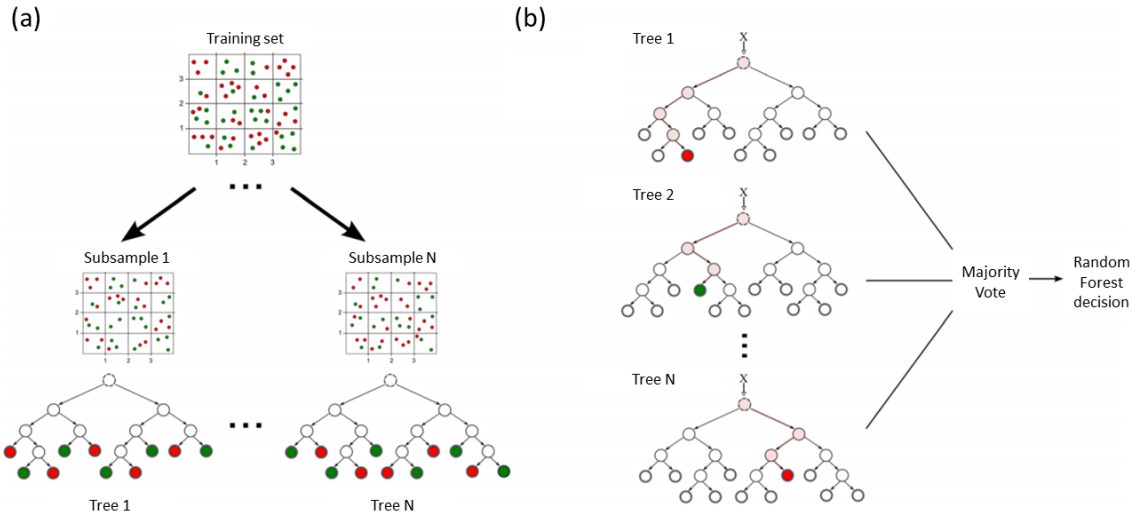

Figure 4.2: A schematic representation of a classification random forest. (a) Each decision tree is built upon a random bootstrap sample of the training data (green and red colors indicate two different classes). (b) The random forest classifies each new instance by tacking the most voted output by the *N* trees of the algorithm. Source: Machado *et al.*, (2015)

Conversely, a neural network is a connected structure of single nodes (called 'neurons') divided in one input layer (where each neuron represents a single feature of the dataset), one output layer (where each neuron is a feature of the result) and a certain quantity of intermediate layers (called 'hidden layers'). The value of each neuron of layer i is obtained by applying a nonlinear function (usually a sigmoid or a rectifier linear unit) to the weighted average of the neurons of layer $i-1$. Each layer i is linked to layer $i+1$ by a $p \times q$ matrix of weights, where q is the number of neurons in the i layer, while q is the number of neurons of the layer $i+1$. The weights matrices are the parameters of the neural network (Figure 4.3). In the case of classification neural networks, the output layer contains many neurons as the number of classes and the choice is made on the class associated to the neuron with the higher output.

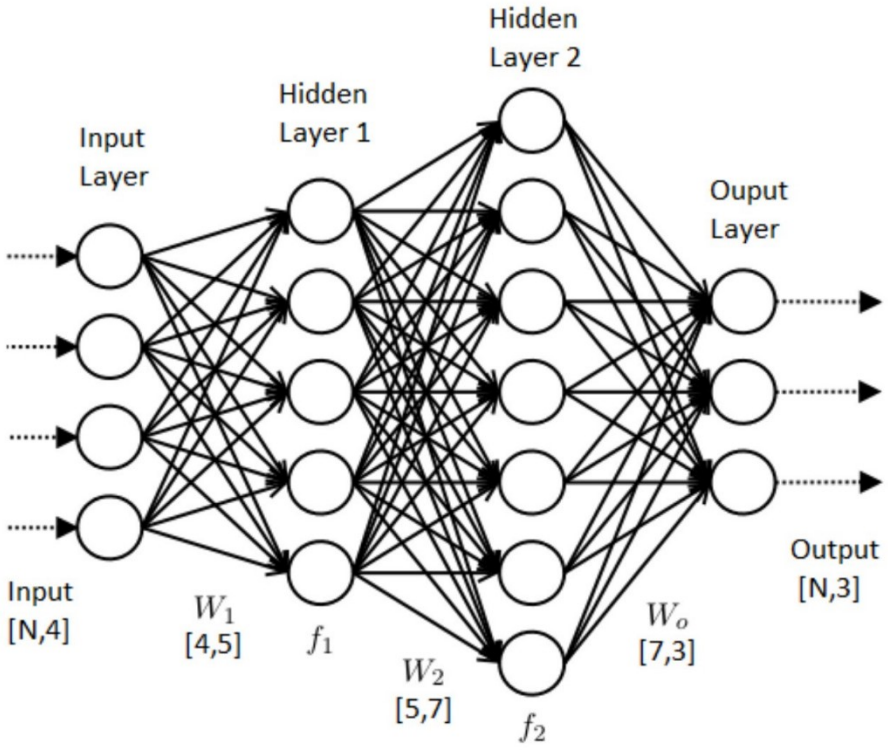

Figure 4.3: A schematic representation of a generic fully connected neural network with two hidden layers (respectively with 5 and 7 neurons). In this case the input dataset has *N* instances and 4 features (i.e. the input layer has 4 neurons, represented by the nodes of the network), while the output is made by 3 variables. Each node performs a nonlinear transformation of the weighted average of the features of the previous layer. Arrows represent the input and the output features of the weighted averages and are described as weight matrices (*W*). Source: *www.datasciencecentral.com*

With reference to the structure of our neural classifier, we did not use only dense layers (i.e. hidden layers where each node is connected with all the nodes of the subsequent layer), but we also explored and tested different alternative architectures. In particular, we added to the fully connected structure some convolutional layers which process by 1D nonlinear filters each of the three time series features of the specific twilight (i.e. the eight after sunrise/pre-sunset light measurements and the two series of the timing of the nine sunrises and sunsets around the specific twilight event), since they turned out to be efficient in dealing with time series for other problems (LeCun and Bengio, 1995). The

convolutional filters[2] extract multiple new features, whose definition is optimized during the training process. These new features, together with the four combined features selected by the expert, are given as input to the last fully connected layers of the DNN which finally performs the classification (Figure 4.4). The dimension of each vector during feature selection is regulated by a *Max Pooling* process, which applicates a piecewise maximum operator at the output of the convolutional filters. At the end of the whole structure, the *Softmax* activation function normalizes to 1 the values of output layer. *Softmax* activation function transforms a n dimensional vector of arbitrary real values (q_i) to a n dimensional vector of real values p_i, each ranging in the interval (0,1) and with sum equal to 1:

$$p_i = \frac{e^{q_i}}{\sum_{j=1}^{n} e^{q_j}}$$

As opposed to other normalization and maximum functions, *Softmax* has the nice properties to be differentiable (helping the DNN training process) and to react differently with clear or imprecise inputs, giving more importance (i.e. higher probability) to the neuron with the maximum value when many other neurons of the network had been activated by a clear input.

Due to the large amount of data available, we decided to randomly split the entire dataset into three sets, for training (70%), cross-validation (15%) and test (15%), respectively. The cross-validation dataset was used to select the best parametrization of each model (e.g. the maximum number of splits of the random forest or the number of hidden layers

[2] Regarding the neural network framework, a convolution operation is an element wise matrix (or vector) multiplication operation, performed between the input data and another matrix (or vector) called filter or kernel. It is usually used to perform feature extraction for images classification. For other information, we suggest Goodfellow et al. (2016).

of the neural network), while the test set was devoted to compare the performances of the resulting models of each class (LR, RF and the different architectures of the DNN).

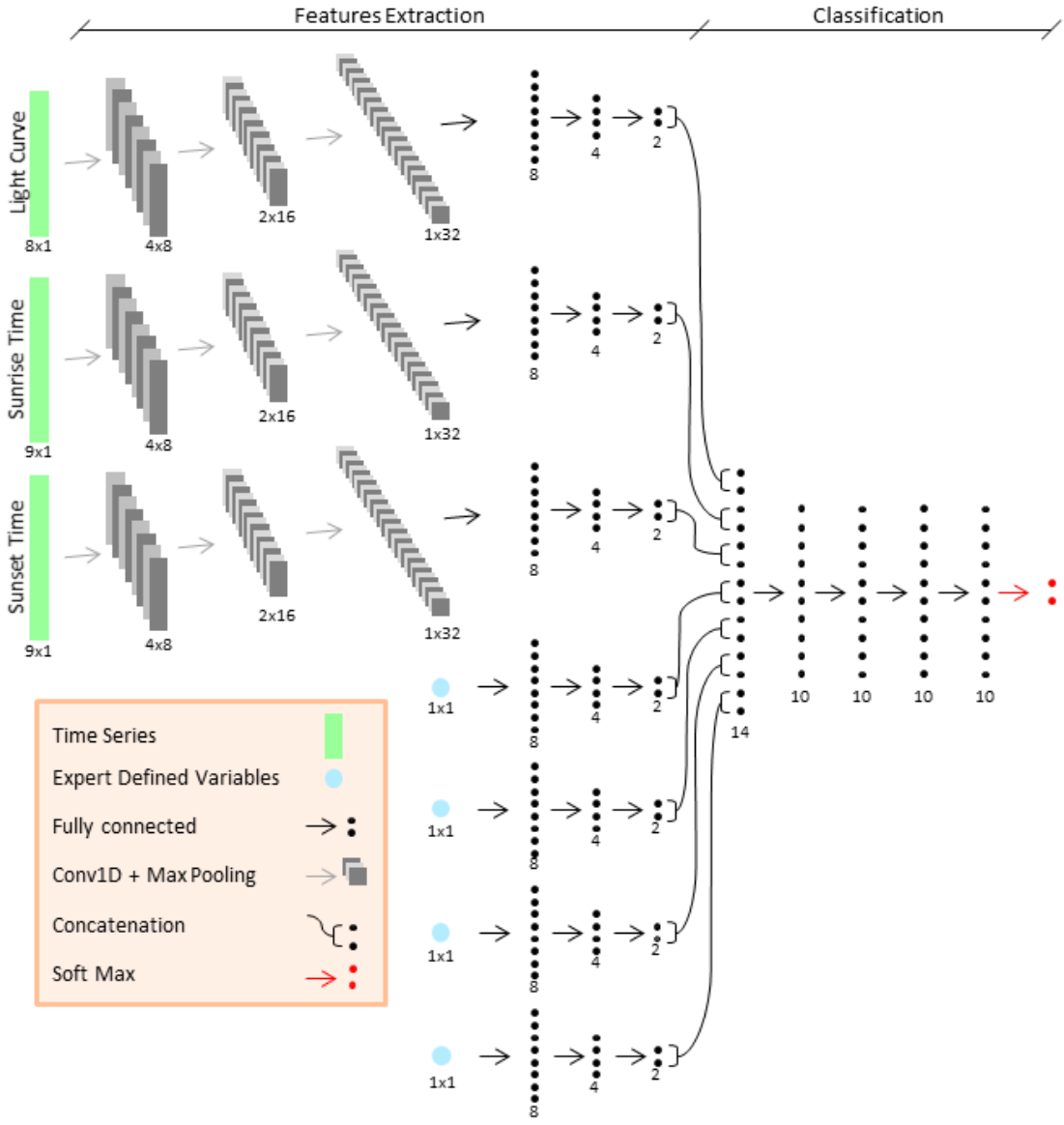

Figure 4.4: Schematic structure of the Deep Neural Network used in our study. A first part of feature extraction is performed on the input variables. The three time series (green vectors: light curve at twilight event, sunrise time of nearby days, sunset time of nearby days) are processed with 1D convolutional filters and then by a fully connected neural network (black dots: neurons). The four expert defined features (4 cerulean single inputs) are not processed with convolutional filters and are directly submitted to the fully connected structure.

We did not adopt more advanced model validation techniques such as *k*-fold or leave-one-out cross-validation, as we didn't notice any overfitting problem during each phase of the work. While we didn't use any precaution to train LR and RF (the former has a

very low number of parameters compared to the task complexity, the latter is an algorithm that is very unlike to overfit if a sufficient number of trees is used; Hastie *et al.*, 2009), we used an early stopping criterion and a regularization for the same procedure in DNN. Early stopping prevents overfitting by interrupting the iterative DNN training process if the performance on the cross-validation dataset is decreasing; regularization takes into account the number of parameters used by the algorithm, adding a value proportional to their sum to the model objective function.

We implemented and trained all ML algorithms using the *Python* packages `scikit-learn` (Pedregosa *et al*., 2012) and `Keras` (Chollet, 2015). We balanced sensitivity and specificity of the result (i.e. we constrained the confusion matrix to have almost the same percentage of true positives and true negatives) by adding and regulating a class weight[3]. This was operatively performed by setting the *class_weight* attribute of each ML algorithm as 'balanced'.

4.2.4 Estimate and comparison of migratory routes

As in the previous chapter, we used `FLightR` *R* package to estimate the migratory tracks of the four target individuals cited before (see Par. 4.2.1). Binding the geolocators measurements with the output of the different twilight classifying methods, for each method and for each individual we generated a TAGS file, used as input in the `FLightR` analysis. The resulting paths (Logistic Regression: LR; Random Forest: RF; Deep Neural Network: DNN; second expert classification: EXP2) were compared to the ones obtained

[3] In the case of binary classification, the weight assigned to the classes is a parameter α within the loss function (e.g. for logistic regression: $Loss = \sum_i \alpha(y_i \cdot \log \hat{y}_i) + (1-\alpha)(1-y_i)\log(1-\hat{y}_i)$. Note that imposing a class weight that guarantees the balance between the classes is equivalent to set the classification threshold in order to make equal the sensitivity and the specificity.

from the first manual classification (EXP1), both visually and using the One-Way-Distance metric (see Par. 3.2.4).

4.3 Results and discussion

4.3.1 Bias and variance trade-off

Figure 4.5 shows the confusion matrix for the three Machine Learning models used in this study and described above, i.e. Logistic Regression (LR), Random Forest (RF) and Deep Neural Network (DNN). As the performances obtained in the three phases of the model calibration (training, validation and test) are nearly the same, we can conclude that we avoided overfitting (i.e. 'high variance'). The RF and the DNN have significantly higher performances compared to the simpler LR classifier, but they perform similarly to each other.

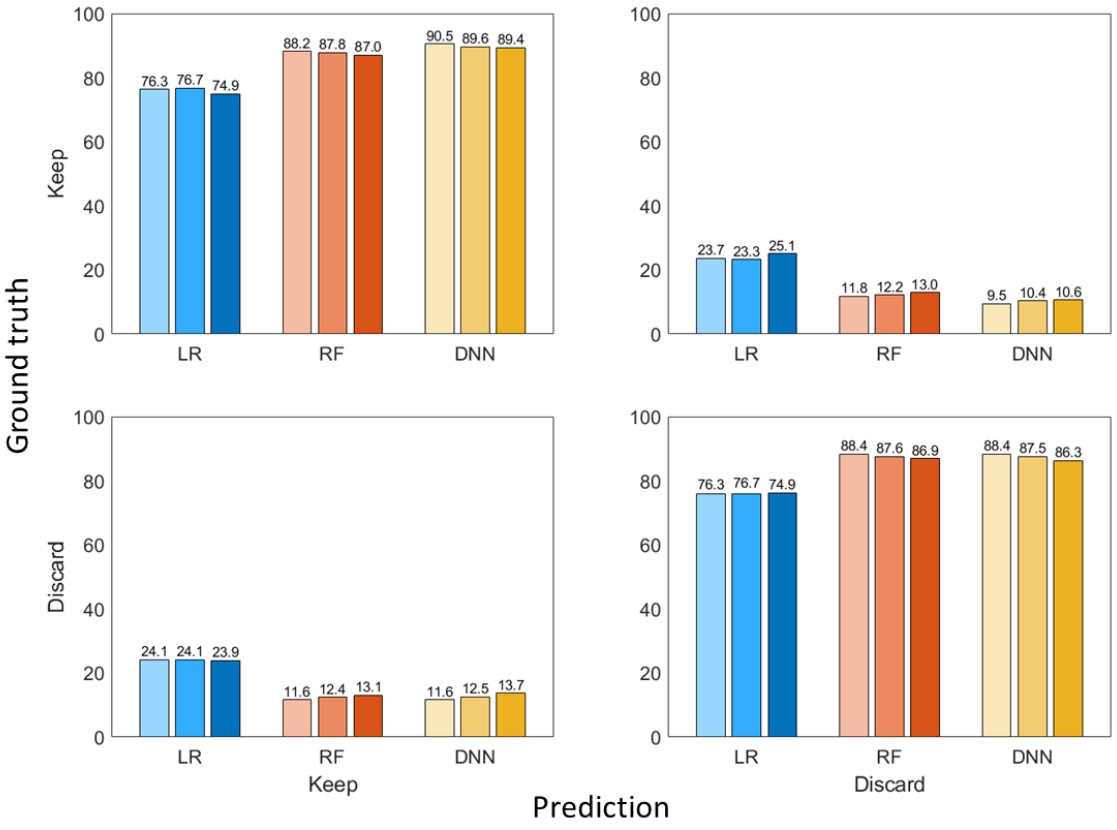

Figure 4.5: Confusion matrix of the three classifier approaches: Logistic Regression (LR, blue), Random Forest (RF, orange) and Deep Neural Network (DNN, yellow). Performances are showed for training (light), validation (medium) and test (dark) sets. Ground truth is referred to the first expert classification (EXP1).

The absence of overfitting, however, does not guarantee *per se* that a model would perform similarly to a human expert. Figure 4.6 compares the performances of the ML algorithms on the classification of the target individuals with the results that we obtained in the second manual classification (performed by the same human expert who classified data for training ML algorithms). It can be noted that the selectivity (true negative/ground truth negative) of the RF and the DNN is comparable with that of a human classifier, while the recall (true positive/ground truth positive) of the two algorithms is slightly lower than that of the expert. Even in terms of overall accuracy the Logistic Regression (LR: 74.3) performs sensibly worse than the other two classifiers (RF: 87.6; DNN: 88.4), which in turn have a slightly lower score respect our expert driven classification (EXP2: 90.7).

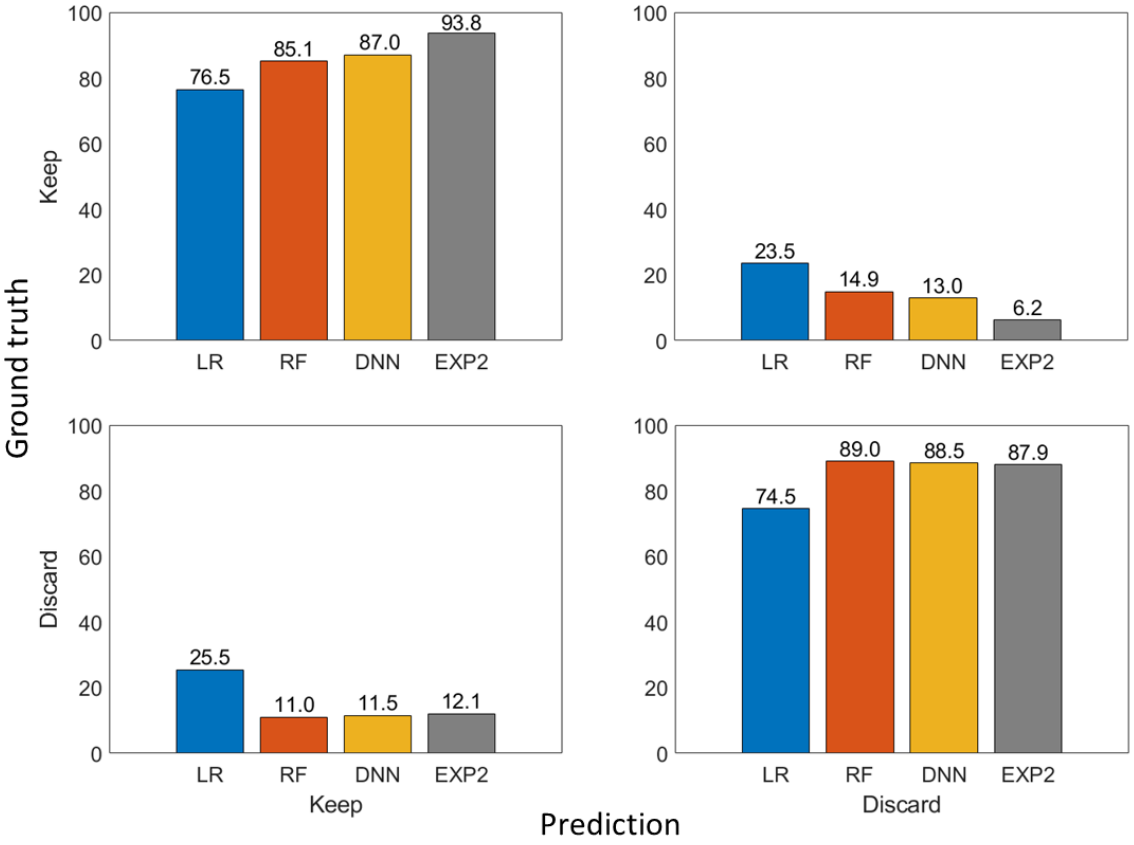

Figure 4.6: Comparison of classifications performed by our Machine Learning algorithms (Logistic Regression, blue; Random Forest, orange; Deep Neural Network, yellow) and a human expert (EXP2, gray) on the twilight data of the target individuals. The ground thrut is referred to the first expert classification (EXP1).

This result, however, highlights the remarks we have reported in Par. 4.2.1 inherently to the difficulty in making a univocal decision for all twilight events: the same expert in

9.3% of cases provided during the second classification (EXP2 a different classification than the one given in the previous one (EXP1).

Regarding the repeatability of the classifiers, Table 4.1 shows the Intraclass Correlation Coefficients calculated from the results of the different classification methods. The value of the ICC between all the methods is pretty high ($ICC_{ALL\ vs\ ALL} = 0.82$), suggesting a generally good consistency between the models we built to classify twilight events and the expert. First of all, the expert classification is the most consistent, as shown by the ICC between his two classifications ($ICC_{EXP1\ vs\ EXP2} = 0.87$). Among the other methods, RF and DNN have similar performance and overperform LR. We can therefore state that both classification procedures operated by the expert and by ML algorithms are repeatable. The ICC at the geolocator level was never higher than 0.0114, implying that the classification of the twilight events did not depend from the features of individual geolocators or of the barn swallows that carried it (i.e. it did not occur, for instance, that twilight events from one geolocator were consistently better than those of another). This means that the classification of twilight events is almost independent from the geolocator, which also explains why the ICC and the confusion matrix gave almost the same results. This result was not strictly predictable as, in principle, individual barn swallows may differ in their behavior during twilight events (e.g. staying in more shaded or more exposed environments), which may affect the light curves on which classification process is based.

Comparison	$ICC_{twilightID\ nested\ in\ geolocatorID}$	$ICC_{geolocatorID}$
ALL vs ALL	0.8243	0.0114
EXP1 vs LR	0.5416	0.0111
EXP1 vs RF	0.8256	0.0092
EXP1 vs DNN	0.8400	0.0109
EXP1 vs EXP2	0.8693	0.0074

Table 4.1: Intraclass Correlation Coefficient values computed for all classification types (ALL vs ALL) and for each separate comparison with the first manual selection (EXP1). The second column shows ICC values at the level if the twilight event identifier (nested within geolocator); the third column indicates ICC values at the level of the geolocator identifier.

4.3.2 Track comparison

Beyond comparing performances of our ML algorithms in terms of mere classification of twilight events, what is key for our problem is to assess whether ML can provide a pre-filtering of twilights data which is reliable enough as to allow a plausible reconstruction of the migration routes of animals based on properly treated light data of the geolocators. Figure 4.7 shows a representative trajectory of one of the target individuals generated by `FLightR` (displayed as average latitude and average longitude at each twilight). The trajectory is estimated starting from the classification operated by the Machine Learning algorithms and by the expert. The path obtained from twilights classified by the LR clearly presents estimation errors, somehow suggesting that this method may be not suitable for safely automating light curves selection (as the high bias in classification performance would preventively suggest). The routes generated from the classification of the RF and the DNN are instead very similar to those obtained using the expert classifications. We obtained similar results also for the other three target individuals (their estimated migratory paths are shown in the Appendix).

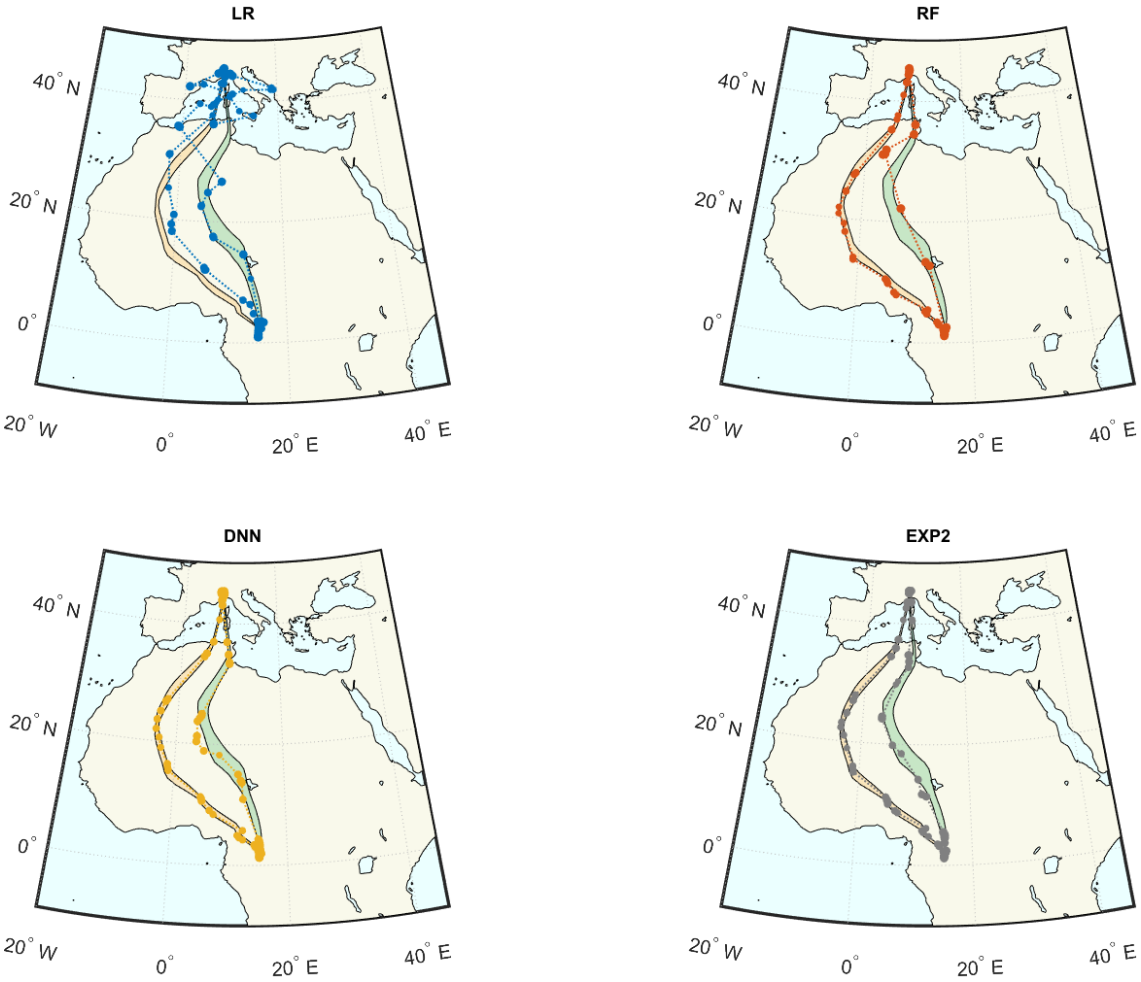

Figure 4.7: Migration paths estimated for one of the 4 target individuals using `FLightR` software with twilight events classified by differents methods: Logistic Regression (LR, blue), Random Forest (RF, orange), Deep Neural Network (DNN, yellow) and expert classification (EXP, gray). Filled polygons refer to first expert classification (orange: fall migration, green: spring migration; boundaries are obtained as mean ± standard deviation of ten repetitions of `FLightR` on EXP1 classification).

The inconsistencies observed between the paths obtained from the RF, DNN, EXP1 and EXP2 classifications are of the same order of magnitude as `FLightR` inter-repetition variability on the same twilights of the same the geolocator (see Par. 3.3.1 at page 62). This could be seen also from Table 4.2, which shows the values of the One Way Distance (defined in Par. 3.2.4 at page 56) calculated by comparing the routes obtained from the classification made by the Logistic Regression, the Random Forest, the Neural Network and the second manual classification with the paths estimated through the first manual classification.

	OWD		Path length (10^3km)		Computation time (s)	
Classification	**Mean**	**Std. Dev.**	**Mean**	**Std. Dev.**	**Mean**	**Std.Dev.**
LR	4.53	1.97	15.3	2.89	<0.001	<0.001
RF	3.68	1.32	11.4	1.22	2.041	0.348
DNN	2.85	1.14	11.1	0.96	15.804	4.872
EXP2	3.40	1.60	11.1	1.10	>1200	>60

Table 4.2: comparison of One Way Distance metric computed on the four test individuals between the routes generated by first expert classification (EXP1) and the other classification methods: Logistic Regression (LR), Random Forest (RF), Deep Neural Network (DNN) and our second manual classification (EXP2).

A mixed effect ANOVA of OWD revealed significant differences according to classification types ($F_{3,9} = 6.04$, $p = 0.015$). Post-hoc tests indicated that OWD of LR was significantly larger than that of EXP2 and DNN ($t_9 \geq 2.79$, $p \leq 0.021$) and marginally not significantly larger than RF ($t_9 = 2.10$, $p = 0.065$). Mixed effect ANOVA test excluding LR showed a marginally not significant difference between the means of the other three classification methods ($F_{2,6} = 4.02$, $p = 0.078$). It can also be noted that the average length of the routes estimated from the sunsets classified by RF is much greater than that of the routes obtained starting from the selections made with the other methods.

4.4 Conclusions

In this chapter we aimed to automate the long manual twilight selection phase that precedes the estimation of the migratory routes in geolocator data analysis. Using a dataset of almost 40,000 expert classified twilight events, we built and calibrated three different Machine Learning algorithms, selecting predictor features that summarize the information processed by the human classifier during his choice.

The performances of complex algorithms such as Random Forests and Deep Neural Networks can be compared with those of the human classifier, both in classification scores, repeatability and in resulting routes estimated by `FLightR` software. Conversely, a simpler technique such as Logistic Regression is not able to correctly classify the

twilights events, causing highly biased outputs in the subsequent phase of route estimation.

For the geolocator models used and for the species analyzed in this study it is therefore possible to automate the twilight events classification procedure and obtain reliable results in the prediction of migration routes. Further twilight measurements from other geolocator models and / or from different species may be useful for a large-scale extension of this automatic procedure in the field of migratory paths reconstruction by light measurements.

In this context, the DNN may have a remarkable advantage with respect to the RF. The dataset of geolocator measurements are usually composed by just a limited number of classified samples, as manual twilight selection is a long time consuming task. In principle, the training process would have to be repeated from scratch, but the small number of records would probably turn out to be insufficient to properly calibrate complex classifiers. A DNN can take advantage of what it learned from bigger dataset, such as the one considered in this paper, thanks to a learning technique known as fine-tuning. The parameters of the front layers, which extract general features, are kept. Conversely, the parameters of the final layers, more task specific, are re-trained on the new dataset. The same process cannot be applied to a RF, which need to be trained again from scratch on the new data. Thus, while the two algorithms have comparable performances, the DNN has a greater flexibility in dealing with new tasks, maintaining the knowledge extracted from previous datasets.

5 CONCLUSION

Migratory birds provide a valuable source of data and information for the study of the impacts of climate change on ecological systems. These species have been monitored for more than a century, but only thanks to technological developments in recent years it has begun to be possible to precisely identify their migratory routes.

The first objective of this thesis was to use ringing data of one of the most studied and known species of migratory birds, the barn swallow, to investigate the possible presence of climatic connections between its wintering and breeding areas in the focal period of spring migration. We found the presence of significant correlations between average temperatures in Africa and in Europe close to the dates of departure and arrival. This climatic signal was stronger in the actual wintering positions of the barn swallows, both at local and continental scale. This result could lead to hypothesize a possible selection of wintering locations based on the climatic connections present with individuals breeding areas. We also analyzed the temporal robustness of the correlations by varying the dates of departure and arrival of the barn swallows, noting that the period when these birds do migrate coincides with the stronger climate connectivity. Finally, we have investigated whether climatic connections between wintering and breeding areas are stable through time, by repeating the calculation of climatic connectivity while shifting the reference year of each individual throughout the time period with available climatic data and found that the most barn swallow were catches in South Africa in the period with the largest number of significant temperature correlations.

In the second part of this thesis, we reconstructed the migratory routes of 88 Italian and Swiss barn swallows from light level geolocator measures, providing for the first time valuable ecological information on a large sample of small migratory birds. We verified the reliability of a software dedicated to the reconstruction of migratory routes, showing how its results could be used in a large-scale analysis of the routes traveled by these birds. From the reconstructed routes, we saw that the barn swallow populations under study adopted different migration strategies, which could be classified in four main types, depending on the propensity of individuals to travel through western routes during the autumn and spring routes. We have therefore analyzed every step of the migration of the reconstructed routes, highlighting the possible carry-over effects of one migratory stage on the following ones. In addition, we identified significant differences in the location of the wintering grounds between the two years in which this study was carried out, consistently to what was already observed by Liechti *et al.* (2015),which used the same geolocator data to identify the wintering grounds of these individuals with a different procedure. This result could be a starting point to investigate the possible influence of local weather conditions on barn swallow migration.

Finally, we have automated a time-consuming manual procedure of the pre-processing of geolocator data: the classification of twilight events based on the light curves associated with them. To achieve this goal, we have implemented three machine learning algorithms, thanks to the amount of data available as a result of the 88 routes reconstruction. The classification performance of two of these methods was comparable with those of an expert human classifier. We tested the reliability of the results of the automatic classification, obtaining a reconstruction of the migratory routes very similar to that provided by the manual selection of the twilight events. This procedure could lead to the complete automation of the light level geolocator analysis process, thus allowing to quickly put in us large amount of data already collected on a wide array of species.

All the analyzes here presented are completely extensible to other species of migratory birds. They provide a contribution to the definition of possible methodologies for investigating the climatic cues used by birds to calibrate their migration and for the reconstruction and the study of individual migratory routes from geolocator data.

APPENDIX

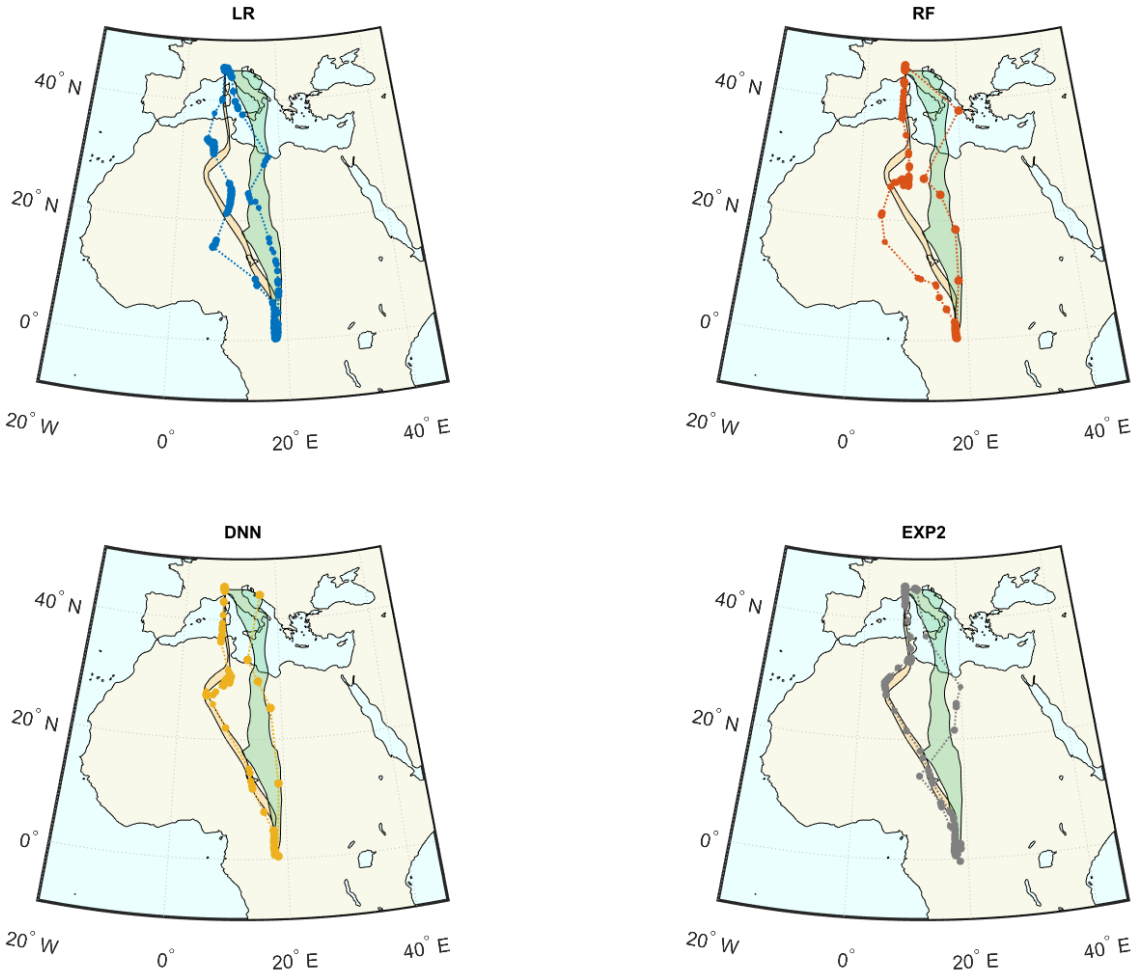

Figure A.1: Migration paths estimated for the second of the four target individuals using `FLightR` software with twilight events classified by differents methods: Logistic Regression (LR, blue), Random Forest (RF, orange), Deep Neural Network (DNN, yellow) and expert classification (EXP, gray). Filled polygons refer to first expert classification (orange: fall migration, green: spring migration; boundaries are obtained as mean ± standard deviation of ten repetitions of `FLightR` on EXP1 classification).

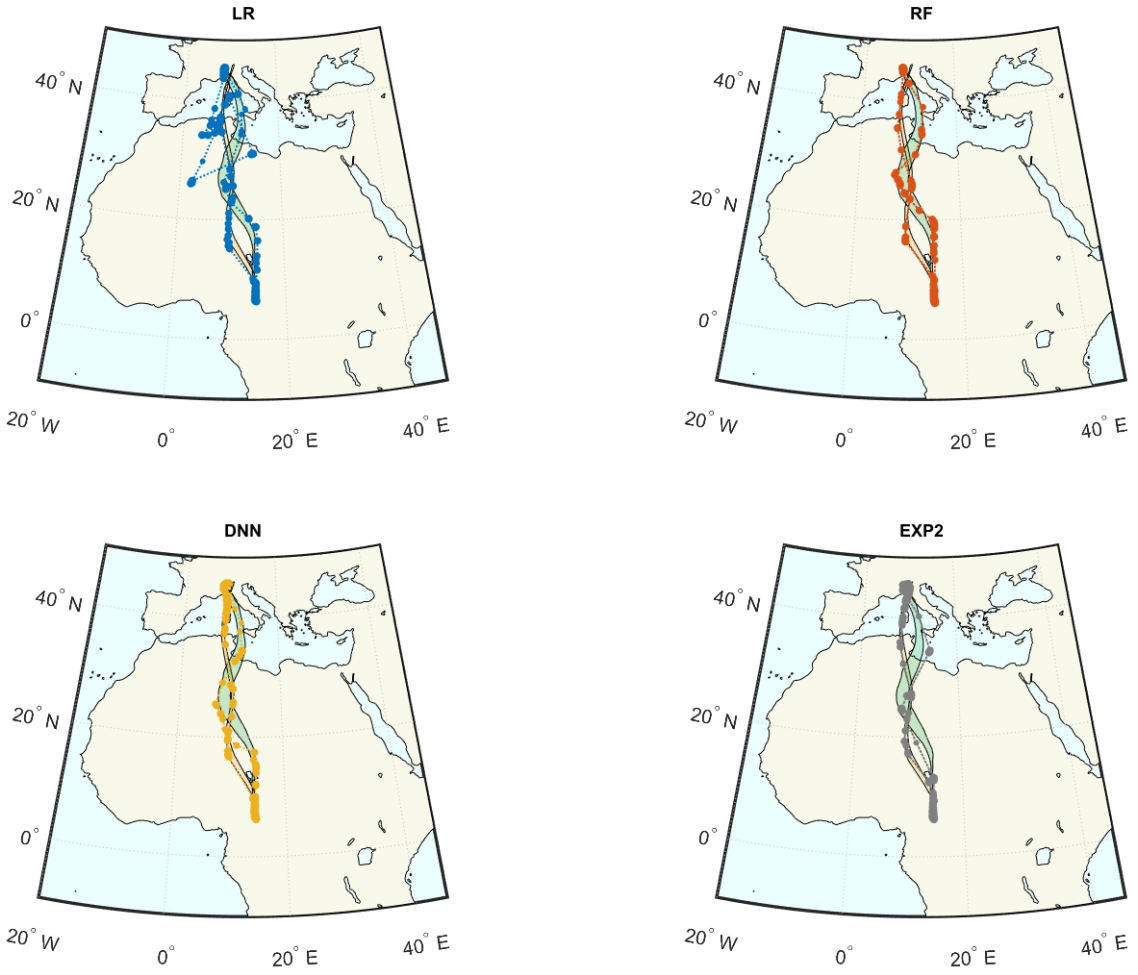

Figure A.2: Migration paths estimated for the third of the four target individuals using `FLightR` software to twilight events classified by differents methods: Logistic Regression (LR, blue), Random Forest (RF, orange), Deep Neural Network (DNN, yellow) and expert classification (EXP, gray). Filled polygons refer to first expert classification (orange: fall migration, green: spring migration; boundaries are obtained as mean ± standard deviation of ten repetitions of `FLightR` on EXP1 classification).

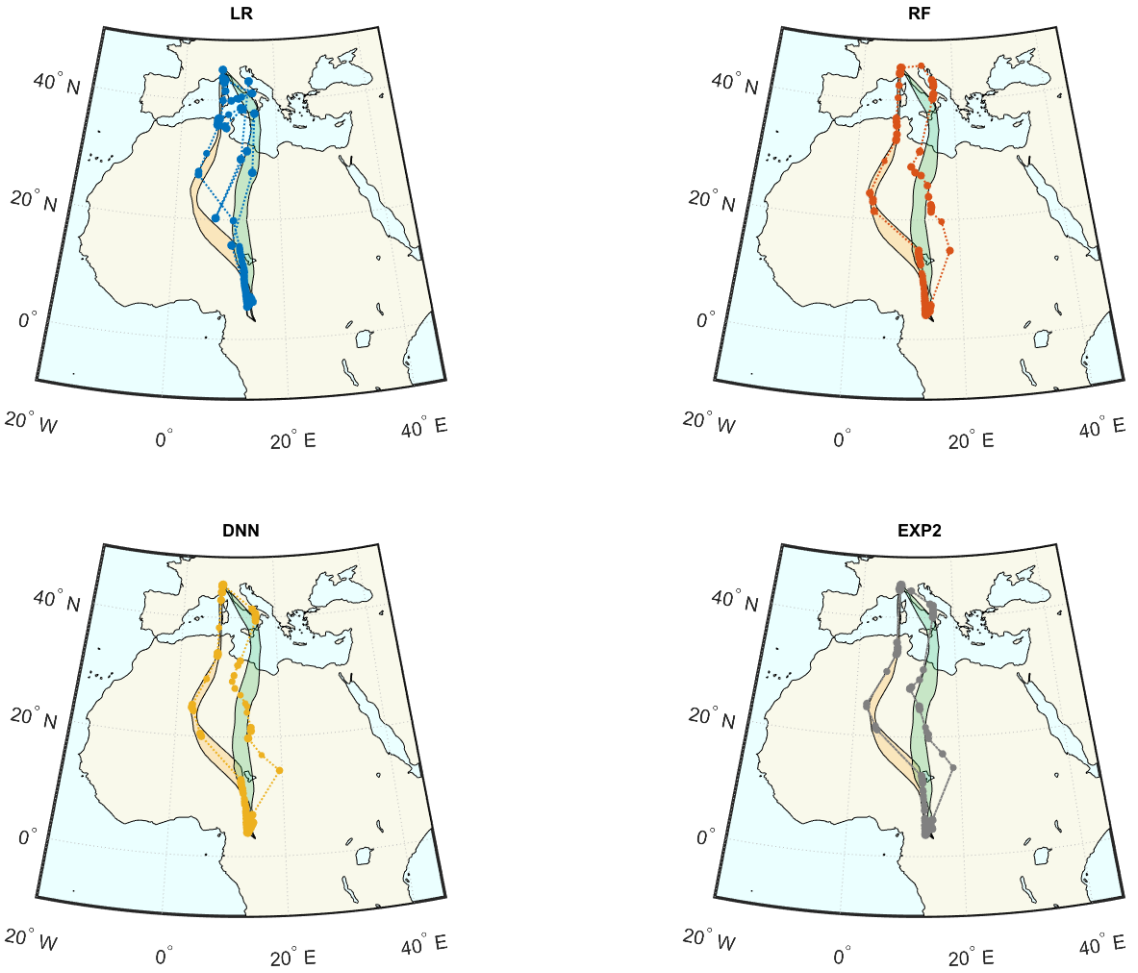

Figure A.3: Migration paths estimated for the last of the four target individuals using `FLightR` software with twilight events classified by differents methods: Logistic Regression (LR, blue), Random Forest (RF, orange), Deep Neural Network (DNN, yellow) and expert classification (EXP, gray). Filled polygons refer to first expert classification (orange: fall migration, green: spring migration; boundaries are obtained as mean ± standard deviation of ten repetitions of `FLightR` on EXP1 classification).

BIBLIOGRAPHY

Altwegg, R. *et al.* (2012) 'Novel methods reveal shifts in migration phenology of barn swallows in South Africa', *Proceedings of the Royal Society B: Biological Sciences*, 279(1733), pp. 1485–1490. doi: 10.1098/rspb.2011.1897.

Ambrosini, R. *et al.* (2002) 'The distribution and colony size of barn swallows in relation to agricultural land use', *Journal of Applied Ecology*. doi: 10.1046/j.1365-2664.2002.00721.x.

Ambrosini, R. *et al.* (2014) 'Modelling the progression of bird migration with conditional autoregressive models applied to ringing data', *PLoS ONE*, 9(7). doi: 10.1371/journal.pone.0102440.

Ambrosini, R. *et al.* (2016) 'Migratory connectivity and effects of winter temperatures on migratory behaviour of the European robin Erithacus rubecula: A continent-wide analysis', *Journal of Animal Ecology*, 85(3), pp. 749–760. doi: 10.1111/1365-2656.12497.

Ambrosini, R., Møller, A. P. and Saino, N. (2009) 'A quantitative measure of migratory connectivity', *Journal of Theoretical Biology*, 257(2), pp. 203–211. doi: 10.1016/j.jtbi.2008.11.019.

Andersen, K. H. *et al.* (2007) 'Using the particle filter to geolocate Atlantic cod (Gadus morhua) in the Baltic Sea, with special emphasis on determining uncertainty', *Canadian Journal of Fisheries and Aquatic Sciences*. doi: 10.1139/f07-037.

Arulampalam, M. S. *et al.* (2007) 'A tutorial on particle filters for online nonlinear/nongaussian bayesian tracking', in *Bayesian Bounds for Parameter Estimation and Nonlinear Filtering/Tracking*. doi: 10.1109/9780470544198.ch73.

Barron, D. G., Brawn, J. D. and Weatherhead, P. J. (2010) 'Meta-analysis of transmitter effects on avian behaviour and ecology', *Methods in Ecology and Evolution*. doi: 10.1111/j.2041-210X.2010.00013.x.

Bates, D. *et al.* (2015) 'Fitting linear mixed-effects models using lme4', *Journal of Statistical Software*. doi: 10.18637/jss.v067.i01.

Bauer, S. and Hoye, B. J. (2014) 'Migratory animals couple biodiversity and ecosystem functioning worldwide', *Science*. doi: 10.1126/science.1242552.

Bengio, Y. (2009) 'Learning Deep Architectures for AI', *Foundations and Trends® in Machine Learning*, 2(1), pp. 1–127. doi: 10.1561/2200000006.

Bertacchi, D., Zucca, F. and Ambrosini, R. (2016) 'The timing of life history events in the presence of soft disturbances', *Journal of Theoretical Biology*. Elsevier, 389, pp. 287–303. doi: 10.1016/j.jtbi.2015.10.028.

Berthold, P. (1996) *Control of bird migration*. London: Chapman & Hall.

Berthold, P. (2001) 'Threats and the conservation and future of migrants', in *Bird migration: a general survey*. Second. Oxford University Press, pp. 180–189.

Biau, G. and Scornet, E. (2015) 'A Random Forest Guided Tour', *ArXiv*. doi: 10.1007/s11749-016-0481-7.

Both, C. *et al.* (2006) 'Climate change and population declines in a long-distance migratory bird', *Nature*, 441(7089), pp. 81–83. doi: 10.1038/nature04539.

Both, C. (2010) 'Flexibility of timing of avian migration to climate change masked by environmental constraints en route', *Current Biology*. Elsevier Ltd, 20(3), pp. 243–248. doi: 10.1016/j.cub.2009.11.074.

Bridge, E. S. *et al.* (2011) 'Technology on the Move: Recent and Forthcoming Innovations for Tracking Migratory Birds', *BioScience*. doi: 10.1525/bio.2011.61.9.7.

Briedis, M. *et al.* (2018) 'Loop migration, induced by seasonally different flyway use, in Northern European Barn Swallows', *Journal of Ornithology*. Springer Berlin Heidelberg, pp. 1–7. doi: 10.1007/s10336-018-1560-1.

Brlík, V. *et al.* (2018) 'First insights into the migration route and migratory connectivity of the Paddyfield Warbler using geolocator tagging and stable isotope analysis', *Journal of Ornithology*. doi: 10.1007/s10336-018-1557-9.

Chollet, F. (2015) ‘Keras Documentation’, *Keras.Io*.

Cooke, S. J. (2008) ‘Biotelemetry and biologging in endangered species research and animal conservation: Relevance to regional, national, and IUCN Red List threat assessments’, *Endangered Species Research*. doi: 10.3354/esr00063.

Cooke, S. J. *et al.* (2013) ‘Tracking animals in freshwater with electronic tags: Past, present and future’, *Animal Biotelemetry*. doi: 10.1186/2050-3385-1-5.

Coppack, T. and Both, C. (2003) ‘Predicting life-cycle adaptation of migratory birds to global climate change’, *Ardea*, 90, pp. 369–378.

Cormier, R. L. *et al.* (2013) ‘Light-Level Geolocators Reveal Strong Migratory Connectivity and Within-Winter Movements for a Coastal California Swainson’s Thrush (Catharus ustulatus) Population’, *The Auk*, 130(2), pp. 283–290. doi: 10.1525/auk.2013.12228.

Cotton, P. a (2003) ‘Avian migration phenology and global climate change.’, *Proceedings of the National Academy of Sciences of the United States of America*, 100(21), pp. 12219–12222. doi: 10.1073/pnas.1930548100.

Cox, D. R. (1958) ‘The Regression Analysis of Binary Sequences’, *Journal of the Royal Statistical Society. Series B (Methodological)*. doi: 10.1007/BF03180993.

Darwin, C. (1859) *On the origin of species by means of natural selection, or preservation of favoured races in the struggle for life*, *Darwin*. London: John Murray. doi: 10.1016/S0262-4079(09)60380-8.

Donald, P. F. *et al.* (2006) ‘Further evidence of continent-wide impacts of agricultural intensification on European farmland birds, 1990-2000’, *Agriculture, Ecosystems and Environment*. doi: 10.1016/j.agee.2006.02.007.

Donald, P. F., Green, R. E. and Heath, M. F. (2001) ‘Agricultural intensification and the collapse of Europe’s farmland bird populations’, *Proceedings of the Royal Society B: Biological Sciences*. doi: 10.1098/rspb.2000.1325.

Doucet, A., Briers, M. and Sénécal, S. (2006) ‘Efficient block sampling strategies for sequential Monte Carlo methods’, *Journal of Computational and Graphical Statistics*. doi: 10.1198/106186006X142744.

Doucet, A., Godsill, S. and Andrieu, C. (2000) 'On sequential Monte Carlo sampling methods for Bayesian filtering', *Statistics and Computing*. doi: 10.1023/A:1008935410038.

Ekstrom, P. (2007) 'Error measures for template-fit geolocation based on light', *Deep-Sea Research Part II: Topical Studies in Oceanography*. doi: 10.1016/j.dsr2.2006.12.002.

Ekstrom, P. P. A. (2004) 'An advance in geolocation by light', *Mem. Natl Inst. Polar Res., Spec. Issue*.

Ensminger, I., Yao-Yun Chang, C. and Bräutigam, K. (2015) 'Tree Responses to Environmental Cues', *Advances in Botanical Research*. doi: 10.1016/bs.abr.2015.05.003.

du Feu, C. R. *et al.* (2016) 'The EURING Data Bank – a critical tool for continental-scale studies of marked birds', *Ringing and Migration*. doi: 10.1080/03078698.2016.1195205.

Fiedler, W., Bairlein, F. and Köppen, U. (2004) 'Using Large-Scale Data from Ringed Birds for the Investigation of Effects of Climate Change on Migrating Birds: Pitfalls and Prospects', *Advances in Ecological Research*. doi: 10.1016/S0065-2504(04)35003-8.

Finch, T. *et al.* (2015) 'A pan-European, multipopulation assessment of migratory connectivity in a near-threatened migrant bird', *Diversity and Distributions*, 21(9), pp. 1051–1062. doi: 10.1111/ddi.12345.

Finch, T. *et al.* (2017) 'Low migratory connectivity is common in long-distance migrant birds', *Journal of Animal Ecology*, 86(3), pp. 662–673. doi: 10.1111/1365-2656.12635.

Fraser, K. C. *et al.* (2012) 'Continent-wide tracking to determine migratory connectivity and tropical habitat associations of a declining aerial insectivore', *Proceedings of the Royal Society B: Biological Sciences*, 279(1749). doi: 10.1098/rspb.2012.2207.

Frederiksen, M. *et al.* (2018) 'Where do wintering cormorants come from? Long-term changes in the geographical origin of a migratory bird on a continental scale', *Journal of Applied Ecology*. doi: 10.1111/1365-2664.13106.

Gilbert, M. *et al.* (2010) 'Flying over an infected landscape: Distribution of highly pathogenic avian influenza H5N1 risk in South Asia and satellite tracking of wild waterfowl', *EcoHealth*. doi: 10.1007/s10393-010-0672-8.

Goodfellow, I; Bengio, Y; Courville, A. (2016) 'Convolutional Networks', in Thomas Dietterich (ed.) *Deep Learning*. Cambridge, Massachusetts; London, England: The MIT Press, pp. 321–359.

Gordo, O. *et al.* (2005) 'Do changes in climate patterns in wintering areas affect the timing of the spring arrival of trans-Saharan migrant birds?', *Global Change Biology*, 11(1), pp. 12–21. doi: 10.1111/j.1365-2486.2004.00875.x.

Gordo, O. (2007) 'Why are bird migration dates shifting? A review of weather and climate effects on avian migratory phenology', *Climate Research*, 35(1–2), pp. 37–58. doi: 10.3354/cr00713.

Guilford, T. *et al.* (2011) 'Migratory navigation in birds: new opportunities in an era of fast-developing tracking technology', *Journal of Experimental Biology*. doi: 10.1242/jeb.051292.

Gunnarsson, T. G. and Tómasson, G. (2011) 'Flexibility in spring arrival of migratory birds at northern latitudes under rapid temperature changes', *Bird Study*, 58(1), pp. 1–12. doi: 10.1080/00063657.2010.526999.

Gwinner, E. (1996) 'Circannual clocks in avian reproduction and migration', *Ibis*, 138, pp. 47–63.

Hahn, S. *et al.* (2013) 'Strong migratory connectivity and seasonally shifting isotopic niches in geographically separated populations of a long-distance migrating songbird', *Oecologia*, 173(4), pp. 1217–1225. doi: 10.1007/s00442-013-2726-4.

Hastie, T., Tibshirani, R. and Friedman, J. (2009) *The Elements of Statistical Learning*, *Bayesian Forecasting and Dynamic Models*. doi: 10.1007/b94608.

Hays, G. C. *et al.* (2014) 'Use of Long-Distance Migration Patterns of an Endangered Species to Inform Conservation Planning for the World's Largest Marine Protected Area', *Conservation Biology*. doi: 10.1111/cobi.12325.

Hill, R. D. (1994) 'Theory of geolocation by light levels', *Elephant Seals: Population Ecology, Behavior, and Physiology*.

Hill, R. D. and Braun, M. J. (2001) 'Geolocation by light level—The next step: Latitude.', *Electronic Tagging and Tracking in Marine Fisheries*. doi: 10.1007/978-94-017-1402-0_17.

Ho, T. K. (1995) 'Random Decision Forests', *Proceedings of 3rd International Conference on Document Analysis and Recognition*, pp. 278–282. doi: 10.1109/ICDAR.1995.598994.

Jones, N. T. and Gilbert, B. (2016) 'Changing climate cues differentially alter zooplankton dormancy dynamics across latitudes', *Journal of Animal Ecology*. doi: 10.1111/1365-2656.12474.

Kardynal, K. J. and Hobson, K. A. (2017) 'The pull of the Central Flyway? Veeries breeding in western Canada migrate using an ancestral eastern route', *Journal of Field Ornithology*. doi: 10.1111/jofo.12207.

Kaufman, L. and Rousseeuw, P. J. (1987) 'Clustering by means of medoids', *Statistical Data Analysis Based on the L 1-Norm and Related Methods. First International Conference*.

Knick, S. T. *et al.* (2014) 'Diffuse migratory connectivity in two species of shrubland birds: Evidence from stable isotopes', *Oecologia*, 174(2), pp. 595–608. doi: 10.1007/s00442-013-2791-8.

Korner-Nievergelt, F. *et al.* (2010) 'Improving the analysis of movement data from marked individuals through explicit estimation of observer heterogeneity', *Journal of Avian Biology*. doi: 10.1111/j.1600-048X.2009.04907.x.

Kramer, G. R. *et al.* (2018) 'Population trends in Vermivora warblers are linked to strong migratory connectivity', *Proceedings of the National Academy of Sciences*. doi: 10.1073/pnas.1718985115.

Lam, C. H., Nielsen, A. and Sibert, J. R. (2008) 'Improving light and temperature based geolocation by unscented Kalman filtering', *Fisheries Research*. doi: 10.1016/j.fishres.2007.11.002.

Lam, C. H., Nielsen, A. and Sibert, J. R. (2010) 'Incorporating sea-surface temperature to the light-based geolocation model TrackIt', *Marine Ecology Progress Series*. doi: 10.3354/meps08862.

LeCun, Y. and Bengio, Y. (1995) ‘Convolutional networks for images, speech, and time series’, *The handbook of brain theory and neural networks*. doi: 10.1109/IJCNN.2004.1381049.

Liechti, F. *et al.* (2015) ‘Timing of migration and residence areas during the non-breeding period of barn swallows Hirundo rustica in relation to sex and population’, *Journal of Avian Biology*, 46(3), pp. 254–265. doi: 10.1111/jav.00485.

Lin, B. and Su, J. (2005) ‘Shapes based trajectory queries for moving objects’, in *Proceedings of the 2005 international workshop on Geographic information systems - GIS ’05*. doi: 10.1145/1097064.1097069.

Lisovski, S. *et al.* (2012) ‘Geolocation by light: Accuracy and precision affected by environmental factors’, *Methods in Ecology and Evolution*. doi: 10.1111/j.2041-210X.2012.00185.x.

Lisovski, S. and Hahn, S. (2012) ‘GeoLight - processing and analysing light-based geolocator data in R’, *Methods in Ecology and Evolution*. doi: 10.1111/j.2041-210X.2012.00248.x.

Machado, G., Mendoza, M. R. and Corbellini, L. G. (2015) ‘What variables are important in predicting bovine viral diarrhea virus? A random forest approach’, *Veterinary Research*. doi: 10.1186/s13567-015-0219-7.

Marshak, S. (2009) *Essentials of Geology*. Third Edit. New York: W. W. Norton & Co.

McClintock, B. T. *et al.* (2012) ‘A general discrete-time modeling framework for animal movement using multistate random walks’, *Ecological Monographs*. doi: 10.1890/11-0326.1.

Meehl, G. A. *et al.* (2000) ‘An Introduction to Trends in Extreme Weather and Climate Events: Observations, Socioeconomic Impacts, Terrestrial Ecological Impacts, and Model Projections *’, *Bulletin of the American Meteorological Society*. doi: 10.1175/1520-0477(2000)081<0413:AITTIE>2.3.CO;2.

Meeus, J. (1991) ‘Astronomical Algorithms’, *Astronomical Algorithms*. doi: 10.1016/B978-0-12-373972-8.00050-4.

Meier, C. M. *et al.* (2018) 'What makes Alpine swift ascend at twilight? Novel geolocators reveal year-round flight behaviour', *Behavioral Ecology and Sociobiology*. doi: 10.1007/s00265-017-2438-6.

Merkel, B. *et al.* (2016) 'A probabilistic algorithm to process geolocation data', *Movement Ecology*. doi: 10.1186/s40462-016-0091-8.

Van Der Merwe, R. *et al.* (2001) 'The Unscented Particle Filter', *Advances in Neural Information Processing Systems*. doi: 10.1152/jn.00126.2006.

Møller, a P., Fiedler, W. and Berthold, P. (2010) 'Long-term time series of ornithological data', in *Effects of climate change on birds*. Oxford Univwersityu Press, pp. 33–38.

Møller, A. P. (1994) *Sexual selection and the Barn Swallow*. Oxford Series in Ecology and Evolution.

Møller, A. P. *et al.* (2004) 'Analysis and interpretation of long-term studies investigating responses to climate change', *Birds and Climate Change*, 35(04), pp. 111–130. doi: 10.1016/s0065-2504(04)35006-3.

Møller, A. P., Rubolini, D. and Lehikoinen, E. (2008) 'Populations of migratory bird species that did not show a phenological response to climate change are declining.', *Proceedings of the National Academy of Sciences of the United States of America*, 105(42), pp. 16195–16200. doi: 10.1073/pnas.0803825105.

Morales, J. M. *et al.* (2004) 'Extracting more out of relocation data: Building movement models as mixtures of random walks', *Ecology*. doi: 10.1890/03-0269.

Mu, T. *et al.* (2018) 'Migratory routes of red-necked phalaropes Phalaropus lobatus breeding in southern Chukotka revealed by geolocators', *Journal of Avian Biology*. doi: 10.1111/jav.01853.

Nadal, J., Ponz, C. and Margalida, A. (2018) 'Population age structure as an indicator for assessing the quality of breeding areas of Common quail (Coturnix coturnix)', *Ecological Indicators*. doi: 10.1016/j.ecolind.2018.06.010.

Newton, I. (2007) *The Migration Ecology of Birds*, *The Migration Ecology of Birds*. doi: 10.1016/B978-0-12-517367-4.X5000-1.

Pancerasa, M. *et al.* (2018) 'Barn swallows long-distance migration occurs between significantly temperature-correlated areas', *Scientific Reports*. doi: 10.1038/s41598-018-30849-0.

Parmesan, C. (2006) 'Ecological and Evolutionary Responses to Recent Climate Change', *Annual Review of Ecology, Evolution, and Systematics*, 37(1), pp. 637–669. doi: 10.1146/annurev.ecolsys.37.091305.110100.

Parmesan, C., Root, T. and Willig, M. R. (2000) 'Impacts of extreme weather and climate on terrestrial biota', *Bulletin of the American Meteorological Society*, 81(3), pp. 1–10. doi: http://dx.doi.org/10.1108/17506200710779521.

Parmesan, C. and Yohe, G. (2003) 'A globally coherent fingerprint of climate change impacts across natural systems.', *Nature*, 421(6918), pp. 37–42. doi: 10.1038/nature01286.

Pedregosa, F. *et al.* (2012) 'Scikit-learn: Machine Learning in Python', *Journal of Machine Learning Research*. doi: 10.1007/s13398-014-0173-7.2.

Phillips, R. A. *et al.* (2004) 'Accuracy of geolocation estimates for flying seabirds', *Marine Ecology Progress Series*. doi: 10.3354/meps266265.

Poli, P. *et al.* (2016) 'ERA-20C : An Atmospheric Reanalysis of the Twentieth Century', *Journal of Climate*, 29, pp. 4083–4097. doi: 10.1175/JCLI-D-15-0556.1.

Przybylo, R., Sheldon, B. E. N. C. and Merila, J. (2000) 'Climatic effects on bredding and morphology: Evidence for phenotypic plasticity', *Journal of Animal Ecology*, 69, pp. 395–403.

Rakhimberdiev, E. *et al.* (2015) 'A hidden Markov model for reconstructing animal paths from solar geolocation loggers using templates for light intensity', *Movement Ecology*. doi: 10.1186/s40462-015-0062-5.

Rakhimberdiev, E. *et al.* (2017) 'FLightR: an r package for reconstructing animal paths from solar geolocation loggers', *Methods in Ecology and Evolution*. doi: 10.1111/2041-210X.12765.

Ranacher, P. and Tzavella, K. (2014) ‘How to compare movement? A review of physical movement similarity measures in geographic information science and beyond’, *Cartography and Geographic Information Science*. doi: 10.1080/15230406.2014.890071.

Reini, M. (1996) ‘Monte Carlo Filter and Smoother for Non-Gaussian Nonlinear State Space Models’, *Journal of Computational and Graphical Statistics*. doi: 10.1080/10618600.1996.10474692.

Robinson, R. A. *et al.* (2009) ‘Travelling through a warming world: Climate change and migratory species’, *Endangered Species Research*, 7(2), pp. 87–99. doi: 10.3354/esr00095.

Robinson, W. D. *et al.* (2010) ‘Integrating concepts and technologies to advance the study of bird migration’, *Frontiers in Ecology and the Environment*. doi: 10.1890/080179.

Rubolini, D. *et al.* (2007) ‘Intraspecific consistency and geographic variability in temporal trends of spring migration phenology among european bird species’, *Climate Research*, 35(1–2), pp. 135–146. doi: 10.3354/cr00720.

Saino, N. *et al.* (2009) ‘Climate change effects on migration phenology may mismatch brood parasitic cuckoos and their hosts.’, *Biology letters*, 5(April), pp. 539–541. doi: 10.1098/rsbl.2009.0312.

Saino, N. and Ambrosini, R. (2008) ‘Climatic connectivity between Africa and Europe may serve as a basis for phenotypic adjustment of migration schedules of trans-Saharan migratory birds’, *Global Change Biology*, 14(2), pp. 250–263. doi: 10.1111/j.1365-2486.2007.01488.x.

Sanderson, F. J. *et al.* (2006) ‘Long-term population declines in Afro-Palearctic migrant birds’, *Biological Conservation*. doi: 10.1016/j.biocon.2006.02.008.

Scandolara, C. *et al.* (2014) ‘Impact of miniaturized geolocators on barn swallow Hirundo rustica fitness traits’, *Journal of Avian Biology*. doi: 10.1111/jav.00412.

Shrout, P. E. and Fleiss, J. L. (1979) ‘Intraclass correlations: Uses in assessing rater reliability’, *Psychological Bulletin*. doi: 10.1037/0033-2909.86.2.420.

Sokal, R. R. and Rohlf, F. J. (1995) *Biometry: the principles and practice of statistics in biological research*. 3rd ed., *Biometry Third edition*. 3rd ed. W.H. Freeman and Company.

Stenseth, N. C. and Mysterud, A. (2002) 'Climate, changing phenology, and other life history traits: nonlinearity and match-mismatch to the environment.', *Proceedings of the National Academy of Sciences of the United States of America*, 99(21), pp. 13379–13381. doi: 10.1073/pnas.212519399.

Sumner, M. D., Wotherspoon, S. J. and Hindell, M. A. (2009) 'Bayesian Estimation of Animal Movement from Archival and Satellite Tags', *PLoS ONE*. doi: 10.1371/journal.pone.0007324.

Teague O'Mara, M., Wikelski, M. and Dechmann, D. K. N. (2014) '50 years of bat tracking: Device attachment and future directions', *Methods in Ecology and Evolution*. doi: 10.1111/2041-210X.12172.

Thomson, D., van Noordwijk, A. and Hagemeijer, W. (2003) 'Estimating avian dispersal distances from data on ringed birds', *Journal of Applied Statistics*, 30(9), pp. 1003–1008. doi: 10.1080/0266476032000076128.

Tomkiewicz, S. M. *et al.* (2010) 'Global positioning system and associated technologies in animal behaviour and ecological research', *Philosophical Transactions of the Royal Society B: Biological Sciences*. doi: 10.1098/rstb.2010.0090.

Turner, A. (2006) *The barn swallow*. London: T & A D Poyser.

Underhill, L. G. and Oately, T. B. (1994) 'The South-African bird ringing unit - 21 years of service and research', *South African Journal Of Science*.

Visser, M. E. and Both, C. (2005) 'Shifts in phenology due to global climate change: the need for a yardstick.', *Proceedings of the Royal Society B*, 272(1581), pp. 2561–2569. doi: 10.1098/rspb.2005.3356.

Wackernagel, H. (1995) 'Ordinary Kriging', in *Multivariate Geostatistics*. Berlin, Heidelberg: Springer Berlin Heidelberg, pp. 74–81. doi: 10.1007/978-3-662-03098-1_11.

Walther, G.-R. *et al.* (2002) 'Ecological responses to recent climate change.', *Nature*, 416(6879), pp. 389–395. doi: 10.1038/416389a.

Wikelski, M. *et al.* (2007) ‘Going wild: what a global small-animal tracking system could do for experimental biologists’, *Journal of Experimental Biology*. doi: 10.1242/jeb.02629.

Williams, C. T. *et al.* (2014) ‘Phenology of hibernation and reproduction in ground squirrels: Integration of environmental cues with endogenous programming’, *Journal of Zoology*. doi: 10.1111/jzo.12103.

Winkler, D. W. *et al.* (2017) ‘Long-Distance Range Expansion and Rapid Adjustment of Migration in a Newly Established Population of Barn Swallows Breeding in Argentina’, *Current Biology*. doi: 10.1016/j.cub.2017.03.006.

Witynski, M. L. and Bonter, D. N. (2018) ‘Crosswise migration by Yellow Warblers, Nearctic-Neotropical passerine migrants’, *Journal of Field Ornithology*. doi: 10.1111/jofo.12237.

Wormworth, J. and Sekercioglu, C. H. (2011) *Winged sentinels: Birds and climate change*, *Winged Sentinels: Birds and Climate Change*. doi: 10.1017/CBO9781139150026.

Wotherspoon, S., Sumner, M. & Lisovski, S. (2016) ‘TwGeos: basic data processing for light-level geolocation archival tags - Version 0.0-1’.